Democratic and Popular Republic of Algeria
Ministry of Higher Education and Scientific Research
Chadli Bendjedid University – El Tarf
Faculty of Sciences and Technology
Process Engineering Department

Professional Master's Thesis

Field: Sciences and Technology

Major: Process Engineering

Specialty: Water Treatment and Desalination

Theme:

Cost-effective and eco-friendly synthesis of a Nano-hybrid material and investigation of its Photocatalytic and Electrocatalytic performance

Presented by:

HAOULI Khaoula

Defended on: 19/06/2025 before the Jury:

Dr. OTMANI Lhadi	**President**	**MCB**	**Univ. El-Tarf**
Dr. KHELLAF Noureddine	**Supervisor**	**MCB**	**Univ. El-Tarf**
Dr. AITBARA Adel	**Examiner**	**MCA**	**Univ. El-Tarf**

Academic Year: 2024/2025

‘ ’The more I learn,

the more I realize how much I don’t know.”

Albert Einstein.

Dedication

To the man who gave me roots and wings my father.'

HAOULI Belkacem

You are the source behind my strength, the quiet voice behind my success, and the reason I never gave up.

This work is for you, with all the love a grateful heart can hold.

Khaoula

Acknowledgment

Knowledge, determination, and grace have guided me on this academic journey. I am most thankful to God Almighty, whose supernatural direction lit my way through every hardship. Thanks to my supervisor, ***Dr. KHELLAF Noureddine***, for your helpful advice, constant support, and faith in my work. The cornerstone of this thesis was built on your guidance.

Heartfelt thanks go to ***Dr. MESKHER Hicham*** for being so deeply involved. It made a big difference. Your gracious feedback, expert advice, and guidance exceeded my expectations. I also recognize the importance of the jury members, as their feedback and suggestions helped me refine my work. I want to thank ***Dr. AITBARA Adel*** and ***Dr. OTMANI Lhadi***.

As I worked on this project, I was lucky to get a lot of technical and practical help from talented engineers. I convey heartfelt appreciation to ***Eng. KHERICI Soufian*** and ***Eng. NADRA***, whose devotion and technical skills at the university laboratory were vital. Your patient support during vital phases of experimentation is sincerely valued.

Over the course of this research, I also profited immensely from collaborative efforts beyond my university. I am extremely grateful to ***Pr. FOUDIA Malika***, ***Dr. AROUI Lynda***, ***Dr.DERBAL Sabrine*** and ***Eng. NECHADI Meriem*** from *FARHAT ABBAS University of Setif*. Your external insights and cooperation gave depth and diversity to my work. Your laboratory's transparency and professionalism made our work meaningful and fruitful.

Undoubtedly, this work would not have been possible without the warmth, love, and steadfast encouragement of my family. To my father, whose memory continues to inspire me; to my mother and, whose prayers, love, and belief in me provided me strength when I needed it most. Every word of support and act of care was a light along the journey.

Laughter and late nights, shared learning and support from friends, students, and peers, added joy to the academic challenge. Thank you for making this experience not just bearable but lovely. Your humour, help, and personal connection lightened the hardest of days and gave life to amazing moments. You were, in every way, my second family.

All of this came together under the dome of a fantastic academic and research environment that encouraged my ideas and personal growth. To all professors, laboratory staff, pedagogical coordinators, and the team members in our lab whose collective commitment created the space where this study could grow. I am extremely thankful to those that guided me, encouraged me, and believed in me every step of the way.

Table of Contents

Dedication ..... **ii**

Acknowledgment ..... **iii**

Table of Contents ..... **iv**

List of Figures ..... **vi**

List of Tables ..... **viii**

List of Abbreviations ..... **ix**

General Introduction **1**

Chapter I: Synthetic Dyes in Wastewater: Challenges and Degradation Technologies **3**

I.1. Introduction ---------- **3**

I.2.Dyes ---------- **3**

I.2.1. Classification of dyes ---------- 3

I.2.2. Structure of dyes ---------- 4

I.2.3 Model Dyes Selected for Study ---------- 5

I.2.4. Toxicity and Environmental Impact of Dyes ---------- 5

I.2.5. Challenges in Dye Degradation ---------- 6

I.2.6. Removal techniques of dyes ---------- 6

I.2.6.1. Physical Methods ---------- 7

I.2.6.2. Chemical Methods ---------- 7

I.2.6.3. Biological Methods ---------- 8

I.2.6.4. Integrated and Hybrid Systems ---------- 9

I.3.Photocatalytic Technologies for Wastewater ---------- **10**

I.3.1. Principles of Photocatalysis ---------- 10

I.3.2. Titanium Dioxide TiO_2 ---------- 10

I.3.2.1. Structure of Titanium Dioxide TiO_2 ---------- 12

I.3.2.2. Properties of Titanium Dioxide TiO_2 ---------- 12

I.3.2.3. Application of Titanium Dioxide TiO_2 in photocatalysis ---------- 13

I.3.2.4. Limitations of Titanium Dioxide TiO_2 and Strategies for Improvement ---------- 13

I.4.Role of Reduced graphene oxide Modifiers ---------- **14**

I.4.1. Reduced Graphene Oxide ---------- 14
I.4.1.1. Structure of reduced Graphene Oxide ---------- 15
I.4.1.2. Properties of reduced Graphene Oxide ---------- 15
I.4.1.3. Application of reduced Graphene Oxide in photocatalysis ---------- 15
I.4.2. TiO_2/rGO Nanohybrids ---------- 16
I.4.2.1. Structure of TiO_2/rGO ---------- 17
I.4.2.2. Properties of TiO_2/rGO ---------- 17
I.4.2.3. Application of TiO_2/rGO in photocatalysis ---------- 17
I.5.Green Synthesis and Sustainability ---------- 18
I.5.1. Plant Extracts in Nanomaterial Synthesis ---------- 18
I.5.2. Plant Extracts used in the study ---------- 18
I.5.2. Synthesis procedures of TiO_2/rGO hybrid ---------- 19
I.5.2.1. Conventional Synthesis Techniques ---------- 19
I.5.2.2. Green Synthesis Approaches ---------- 19
I.5.3. Cost-Effective Methods ---------- 20
I.6. Literature Gaps and Research Need ---------- 21
I.7.Conclusions ---------- 21

Chapter II: Materials and methods 22

II.1. Introduction ---------- 23
II.2. Materials and Chemicals ---------- 23
II.3. Preparation of Ficus Leaf Extract ---------- 25
II.4. Synthesis of TiO_2 Nanoparticles via Sol-Gel Method ---------- 26
II.5. Synthesis of GO via modified Hummers method ---------- 27
II.6. Green Synthesis of TiO_2/rGO Nano-Hybrids ---------- 28
II.7. Working Dye Solutions ---------- 29
II.7.1. Calibration Curve ---------- 29
II.7.2. Preparation of Working Dye ---------- 30
II.8. Photocatalytic Activity Tests ---------- 30
II.8.1. Photolysis: Degradation without Catalyst ---------- 30
II.8.2. Photocatalysis ---------- 31
II.8.3. Electrocatalysis ---------- 32
. II.8.4. Electrolysis : Direct Electrochemical Oxidation ---------- 33
II.9. Characterization Techniques ---------- 34
II.9.1. Thin-Layer Chromatography ---------- 34

II.9.2 X-ray Diffraction ---------- 34
II.9.3. Scanning Electron Microscopy and Energy Dispersive X-ray spectroscopy ---------- 35
II.9.4. Fourier Transform Infrared Spectroscopy ---------- 36
II.9.5. UV–Visible Spectrophotometry (UV–Vis) ---------- 36
II.10. Limitation of methodology ---------- 37
Chapter III: Results and Discussion ---------- 38
III.1. Introduction ---------- 38
III.2. Plant extract identification ---------- 38
III.2.1.TLC ---------- 38
III.3. Structural and Morphological Characterization ---------- 39
III.3.1 Fourier Transform Infrared Spectroscopy (FTIR) ---------- 39
III.3.2. Scanning Electron Microscopy and Energy Dispersive X-ray Spectroscopy ---------- 40
III.3.3. X-ray Diffraction (XRD) ---------- 41
III.3.3.1. XRD of Titanium Dioxide TiO_2 ---------- 41
III.3.3.2. XRD of Graphene Oxide GO ---------- 42
III.3.3.3. XRD of TiO_2/rGO ---------- 43
III.4. Optical Properties and Spectral Calibration ---------- 45
III.4.1. UV spectrum of Dyes ---------- 45
III.4.1.1. UV spectrum of Congo Red ---------- 45
III.4.1.2. UV spectrum of Crystal Violet ---------- 46
III.4.2. Calibration Curves ---------- 47
III.4.2.1. Calibration Curve of Congo Red ---------- 47
III.4.2.2. Calibration Curve of Crystal Violet ---------- 48
III.4.3. Kubelka–Munk function for Bandgap Estimation ---------- 48
III.5. Photolysis Activity ---------- 49
III.5.1. Photolysis (Homogenous) ---------- 49
III.6. Photocatalytic Degradation Analysis ---------- 50
III.6.1. Photocatalytic of Congo Red ---------- 50
III.6.2. Photocatalytic of Crystal Violet ---------- 53
III.7. Electrochemical Characterization and Activity ---------- 55
III.7.1. Cyclic Voltammetry of CR and CV ---------- 55

III.7.2. Electrocatalytic Degradation Performance ---------- 57
III.7.2.1. Electrocatalytic Degradation Performance of Congo Red ---------- 57
III.7.2.2. Electrocatalytic Degradation Performance of Crystal Violet ---------- 58
III.8. Electrolysis degradation Analysis ---------- 59
III.8.1. Electrolysis of Congo Red ---------- 59
III.8.2. Electrolysis of Crystal Violet ---------- 60
III.9. Comparative Analysis of Degradation Systems ---------- 61
III.10. Conclusions ---------- 62
General Conclusions 64
General Introduction References 66
Chapter I References 67
Chapter II References ---------- 78
Appendix 80
Résumé 84
ملخص **84**
Abstract 84

List of Figures

Figure I- 1.General structure of an organic dye ---------- 4

Figure I- 2.Molecular structure of Crystal Violet ---------- 5

Figure I- 3..Molecular structure of Congo Red ---------- 5

Figure I- 4. Summary of Dye Removal Method from Wastewater. ---------- 6

Figure I- 5. Schematic diagram of the photoexcitation of TiO_2 under UV light irradiation from. ---------- 11

Figure I- 6.Unit cells of rutile, anatase, and brookite showing TiO_6 octahedral geometry. Reproduced from from the American Chemical Society. ---------- 12

Figure I- 7. Structures of graphene (G), graphene oxide (GO), and reduced graphene oxide (rGO). According to the adaptive natural density partitioning analysis and the electron sharing indices. -- 14

Figure I- 8. The photocatalytic mechanisms of rGO@TiO2 nanocomposite for MB dye degradation.16

Figure I- 9. Mature leaves of Ficus retusa photos. ---------- 19

Figure II- 1. Schematic representation of the preparation steps of Ficus retusa leaf extract 26

Figure II- 2. Schematic representation of Sol-gel synthesis process of TiO_2 nanoparticles. 27

Figure II- 3. Schematic of graphene oxide synthesis via the modified Hummers' method. 28

Figure II- 4. Schematic of Green synthesis of TiO_2/rGO nanohybrids. 29

Figure II- 5. Schematic representation of the photolysis chambre. 31

Figure II- 6. Schematic representation with real photo of the Photocatalytic degradation. 32

Figure II- 7. Schematic diagram with real photo of the electrocatalytic degradation setup. 33

Figure II- 8. Electrolysis cell for CV/CR dyes degradation. 34

Figure II- 9. Bruker D8 ADVANCE X-ray Diffractometer (XRD) system. 35

Figure II- 10. Shimadzu UV-1800 UV-Visible Spectrophotometer 37

Figure III- 1. TLC analysis under UV light of phenolic standards (Ph) and the plant extract (PE) 38

Figure III- 2. FTIR spectra of TiO_2/GO with varying GO compared to pure TiO_2 synthesized by the sol-gel method. 40

Figure III- 3. SEM image and EDX spectrum of TiO_2 nanoparticles. 41

Figure III- 4. X-ray diffractogram of pure anatase TiO_2 nanoparticles. 42

Figure III- 5. X-ray diffractogram of graphene oxide. 43

Figure III- 6. X-ray diffractogram of TiO_2/rGO synthesized with varying rGO contents (0.02%, 0.04%, and 0.06%), compared with TiO and graphene oxide. 45

Figure III- 7. Absorbance spectrum of Congo Red. 46

Figure III- 8. Absorbance spectrum of Crystal Violet. 47

Figure III- 9. Calibration curve of Congo Red. 48

Figure III- 10. Calibration curve of Crystal Violet. 48

Figure III- 11. Plot of the Kubelka-Munk transformTiO_2. 49

Figure III- 12. Photolysis kinetics and efficiencies degradation of CR and CV. 50

Figure III- 13. Kinetics of decolorization of CR byTiO2/rGO (0.02g;0.04g and 0.06g) 51

Figure III- 14. Photocatalytic kinetics of degradation of CR 20 ppm. 52

Figure III- 15. Pseudo-first order kinetics of photocatalytic removal of CR 53

Figure III- 16. Kinetics degradation of CV10 ppm. 54

Figure III- 17. Pseudo-first-order kinetics of photocatalytic removal of CR. 55

Figure III- 18. Cyclic voltammograms of CR degradation in 1 M NaCl at a scan rate of 50 $mV \cdot s^{-1}$, using Ag/AgCl as the reference electrode. 56

Figure III- 19. Cyclic voltammograms of CV degradation in 1 M NaCl at a scan rate of 50 $mV \cdot s^{-1}$, using Ag/AgCl as the reference electrode. 57

Figure III- 20. Absorbance spectra illustrating the degradation of CR during Electrocatalysis. 58

Figure III- 21. Absorbance spectra illustrating the degradation of CV during Electrocatalysis. 59

Figure III- 22. Absorbance spectra illustrating the degradation of CR during Electrolysis. 60

Figure III- 23. Absorbance spectra illustrating the degradation of CV during Electrolysis. 61

Figure III- 24. Bar chart presents the degradation efficiency (%) of CR. 62

Figure III- 25. Bar chart presents the degradation efficiency (%) of CV. 62

List of Tables

Table I- 1.Classification of Dyes Based on Chemical Structure and Application ---------- 3

Table I- 2.Summary of the properties, industrial uses, and environmental risks associated with CV / CR. 5

Table I- 3. Key Properties of TiO_2 and Their Implications for Photocatalytic Applications ---------- 12

Table I- 4.. Summary of TiO_2 modification strategies and their enhancements in photocatalytic performance. Adapted from. ---------- 14

Table I- 5. Key Properties of Reduced Graphene Oxide (rGO) and Their Implications. ---------- 15

Table I- 6. Properties of rGO/TiO2. ---------- 17

Table I- 7. Examples of plant extracts used for nanomaterial synthesis ---------- 18

Table I- 8. Conventional Synthesis Methods for rGO–TiO_2.---------- 19

Table I- 9.Comparative Performance of Plant-Extract-Derived TiO_2 and TiO_2/rGO Photocatalysts ------ 20

Table I- 10.Comparative Analysis of Green vs. Conventional Synthesis of TiO_2/rGO Nanocomposites --- 20

Table II- 1. List of materials, chemicals, and equipment used during the experimental procedures 23

Table II- 2.Parameters in Bragg's Law and Scherrer Equation. 35

Table II- 3. Analytical Methods, Governing Equations, and Their Specific Roles in the Photocatalytic Study 36

Table III- 1. Key Diffraction Peaks for Anatase. 41

List of Abbreviations

AOPs	Advanced Oxidation Processes
CB	Conduction Band
CR	Congo Red
CV	Crystal Violet
EDX	Energy Dispersive X-ray Spectroscopy
Epa	Anodic Peak Potential
Epc	Cathodic Peak Potential
FTIR	Fourier Transform Infrared Spectroscopy
GO	Graphene Oxide
HCl	Hydrochloric Acid
H_2O_2	Hydrogen Peroxide
H_2SO_4	Sulfuric Acid
IPCE	Incident Photon-to-Current Conversion Efficiency
ICCD	International Centre for Diffraction Data
$KMnO_4$	Potassium Permanganate
KOH	Potassium Hydroxide
LSV	Linear Sweep Voltammetry
MB	Methylene Blue
MBR	Membrane Bioreactor
mA	milliAmpere

NHE	Normal Hydrogen Electrode
NaCl	Sodium Chloride
PL	Photoluminescence
ROS	Reactive Oxygen Species
RhB	Rhodamine B
SEM	Scanning Electron Microscopy
TEM	Transmission Electron Microscopy
TLC	Thin Layer Chromatography
TTIP	Titanium (IV) Isopropoxide
TiO_2	Titanium Dioxide
UV	Ultraviolet
UV-Vis	Ultraviolet Visible
VB	Valence Band
XRD	X-ray Diffraction
ZVI	Zero-Valent Iron
eV	Electron Volt (energy unit)
e^-	Electron (negative charge carrier)
h^+	Hole (positive charge carrier)
rGO	Reduced Graphene Oxide
°C	Degrees Celsius
ζ	Photocatalytic Efficiency
λ_{max}	Wavelength of Maximum Absorbance

General Introduction

There are profound fears regarding human and environmental health resulting from the amplified discharge of artificial dyes into water bodies, resulting from the geometric growth of industrial activity, especially in textile, paper, leather, cosmetics, and pharmaceuticals [1]. These dyes are specifically designed to withstand photochemical degradation, hydrolysis, and microbiological activity[2]. They have elaborated aromatic molecules and stability[3]. As a result, they remain in natural water bodies, interfering with aquatic photosynthesis, limiting light penetration, and potentially being carcinogenic and mutagenic through the creation of harmful intermediates[1]. Dyes like Congo Red (CR) and Crystal Violet (CV) are relatively resistant to these pollutants and have been used as model representatives within wastewater treatment studies.[4]

The efficiency, operating cost, and environmental friendliness of conventional degradation treatments such as adsorption, membrane filtration, coagulation-flocculation, and biological treatment have been discovered to be limited[5]. In addition, biodegradation of the dye normally creates more harmful byproducts, forcing researchers to invent new and more efficient treatment technologies[6]. The use of semiconductor material when illuminated to create reactive oxygen species (ROS) that can destroy complex organic molecules into harmless products has put photocatalytic oxidation processes (AOPs) in the spotlight as a feasible choice here.[7]

Owing to its good oxidative ability, photochemical durability, low cost, and non-toxicity, titanium dioxide (TiO_2) has been predominantly utilized as a standard photocatalyst. Its large bandgap (~3.2 eV) limits its photocatalytic behavior to the UV region, which forms a negligible portion of the solar spectrum. Moreover, the easy recombination of the photogenerated electron-hole pairs in TiO_2 intensely lowers its quantum efficiency[8]. Hybridization with carbonaceous material, i.e., reduced graphene oxide (rGO), has been suggested as a remedy to these shortcomings. Increased surface area, improved electrical conductivity, and charge separation and interfacial interaction-functionalizing groups are all provided by rGO, which promotes visible light and ultraviolet light photocatalytic activity[9].

At the same time, environmentally friendly nanomaterial synthesis processes have seen increased interest owing to the green chemistry revolution. Biological materials such as plant

extracts containing polyphenols, flavonoids, and antioxidants are used in green synthesis as green reducing and stabilizing agents. The process minimizes energy consumption, stops the use of harmful chemicals, and is useful in attaining sustainable development objectives. TiO_2/rGO nanohybrids can be successfully and sustainably synthesized using ***Ficus retusa***, which contains phytochemicals. This promotes both material functionality and environmental security[10,11].

In this thesis:

- Chapter I, is a comprehensive literature review of synthetic dye chemical composition, environmental toxicity, and classification and conventional and novel degradation techniques. Emphasis is placed on the photocatalytic aspect of titanium dioxide (TiO_2) and its limitation to introduce a more sophisticated investigation of hybrid nanomaterials such as TiO_2/reduced graphene oxide (rGO) composites. The use of rGO is explored for photocatalytic efficiency enhancement under visible light, and the green synthesis route with plant extracts is being considered as a green, cost-effective, and eco-friendly route.
- Chapter II describes the experimental process for the synthesis of TiO_2/rGO nanohybrids using an eco-friendly route with ***Ficus retusa*** leaf extract. It describes the synthesis procedure, material preparation, and equipment for structural and photocatalytic characterization.
- Chapter III is the characterization and performance output of the green-synthesized nanohybrids. Structural, optical, and electrochemical characterizations via FTIR, SEM, XRD, and UV-Vis spectroscopy are outlined with the Congo Red and Crystal Violet dyes degradation kinetics measurement under UV light irradiation exposure. The outcome highlights the synergistic action of rGO and TiO_2 on the improvement of photocatalytic degradation and validate the effectiveness of green-synthesized nanocomposites as future industrial wastewater treatment agents.

Chapter I: Synthetic Dyes in Wastewater: Challenges and Degradation Technologies

I.1. Introduction

As industrial development is increasing all over the world, dye-containing wastewater has increased many times with vast applications of synthetic dyes in textile, cosmetic, leather, paper, plastic, and pharmaceutical industries. All these dyes have extensive applications due to their stability, shade range, and solubility, but are grave environmental threats due to their complex aromatic ring system, low biodegradability, and potential toxicity[1,2,3]

Methylene blue (MB), rhodamine B (RhB), methyl orange (MO), Congo red (CR), crystal violet, methyl red, and Disperse Violet 26, [1] They are some of the most commonly adopted dyes. These dyes find their entry into aquatic ecosystems as industrial effluent wastewater, which alters aquatic ecosystems through an impact upon photosynthesis, oxygen balance, and induces carcinogenicity and mutagenic hazards for aquatic organisms[4,5].

I.2.Dyes

The term dye is applied to a substance that imparts color to a substrate due to light absorption selectivity. Conjugated structures in the molecule enable them to absorb radiation from ultraviolet (UV) and visible (typically 380–750 nm) regions of the electromagnetic spectrum [5], They are a significant category of industrial impurities as they are human-made and non-biodegradable in nature. [6,7]

I.2.1. Classification of dyes

Table I- 1.Classification of Dyes Based on Chemical Structure and Application

Category	Sub-type	Description	Example	Ref
Chemical Structure	**Azo Dyes**	Contain one or more azo (–N=N–) linkages; typically bright colors	Methyl Orange	[8,9]
	Anthraquinone Dyes	Based on anthraquinone; excellent lightfastness and deep shades	Disperse Blue 1	[10]
	Triphenylmethane	Central carbon linked to three aromatic rings; intense coloration	Crystal Violet	[11,12]
	Squaraine Dyes	Contain a squaric acid core; strong NIR absorption	Bis(3,4-dihydroxyphenyl)squaraine	[13]
Applications	**Reactive Dyes**	Form covalent bonds with fibers; good wash fastness	Procion Red	[14]
	Disperse Dyes	Water-insoluble; suitable for hydrophobic fibers	Disperse Violet 26	[15]

	Acid Dyes	Anionic; used on protein fibers like wool and silk	Acid Orange 7	[16]
	Basic (Cationic) Dyes	Cationic; used on acrylic fibers and paper	Methylene Blue	[17]

I.2.2. Structure of dyes

The structural framework of synthetic dyes is the principal determinant of their optical properties, chemical reactivity, and environmental persistence. Most dye molecules comprise two essential components: chromophores, responsible for color through the absorption of visible light, and auxochromes, which modify color intensity and enhance dye–substrate interactions.

Chromophores: Chromophores are conjugated systems with unsaturated functional groups such as azo (–N=N–), carbonyl (C=O), nitro (–NO_2), or quinoid structures. These allow delocalized π electron systems to be able to absorb electromagnetic radiation within the ultraviolet-visible (UV-Vis) range (380–750 nm) and produce visible color. [18]

Auxochromes: Auxochromes, such as hydroxyl (–OH), amino (–NH_2), sulfonic acid (–SO_3H), or carboxyl (–COOH) groups, are not themselves chromogenic. However, they modulate the electronic characteristics of the chromophore, shifting the absorption maxima and improving water solubility and dye–fiber binding.[19]

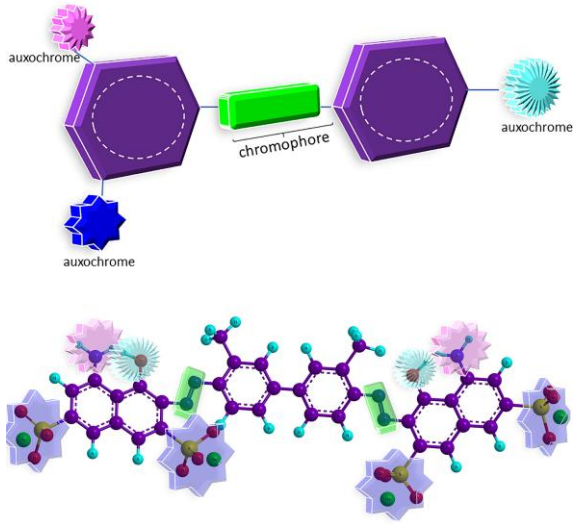

Figure I- 1.General structure of an organic dye. [19]

I.2.3 Model Dyes Selected for Study

Table I- 2.Summary of the properties, industrial uses, and environmental risks associated with CV / CR.

Property	Crystal Violet	Congo Red
Chemical Class	Triphenylmethane dye	Azo dye
Molecular Structure	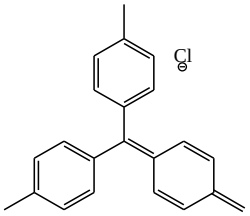 **Figure I- 2.Molecular structure of Crystal Violet**	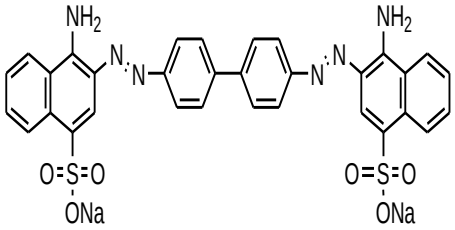 **Figure I- 3.Molecular structure of Congo Red**
Ionic Nature	Cationic	Anionic
Molecular Formula	$C_{25}H_{30}ClN_3$	$C_{32}H_{22}N_6Na_2O_6S_2$
Molar Mass	~407.98 g/mol	~696.66 g/mol
λmax (nm)	590–600	~497
Industrial Applications	Inks, textiles, microbiology staining	Textile dyeing, paper, histological staining
Environmental Concerns	Mutagenic, cytotoxic, resistant to biodegradation	Degrades into carcinogenic aromatic amines
Solubility	Soluble in water and ethanol	Water-soluble
Ref	[20,21]	[22]

I.2.4. Toxicity and Environmental Impact of Dyes

Synthetic dyes are environmentally persistent and pose a major ecological and health problem. They are resistant to conventional biological treatment methods, whereby they remain in aqueous systems. The major implications are

- Impaired Light Penetration: Dyeing water inhibits sun penetration, impacting algal and aquatic plant photosynthesis [23]
- Oxygen depletion: The degradation of dyes consumes dissolved oxygen, causing death to fish and other aquatic life.[24,25]
- Toxicity and Mutagenicity: Some dyes and degradation products are carcinogens, mutagens, or teratogens [26,27]

Azo dyes can be split to produce aromatic amines, which are themselves toxic and potentially carcinogenic [28]

I.2.5. Challenges in Dye Degradation

The major problems for dye removal from wastewater are:

- **Chemical stability:** The hydrolytic stability of the dye molecules remains unaltered.
- **Low biodegradability**: Conventional wastewater treatment plants are not effective in dye removal
- **High Colour Intensity**: Highly coloured water with a small concentration.
- **Generation of Toxic By-products**: Incomplete degradation can lead to more toxic intermediate by-products. [29,27,30,31]

These challenges necessitate the development of advanced treatment technologies beyond conventional physical and biological processes.

I.2.6. Removal techniques of dyes

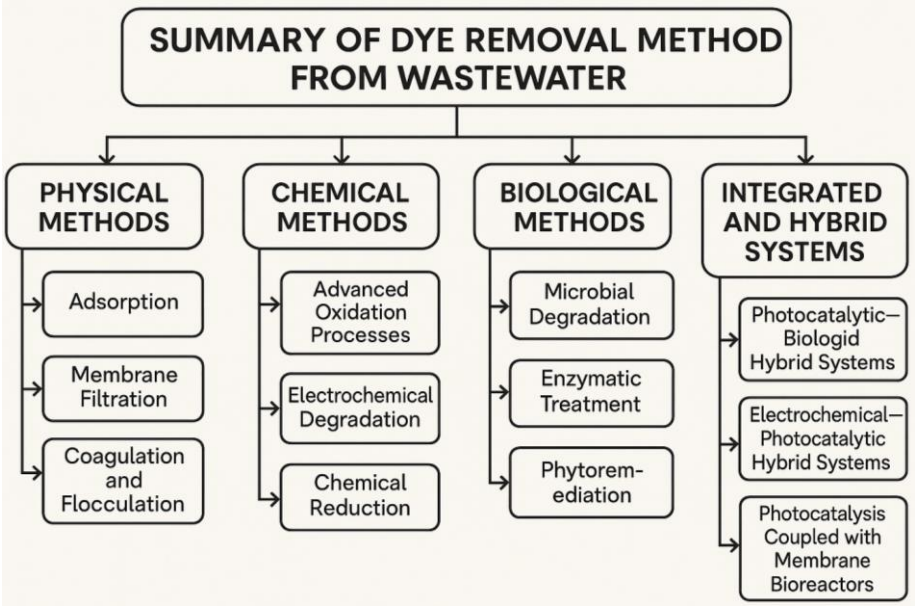

Figure I- 4. Summary of Dye Removal Method from Wastewater.

I.2.6.1. Physical Methods

I.2.6.1.1. Adsorption

Simple, cost-effective, and efficient, adsorption is one of the most often used techniques for color removal. Biochar has been discovered as an excellent adsorbent due to its high surface area and porosity, making it suited for extracting azo dyes from aqueous solutions. [32,33,34].

I.2.6.1.2. Membrane Filtration

Ultrafiltration and nanofiltration are among the advanced membrane technologies whose efficiency in dye removal from wastewater has been much investigated. Though they are sometimes connected with difficulties like membrane fouling and excessive energy consumption, these technologies show great possibilities. [35]

I.2.6.1.3. Coagulation and Flocculation

Chemical coagulation employing substances like potassium ferrate has been studied for its capacity to remove azo colors via concurrent oxidation and coagulation. This method has proven good success treating wastewater including Orange II's color. [36,37]

I.2.6.2. Chemical Methods

I.2.6.2.1. Advanced Oxidation Processes (AOPs)

AOPs produce strongly reactive hydroxyl radicals (**$OH^{\bullet}$**) which can degrade most organic contaminants, such as azo dyes. The radicals are typically formed under the use of UV light, ozone, hydrogen peroxide, or through the use of photocatalysts in combination.

Graphene oxide (GO) is proving to be an effective material for advanced oxidation processes (AOPs) as it possesses high surface area and numerous functional groups. This enables GO to absorb dyes and form radicals.[38] degradation of methyl orange within 20 minutes using a UV/H_2O_2/GO system under optimized pH and light intensity conditions.

I.2.6.2.2. Electrochemical Degradation

Ectrical current is employed during electrochemical treatment to initiate redox reactions that degrade dyes directly at the electrode surface or through oxidants derived from electricity. Combining photocatalysis with electrochemical oxidation can significantly enhance how degradation occurs.

Tungsten trioxide (WO_3) heterojunction photocatalysts are effective under visible light, particularly for use in electrochemical systems [39]. A hybrid WO_3-based photocatalytic-

electrochemical system achieved >95% decolorization of Congo red under visible light in less than 30 minutes.

I.2.6.2.3. Chemical Reduction

Chemical reducing agents such as sodium dithionite and zero-valent iron (ZVI) can cleave the azo bond, thereby causing effective azo dye decolorization. The advantage of reduction is that it specifically targets the azo linkage with virtually no formation of toxic aromatic amines if it is properly regulated.

Amorphous alloys have been the focus of attention more lately owing to their high surface activity and ability to produce electrons for azo dye reduction in multi-component industrial wastewater [40]. Iron-based amorphous alloys were shown to remove >90% of Acid Orange 7 within 15 minutes, with low sludge production and high reusability.

I.2.6.3. Biological Methods

I.2.6.3.1. Microbial Degradation

Microorganisms such as bacteria, fungi, and algae are capable of degrading azo dyes through biochemical reactions to form non-toxic byproducts. A recent detailed review of existing literature has indicated that there is great potential in using various microbial species for application in environmental remediation with respect to toxicity and considering limitations for such biodegradation. [41] Bacterial strains such as Pseudomonas putida, Bacillus subtilis, and Enterococcus faecalis have been reported to decolorize dyes like Congo Red and Reactive Black 5 with efficiencies exceeding 85% under optimized lab-scale conditions.

I.2.6.3.2. Enzymatic Treatment

The breakdown of azo dyes is catalyzed by oxidoreductase enzymes, such as peroxidase, azoreductase, and laccase, to form more basic compounds. A recent study using an inter-disciplinary approach to azo dye biodegradation focused on enzymatic mechanisms and gave prominence to them in the field of environmentally sustainable technologies. [42] A multidisciplinary study reported that laccase immobilized on silica gel could degrade over 90% of Reactive Orange 16 in 6 hours at pH 5.5, with minimal enzyme loss over multiple cycles.

I.2.6.3.3. Phytoremediation

Some plant species like Eichhornia crassipes and Lemna minor, respectively identified as water hyacinth and duckweed, are found to exhibit enormous potential for adsorption and

biodegradation of azo dyes in contaminated water bodies. Studies on using compost as a plant-based environmentally friendly adsorbent for azo dye removal are producing optimistic results and are improving phytoremediation methods. [43] Water hyacinth cultivated in dye-contaminated water removed up to 80% of Methylene Blue and Acid Red within 10 days, demonstrating significant adsorption and degradation capacity

I.2.6.4. Integrated and Hybrid Systems

I.2.6.4.1. Photocatalytic–Biological Hybrid Systems:

Photocatalytic oxidation alone can produce intermediates, which are partly degraded and still toxic and non-biodegradable. This can be followed by combining the same with biotreatment, and the intermediates can be mineralized to innocuous products. A hybrid system combining TiO_2/g-C_3N_4 photocatalysis with microbial degradation achieved a 25% increase in total organic carbon (TOC) removal compared to photocatalysis alone. This approach is particularly effective for treating textile wastewater, which is typically rich in recalcitrant azo dyes [44].

I.2.6.4.2. Electrochemical-Photocatalytic Hybrid Systems

The photcatalysis and electrochemical oxidation combination speeds up the generation of reactive oxygen species (e.g., **$OH^{\bullet}$** radicals) and causes more rapid and complete degradation of the dye. New studies have been focusing on using MXene photocatalyst coupled with electrochemical cells for improving the efficiency of the process. MXene-integrated electrochemical-photocatalytic systems achieved over 90% azo dye degradation in under 30 minutes of visible light exposure, while also reducing energy consumption compared to standalone electrochemical systems [45,46].

I.2.6.4.3. Photocatalysis Coupled with Membrane Bioreactors (MBRs)

MBRs excel at dye removal since they can filter out detrimental chemicals and further degrade them. They are, however, plagued by issues such as membrane fouling and are unable to degrade complex dye structures.

For it to function effectively, substances such as ZnO or TiO_2 nanoparticles can be incorporated into the membrane or applied in the MBR system. Incorporation of these substances eliminates color and aids in the degradation of harmful substances [47]. A submerged MBR system using ZnO-modified membranes demonstrated over 90% removal

efficiency for azo dyes under visible light, though challenges like membrane fouling and catalyst leaching remain.

I.3.Photocatalytic Technologies for Wastewater

I.3.1. Principles of Photocatalysis

Photocatalysis is a light-induced catalytic process that utilizes a semiconductor material to accelerate chemical reactions without undergoing permanent change. In environmental remediation, particularly wastewater treatment, photocatalysis exploits light energy (typically UV or visible light) to generate reactive oxygen species (ROS), such as hydroxyl radicals (**$OH^{\bullet}$**) and superoxide ions ($O_2^{\bullet-}$), which degrade organic pollutants into less harmful substances like CO_2 and H_2O [48,49].

The fundamental mechanism involves photon absorption by a semiconductor, leading to excitation of an electron from the valence band (VB) to the conduction band (CB), generating an electron-hole (e^-/h^+) pair:

$$\textbf{Semiconductor} + h\nu \rightarrow e_{CB}^- + h_{VB}^+ \quad \textbf{(I-1)}$$

These charge carriers participate in redox reactions at the semiconductor surface. The effectiveness of the process is determined by factors such as bandgap energy, surface area, crystallinity, and light intensity.[50]

Photocatalytic reactions may be categorized into two on the basis of the physical state of reactants.

- **Homogeneous photocatalysis:** is when reactant and semiconductor are in the same phase solid, liquid, or gas during photocatalytic reactions.
- **Heterogeneous photocatalysis:** occurs when the reactant and semiconductor exist in distinct phases, which classifies such photocatalytic reactions as heterogeneous photocatalysis.[51,52]

I.3.2. Titanium Dioxide TiO_2

Photocatalysis, driven by light-activated semiconductors offers a clean approach to energy conversion and environmental purification. Among numerous photocatalysts, titanium dioxide (TiO_2) has been among the most widely researched materials due to its high oxidative power, chemical durability, non-toxicity, and low price [53]. Its large bandgap (~3.2 eV for

anatase) restricts its photocatalytic activity to the UV range, which constitutes only about 5% of the solar spectrum, and therefore significantly lowers its utilization of solar energy. Under UV light (λ = 387 nm), TiO_2 absorbs photons, promoting electrons to the conduction band and leaving holes in the valence band:[54]

$$TiO_2 + h\nu \rightarrow e^-_{CB} + h^+_{VB} \quad \text{(I-2)}$$

$$e^-_{(CB)} \rightarrow e^-_{(degradation)} \quad \text{(I-3)}$$

$$h^+_{(VB)} \rightarrow h^+_{(degradation)} \quad \text{(I-4)}$$

$$e^-_{(degradation)} + h^+_{(degradation)} \rightarrow heat \quad \text{(I-5)}$$

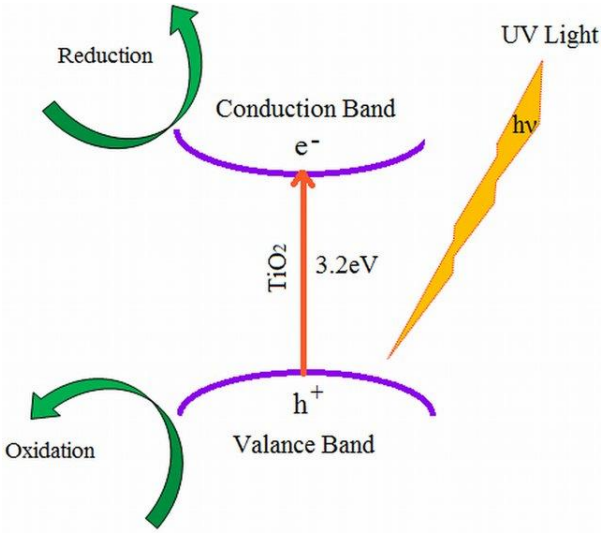

Figure I- 5. Schematic diagram of the photoexcitation of TiO_2 under UV light irradiation from.[55]

Recent studies have sought to enhance the visible-light activity of TiO_2 by optimizing its structure. For example, the integration of carbon dots (C-dots) into titanate nanotubes has shifted light absorption from the UV into the visible light region, improving organic contaminant degradation efficiency by several orders of magnitude [64]. Similarly, bismuth (Bi) doping has been reported to enhance electron mobility as well as visible-light absorbance, enhancing the ability of TiO_2 to perform more efficiently in applications like water splitting as well as environmental decontamination [56,53].

I.3.2.1. Structure of Titanium Dioxide TiO_2

TiO_2 exists in three main crystalline forms: anatase, rutile, and brookite, each with varying physicochemical and photocatalytic properties [57].

- **Anatase:** Most photocatalytically active owing to high surface area, low rate of recombination, and effective charge transfer [58].
- **Rutile:** Thermodynamically stable but less photocatalytically active owing to faster electron–hole recombination [59].
- **Brookite:** Uncommon and hard to synthesize, with single crystal geometry and limited photocatalytic application [60].

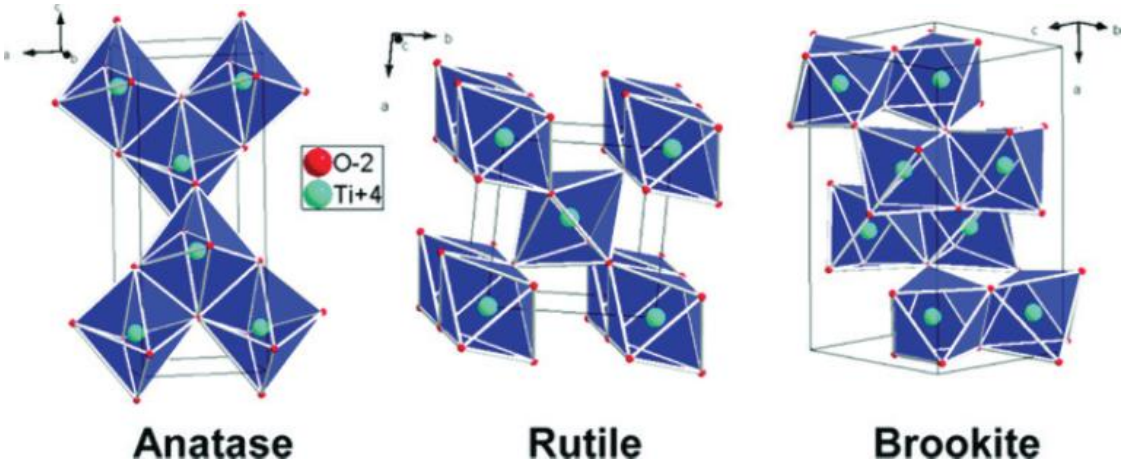

Figure I- 6.Unit cells of rutile, anatase, and brookite showing TiO_6 octahedral geometry. Reproduced from the American Chemical Society. [61]

I.3.2.2. Properties of Titanium Dioxide TiO_2

Table I- 3. Key Properties of TiO_2 and Their Implications for Photocatalytic Applications

Property	Description	Implication in Applications	Ref
Bandgap Energy	~3.2 eV for anatase, ~3.0 eV for rutile	Limits activity to UV light; visible-light response requires doping	[57,62]
Crystal Phases	Anatase, rutile, brookite	Anatase preferred for photocatalysis due to superior charge dynamics	[57,60]
Charge Carrier Dynamics	Slower recombination in anatase vs rutile	Enhances efficiency of photocatalytic reactions	[58,59]

Chemical Stability	High resistance to corrosion, acids, and oxidation	Ideal for harsh environmental conditions	[62]
Non-toxicity	Biocompatible and safe for environmental and medical uses	Suitable for self-cleaning, antimicrobial coatings, and drug delivery	[63,64]
Surface Area	High specific surface area (especially in nanostructures)	Increases active sites for photocatalytic reactions	[58,63]
Photocatalytic Activity	Ability to generate ROS (e.g., •OH, $•O_2^-$) under UV irradiation	Enables degradation of dyes, microbes, and pollutants	[65,63]
Modifiability	Can be doped with metals/non-metals or composited with materials like rGO	Improves visible-light response and catalytic performance	[63,66]

I.3.2.3. Application of Titanium Dioxide TiO_2 in photocatalysis

TiO_2 plays a pivotal role in a variety of photocatalytic processes, including:

- ✓ **Wastewater treatment:** Degradation of azo dyes, pesticides, and pharmaceuticals
- ✓ **Hydrogen production:** Water splitting via photoelectrochemical cells
- ✓ **CO_2 reduction:** Conversion of CO_2 into solar fuels
- ✓ **Self-cleaning coatings:** On glass, textiles, and medical implants
- ✓ **Antimicrobial surfaces:** Used in healthcare settings for infection control [57,64,67].

I.3.2.4. Limitations of Titanium Dioxide TiO_2 and Strategies for Improvement

Despite its advantages, TiO_2 suffers from several limitations:

- limited visible light response due to its wide bandgap,
- fast recombination of photogenerated electron-hole pairs,
- relatively low surface adsorption for organic molecules.[68]

Several strategies have been developed to overcome these challenges:

- **Doping with metals or non-metals** to narrow the bandgap.[69]
- **Coupling with other semiconductors** (e.g., ZnO, CdS) to form heterojunctions.[70,71]
- **Surface modification** with carbon-based materials such as graphene and reduced graphene oxide (rGO).[72,73].

- **Morphological tuning** (e.g., nanotubes, nanorods) to enhance surface area.[74,75]

Table I- 4.. Summary of TiO_2 modification strategies and their enhancements in photocatalytic performance. Adapted from.

Strategy	Effect	Reference
Metal doping (e.g., Fe, Cu)	Bandgap narrowing, visible light response	[76]
TiO_2/ZnO heterojunction	Improved charge separation	[77]
TiO_2/rGO composite	Enhanced electron mobility	[78]

I.4.Role of Reduced graphene oxide Modifiers

I.4.1. Reduced Graphene Oxide

Reduced graphene oxide (rGO) is also a promising functional material that has been widely studied for energy conversion, environmental detoxification, and photocatalysis. Even without the ideal structure of pristine graphene lower solubility and non-uniform bandgap, rGO possesses most of the favorable properties of graphene, like high electrical conductivity, thermal stability, and tunable surface chemistry [79,80].

Graphene oxide (GO), a precursor to rGO, is chemically oxidized graphite and possesses a high oxygen-containing functional group density such as hydroxyl, carboxyl, and epoxide moieties. These make GO very dispersible in polar solvents but greatly reduce its conductivity [88]. rGO is obtained by the partial removal of these oxygenated groups to restore the π-conjugated network and to improve electronic performance. Heterostructures between TiO_2 and rGO make use of the conductivity of rGO and reactivity of the GO surface, leading to efficient and processable photocatalysts [81,82].

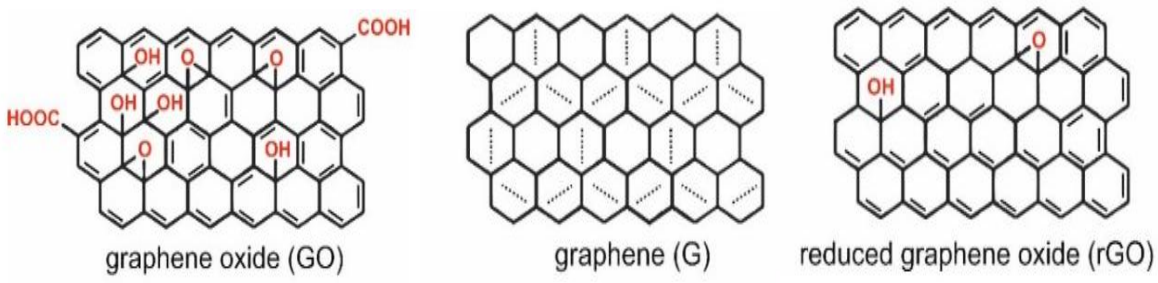

Figure I- 7. Structures of graphene (G), graphene oxide (GO), and reduced graphene oxide (rGO). According to the adaptive natural density partitioning analysis and the electron sharing indices.[83]

I.4.1.1. Structure of reduced Graphene Oxide

Structurally, rGO is a partly reduced graphene oxide, with the elimination of oxygen-containing groups and the rebuilding of the π-conjugated carbon network to a certain degree [92]. While pristine graphene exhibits a defect-free sp^2-hybridized honeycomb lattice, rGO continues to contain defects, vacancies, and sp^3-hybridized domains. These structural imperfections are significant, for they:

- Change interlayer spacing (rGO: 0.335–0.446 nm; GO: ~0.721 nm)
- Affect electronic properties
- Enable functionalization for composite preparation [84]

The degree of reduction controls the electronic conductivity, number of layers, and surface reactivity of rGO.

I.4.1.2. Properties of reduced Graphene Oxide

Table I- 5. Key Properties of Reduced Graphene Oxide (rGO) and Their Implications.

Property	Description	Implication	Ref
Electrical Conductivity	Higher than GO due to restored sp^2 structure, but lower than pristine graphene	Enables charge transport in photocatalytic composites	[85]
Mechanical Strength	High tensile strength and modulus, reduced slightly by defects	Useful in flexible membranes and nanocomposite films	[79]
Thermal Stability	Stable under high temperatures; good thermal conductivity	Suitable for heat dissipation and sensor applications	[79]
Surface Area & Porosity	High surface area, particularly in exfoliated form	Facilitates adsorption and catalytic reactions	[80]
Functionalizability	Rich in residual –OH, –COOH, and epoxy groups	Enhances binding with metal oxides or dopants	[86]

I.4.1.3. Application of reduced Graphene Oxide in photocatalysis

rGO contributes significantly to photocatalytic systems via overcoming traditional semiconductors' limitations.

- **Charge Separation and Transport**

Due to its higher conductivity, rGO works as an electron acceptor and shuttle, which suppresses recombination of photo-generated electron-hole pairs and promotes quantum efficiency. Studies show that rGO-semiconductor hybrids excel over bare semiconductors in dye and organic pollutant degradation uniformly.[87]

- **Aerobic Oxidation and Degradation**

The conjugated π-system of the rGO absorbs visible light and extends the spectral range of the composite photocatalyst. It enables sunlight-powered photocatalysis, central to sustainable use .[88]

- **Adsorption and Surface Interaction**

The rGO's high surface area and groups enhance dye molecule adsorption, enabling effective mass transfer of photocatalysts. Enhanced adsorption enhances exposure of pollutants with active sites, hence enhancing the efficiency of degradation. [87]

- **Green Synthesis for Photocatalytic Application**

Plant-synthesized rGO possesses greater surface functional groups, which facilitate not only dispersion and composite development but also dye adsorption and reactivity. For instance, plant extract-synthesized rGO has demonstrated impressive removal of methylene blue under visible light, indicative of significant potential in green water treatment.[89]

I.4.2. TiO_2/rGO Nanohybrids

The rGO/TiO_2 hybrid has emerged as a new way to address the inherent disadvantage of pure TiO_2, i.e., low quantum yield, poor visible light absorption, and rapid electron–hole recombination. The formed rGO/TiO_2 nanocomposites inherit the high surface area and conductivity of rGO and the strong oxidative ability of TiO_2 to create a synergistic heterojunction of high photocatalytic activity [90,91].

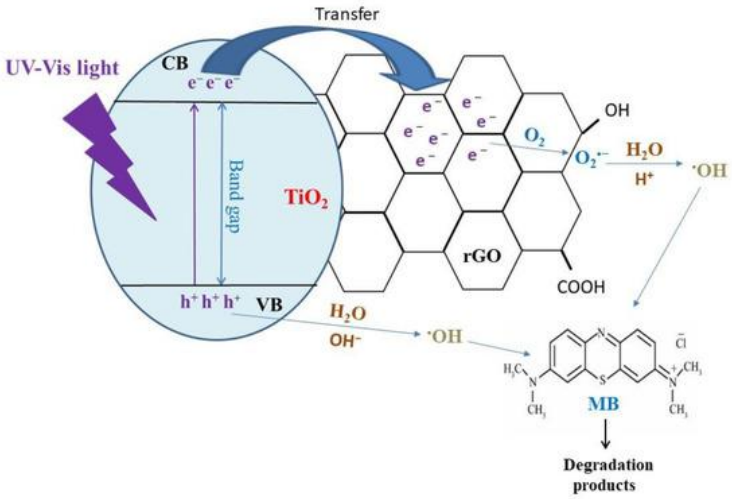

Figure I- 8. The photocatalytic mechanisms of rGO@TiO2 nanocomposite for MB dye degradation.[92]

I.4.2.1. Structure of TiO_2/rGO

Structurally, rGO/TiO_2 hybrids exhibit:

- 6–20 nm TiO_2 nanoparticles homogeneously attached on rGO sheets
- Formation of C–O–Ti bonds and Ti–O–C bridges, allowing fast charge transfer
- High-resolution TEM confirms retained hexagonal rGO lattice in association with (101) anatase TiO_2 planes (d ≈ 0.35 nm) [93,94].

I.4.2.2. Properties of TiO_2/rGO

Table I- 6. Properties of rGO/TiO2.

Property	Description	Impact	Ref
Particle Size	2–2.8 nm crystallites observed under SEM and HR-TEM	Enhances surface reaction kinetics	[95,96]
Specific Surface Area	Up to 330 m^2/g (hydrophilic portion ~50%)	Promotes dye adsorption and redox activity	[95]
Capacitance	rGO/TiO_2: 585 F/g at 1 A/g vs rGO: 174 F/g; TiO_2: 66 F/g	Suitable for photocatalysis and energy storage	[95]
Pseudo capacitance	Up to 1200 C/g with rapid redox behavior	Indicates rapid charge storage and electron cycling	[95]
Hydrophilicity	Improved by residual oxygen groups; tunable via surface engineering	Crucial for aqueous-phase degradation and MBR applications	[94,97]
Stability	>100% retention after 5000 cycles	High recyclability and longevity	[95]

I.4.2.3. Application of TiO_2/rGO in photocatalysis

rGO/TiO_2 nanocomposites have displayed improved performance in various photocatalytic applications:

- **Environmental Remediation**

  - Complete degradation with high efficiency of azo dyes, pharmaceuticals, and pesticides
  - Degradation of imidacloprid up to 25% in 3 hours under visible light (MBR membrane systems) [97]
  - Improved activity due to:
    - Charge separation by Ti–C and C–O–Ti bonds
    - π–π interaction of rGO with the aromatic dye structure

- **Water Splitting and Hydrogen Generation**

  - $CoFe_2O_4$–TiO_2/rGO ternary systems exhibit H_2 production rates of 76,559 µmol g^{-1} h^{-1} under simulated sunlight [95]

- **Photoreduction of CO_2**

  - Enhanced CO_2-to-CO and CO_2-to-CH_4 conversion due to efficient charge separation
  - Stability across several cycles without catalyst degradation [98,99]

‘'The synergy of TiO_2 and rGO not only supports mobility of the charge carriers, but also increases long-term endurance and operational stability in environmental applications as well as energy-related processes.’’

I.5.Green Synthesis and Sustainability

I.5.1. Plant Extracts in Nanomaterial Synthesis

Green synthesis leverages biological materials, such as plant extracts, for the eco-friendly fabrication of nanomaterials. These extracts serve as both reducing and stabilizing agents. Phytochemicals like polyphenols, flavonoids, and alkaloids play a vital role in reducing metal ions to nanoparticles[100,101].

TiO_2 and rGO have been synthesized using green routes involving extracts from neem, tea leaves, aloe Vera, and others. This method minimizes toxic solvents, reduces cost, and enhances biocompatibility.[102]

Table I- 7. Examples of plant extracts used for nanomaterial synthesis

Plant Extract	Nanomaterial Synthesized	Ref
Green tea	TiO_2 nanoparticles	[103]
Neem	ZnO, TiO_2 nanoparticles	[104]
Aloe vera	rGO, Ag nanoparticles	[105]

I.5.2. Plant Extracts used in the study

In the current work, ***Ficus retusa*** leaf extract is used as a green reducing agent and stabilizing agent to prepare TiO_2/rGO nanohybrids. ***F. retusa*** contains a rich amount of bioactive phytochemicals like phenolic acids (gallic acid and caffeic acid), flavonoids (quercetin and rutin), and tannins. These phytochemicals are excellent antioxidants and have been used to reduce the graphene oxide to reduced graphene oxide efficiently under mild

conditions. Use of these phytochemicals not only simplifies the reduction process but also stabilizes the produced nanoparticles to make them dispersive and functional. Use of F. retusa's leaf extract is based on green chemistry and represents a green, eco-friendly alternative to chemical reducing agents.[106],[107],[108].

Figure I- 9. Mature leaves of Ficus retusa photos.[109]

I.5.2. Synthesis procedures of TiO_2/rGO hybrid

The morphology, crystallinity, interfacial interaction, and photocatalytic activity of TiO_2/rGO nanocomposites significantly depend on the synthesis route. These methods can be categorized into conventional and green synthesis routes:

I.5.2.1. Conventional Synthesis Techniques

Table I- 8. Conventional Synthesis Methods for rGO–TiO_2.

Method	Key Features	Limitations	Ref
Hydrothermal/ Solvothermal	Produces well-crystallized TiO_2 on rGO under high temp/pressure; ethanol enhances dispersion	Energy-intensive; organic solvents used	[96,110]
Sol–Gel	Enables uniform TiO_2 growth on GO under low temperature conditions	Requires calcination; uses toxic solvents	[111]

I.5.2.2. Green Synthesis Approaches

Plant extracts, microbial enzymes, or biotemplates are employed in green synthesis to reduce GO and concurrently synthesize TiO_2. Polyphenols, flavonoids, and terpenoids are examples of phytochemicals acting as reducing, stabilizing, and capping agents and enabling

- Low-temperature synthesis
- No application of toxic reagents (e.g., hydrazine, $NaBH_4$)
- Enhanced interfacial bonding

Azadirachta indica (neem) extract was used to reduce GO and synthesize anatase-phase TiO_2 nanoparticles, resulting in 92% degradation of methylene blue under visible light in 45 minutes [112],[113]

Table I- 9.Comparative Performance of Plant-Extract-Derived TiO_2 and TiO_2/rGO Photocatalysts

Photocatalyst	Plant Extract Used	Degradation Efficiency (%)	Irradiation Time (min)	Improvement Over Pure TiO_2 (%)	Ref
Pure TiO_2	*Impatiens rothii*	98	100	—	[114]
TiO_2/rGO	*Citrus sinensis* & *Musa acuminata*	94.28	Not specified	+52.28	[113]

I.5.3. Cost-Effective Methods

Green synthesis is also economically viable. It eliminates the need for high-temperature calcination, hazardous chemicals, and energy-intensive procedures. Furthermore, utilizing agricultural waste or surplus biomass makes the process sustainable and scalable[115].

Some recent works have even integrated solar energy in the synthesis step, further reducing energy consumption and carbon footprint. [116,117]

Table I- 10.Comparative Analysis of Green vs. Conventional Synthesis of TiO_2/rGO Nanocomposites

Aspect	Green Synthesis	Conventional Synthesis	Ref
Efficiency (Yield & Rate)	Moderate to high yield (85–92%) but with slower reaction rates	High yield with faster reaction kinetics	[118]
Cost	Low-cost due to natural extracts and room-temperature processing	Higher cost involving pure chemicals and energy-intensive steps (e.g., calcination)	[119]
Environmental Impact	Minimal: avoids toxic reagents and reduces hazardous byproducts	Generates more chemical waste and has a higher environmental burden	[120]
Material Consistency	Can vary based on plant species, extract composition, and seasons	High reproducibility with consistent particle size and morphology	[121]

Morphology Control	Limited control, often resulting in irregular shapes and broader size distributions	Precise control via surfactants, pH, and temperature tuning	[122]
Reduction Quality	Partial reduction may leave oxygenated groups—useful for functionalization but lowers conductivity	Near-complete reduction results in purer, more conductive rGO	[123]

I.6. Literature Gaps and Research Need

Despite significant advances, several gaps persist in the current literature:

- Insufficient understanding of charge transfer dynamics in TiO_2/rGO systems under natural sunlight.
- Lack of standardization in green synthesis protocols makes results difficult to reproduce.
- The scalability and long-term stability of green-synthesized photocatalysts remain underexplored.
- Mechanistic insight into degradation pathways for complex wastewater pollutants is limited.

I.7.Conclusions

In summary, this chapter examined the problems posed by synthetic dyes in industrial wastewater, Including their structural stability, environmental recalcitrance, and toxicity. Although various physical, chemical, biological, and hybrid removal techniques, are available for dye removal each has limitations in terms of efficiency, operating cost, or secondary pollution. In this context, green synthesis emerges as a promising approach, enabling the development of photocatalytic materials through eco-friendly processes that minimize toxic byproducts and reduce energy consumption. This insight lays the foundation for investigating innovative materials such as TiO_2/reduced graphene oxide (rGO) nano-hybrid material with emphasis on assessing its photocatalyst activity in the degradation of synthetic dyes, in alignment with the general objective of developing an efficient and affordable wastewater treatment system.

Chapter II: Materials and methods

II.1. Introduction

This investigation showcases an eco-friendly production approach for **TiO_2/rGO** nanohybrids utilizing ***Ficus retusa*** leaf extract. Titanium dioxide was synthesized through a sol-gel method, while graphene oxide was produced using a modified Hummers approach. The natural extract functioned as a reducing and stabilizing agent, facilitating an environmentally friendly process. The synthesis was carried out at the pedagogical laboratory of FST-UCBET and the Laboratory of Physical Chemistry of Materials (Univ-Eltarf), which provided hands-on experience. Meanwhile, photocatalytic,electrocatalytic activity tests and FTIR analysis were performed in the Solid-State Energetics and Electrochemistry research laboratory at UFAS. The project proposes to build effective photocatalysts for dye degradation in wastewater treatment utilizing an environmentally friendly method.

II.2. Materials and Chemicals

Table II- 1. List of materials, chemicals, and equipment used during the experimental procedures

CATEGORY	MATERIAL / EQUIPMENT	PURPOSE / ROLE
TITANIUM DIOXIDE SYNTHESIS	Titanium (IV) isopropoxide (**TTIP, 97%**)	Titanium precursor to **TiO_2**
	Isopropanol	Solvent of TTIP, stabilizes sol-gel reaction
	Deionized Water	Used during synthesis and sample preparation
GRAPHENE OXIDE (GO) SYNTHESIS	Graphite Powder	Starter material for **GO**
	Sulfuric Acid (**H_2SO_4, 98%**)	Acid medium in **GO** oxidation
	Phosphoric Acid (H_3PO_4)	Improves oxidation efficiency and safety
	Potassium Permanganate (**$KMnO_4$**)	Oxidizing agent that brings oxygen into graphite
	Hydrogen Peroxide (**H_2O_2**) **30%**	Stops oxidation reaction, lowers residual manganese compounds
	Hydrochloric Acid (**HCl**) 2M	Removes impurities and metal ions
	Ice Bath	Regulates temperature when adding **$KMnO_4$**
GREEN SOL-GEL SYNTHESIS (TIO_2/RGO)	***Ficus retusa*** Leaf Extract	Natural stabiliser and reducing agent for green synthesis

	GO (0.02;0.04;0.06 g)	Incorporated for nanohybrid formation, electronic enhancement
	Sonicator	Spread **GO** evenly into water
	Magnetic Stirrer / Hot Plate	Ensures uniform blending throughout the synthesis processes
	Dropper	For controlled addition of Ficus extract
	Centrifuge	Separates solid **TiO_2/rGO** from aqueous
	Drying Oven (80°C)	Precipitate prior to calcination
	Muffle Furnace (500°C)	Removes the organic content and crystallizes the **TiO_2** phase
POLLUTANTS AND TESTING	Crystal Violet (CV)	Standard dye pollutant (10 ppm from 1000 ppm stock solution)
	Congo Red (CR)	20 ppm of model pollutant from 1000 ppm stock
	UV-A Lamp (365 nm)	Light source used in photocatalytic degradation
	Pyrex Glass Photocatalytic Reactor	Reactor vessel that permits light transmittance
	Air Pump	Provides oxygen to support aeration throughout reaction
	Cooling Jacket / Ice Bath	Sustains reaction temperature
	Sampling Ports	Enables sample withdrawal under conditions of photocatalysis
	0.45 µm Syringe Filter	Filters the post-reaction samples to analyze
ELECTROCHEMICAL ANALYSIS	VoltaLab PGP201 Potentiostat/Galvanostat	Regulates potential/current of electrochemical measurements
	VoltaMaster 4 Software	Interface with PGP201 to collect data and control
	Working Electrode (Glassy Carbon)	Location of the electrochemical reaction
	Reference Electrode (Ag/AgCl)	Retains a steady potential to make accurate measurements
	Counter Electrode (Platinum Wire)	It completes the circuit by enabling current flow
	Electrochemical Cell	Includes the electrolyte and electrodes

	NaCl Solution (1M)	Supporting electrolyte; maintains ionic strength without interfering with reaction
	Connecting Cables and Electrodes Kit	Attaches electrodes to potentiostat
GENERAL LABORATORY EQUIPMENT	Analytical Balance	Accurately measures chemicals
	Beakers, Glassware	Reaction vessels and transfer tools
	Vacuum Filtration Unit	Used in purification and accumulation of precipitates
CHARACTERIZATION TECHNIQUES	FTIR Spectrometer	These identify chemical bonds and functionalities in TiO_2 and /rGO
	XRD (X-Ray Diffraction)	Determines the crystalline phases and crystallite dimensions of TiO_2
	UV-Vis Spectrophotometer	Investigate optical properties and efficiency of photocatalytic degradation
FUNCTIONAL TESTS	TLC	Used to identify phenolic compounds in ***Ficus extract***

II.3. Preparation of Ficus Leaf Extract

1. **Collecting and Purifying:** The ***Ficus retusa*** plant's adult leaves were harvested from el-Tarf city and rinsed using distilled water gently to remove any surface impurities.
2. **Drying:** The leaves were dried at room temperature over a few days until they were completely moisture-free.
3. **Grinding:** The dried leaves were then ground into a fine powder with a grinder.
4. **Extraction:** A total of **10 g** of the powdered leaves was added to **100 mL** of deionized water.
5. **Heating:** The solution was subsequently heated at **45°C** for 1 hour to facilitate the release of bioactive components like antioxidants and phenolic acids.
6. **Filtration:** When the solution was heated, it was filtered using a sous vide vacuum filtration device to remove any solid residues.
7. **Storage:** The filtrate was preserved at 4°C for further application in the green synthesis of **TiO_2/rGO** nanohybrids. [1]

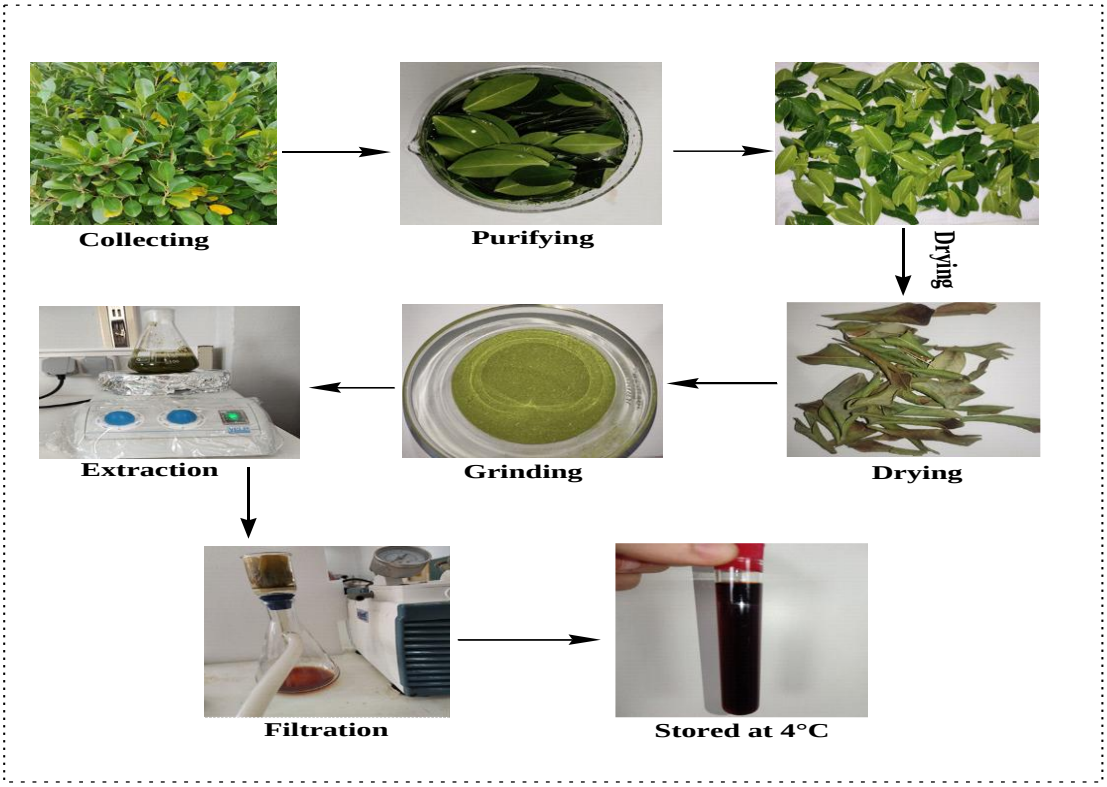

Figure II- 1. Schematic representation of the preparation steps of Ficus retusa leaf extract

II.4. Synthesis of TiO_2 Nanoparticles via Sol-Gel Method

TiO_2 nanoparticles were synthesized using a sol-gel process. For a general process, **10 mL** of TTIP was added to a reaction system of **10 mL** of isopropanol for 16 hours. After that, **10 mL** of deionized water was gradually added under stirring to initiate hydrolysis. The solution was stirred at a low temperature under continuous stirring to allow the formation of a uniform sol. The sol was aged under 24-hour conditions and dried at **80°C** to give a gel. The powder resulting from drying was calcinated at **450°C** for 1 hours to produce crystalline **TiO_2** nanoparticles.[2]

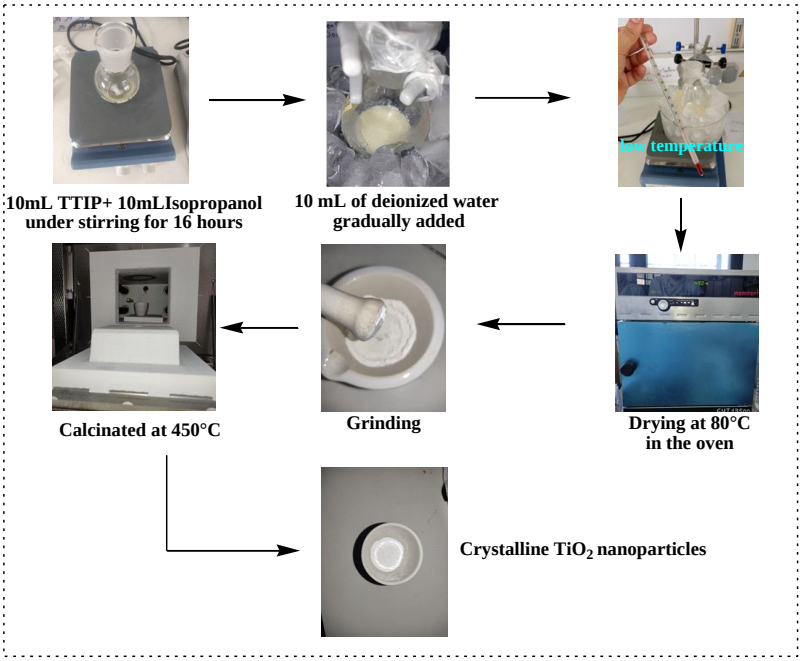

Figure II- 2. Schematic representation of Sol-gel synthesis process of TiO_2 nanoparticles.

II.5. Synthesis of GO via modified Hummers method

At first, **2 g** of graphite powder was sonicated with **50 mL** of **H_2SO_4** for 1 hour, then **30 mL** of **H_3PO_4** was added to the mixture under stirring to initiate the oxidation process. Later on,**6g** of **$KMnO_4$** was gradually added under low temperature (in an ice bath) to avoid overheating. The reaction was carried out, and it was mixed with **100 mL** of pure water afterward. Then, **H_2O_2** was employed in order to eliminate remaining dirt. Thereafter, the product was washed with pure water and **HCl** in order for it to be purified. Lastly, it was centrifuged and filtrated then baked in the oven at **100 °C** in order for it to be a powder of graphene oxide.[3]

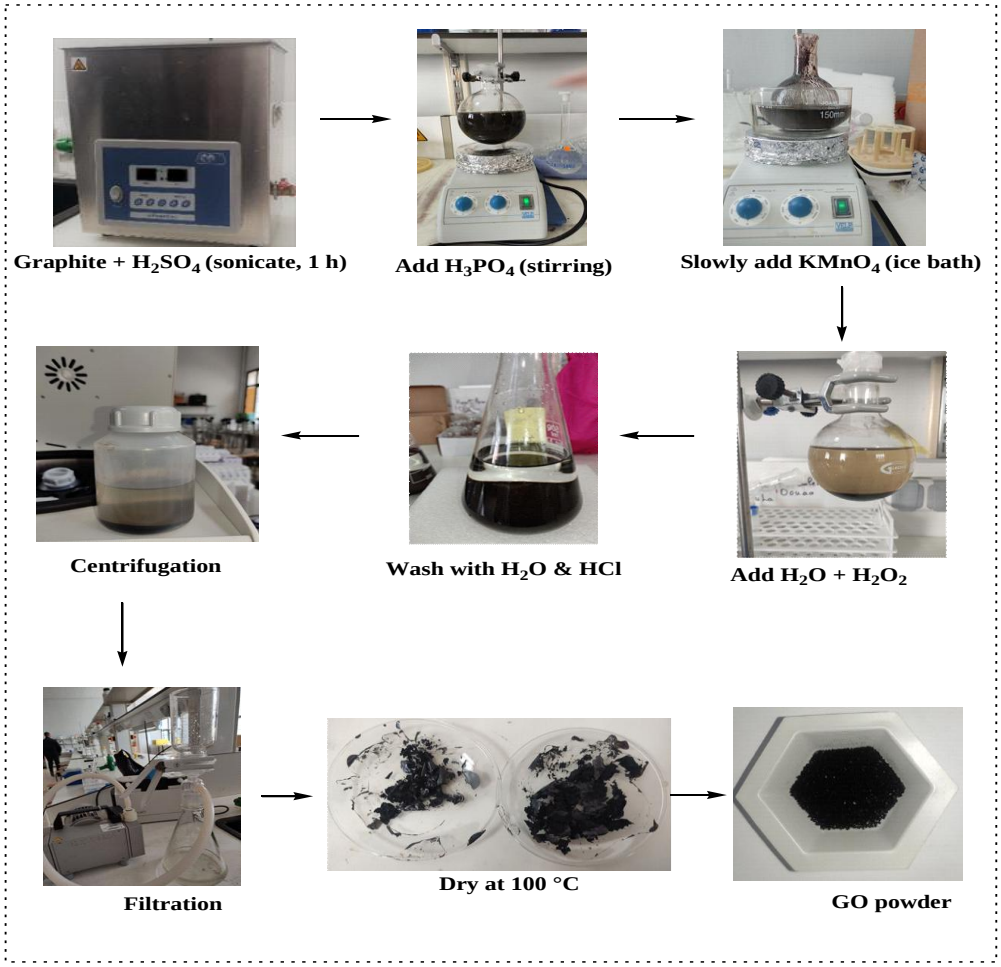

Figure II- 3. Schematic of graphene oxide synthesis via the modified Hummers' method.

II.6. Green Synthesis of TiO_2/rGO Nano-Hybrids

Titanium dioxide (TiO_2) combined with reduced graphene oxide (rGO) was prepared using an eco-conscious sol-gel method. Instead of leaning on synthetic chemicals, the process made use of Ficus retusa leaf extract, which helped both reduce GO and stabilize the particles, making the whole method a lot more in line with green chemistry goals.

1. A small amount 1 mL of titanium isopropoxide (TTIP) was blended with 3 mL of isopropanol. This was stirred for a full 6 hours. That long stirring helped trigger the first changes needed to start forming the sol.
2. GO suspension, 0.02 g, 0.04 g, or 0.06 g of graphene oxide (GO). Each amount was mixed into 10 mL of deionized water and then sonicated for 30 minutes.
3. The GO suspension was slowly poured into the TTIP solution, and the whole thing was stirred for 3 hours.

4. The Ficus retusa leaf extract was added little by little, drop by drop, while the mixture kept stirring.
5. Once the reaction was wrapped up, the material was centrifuged. That's a way of spinning the mix fast enough to separate the solid product from the liquid. The solid was then washed several times with distilled water. finally filtrated
6. After filtration, the solid was left to dry overnight at 80°C. Then it was calcinated at 450°C for 2 hour. [1]

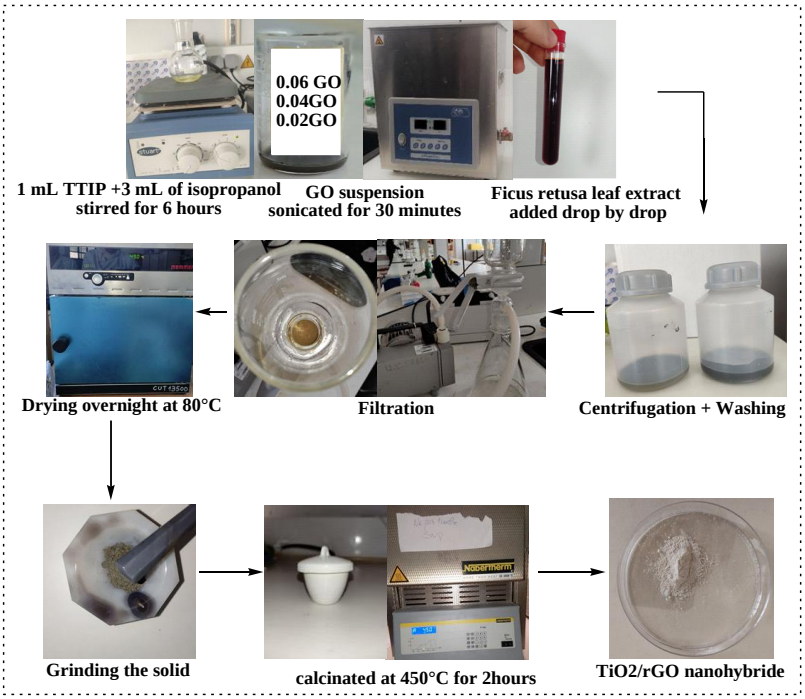

Figure II- 4. Schematic of Green synthesis of TiO_2/rGO nanohybrids.

II.7. Working Dye Solutions

II.7.1. Calibration Curve

A calibration curve is prepared using standard solutions of known concentration. The process allows you to quantify exactly the concentrations of residual dye through comparison of absorbance and concentration values. Thus, you are certain of the test outcome of the degradation efficiency.

We have prepared a 1000 ppm stock solution of CR and CV using the appropriate quantity of the dye and dissolving the same in distilled water. Standard solutions of 5, 7, 10, 15, 20, and 25 ppm were then prepared through serial dilution.

- **Instrument:** Shimadzu UV-1800 UV–Vis spectrophotometer

- **The wavelength of the measurement:** λmax = 664 nm.
- **The cuvettes:** quartz with a path length of 1 cm.
- **The blank solution:** distilled water.

We measured the absorbance of each standard solution and then plotted the results to make the calibration curve, for optimal measurement results and to comply with the Lambert-Beer Law.[4]

II.7.2. Preparation of Working Dye

Dye solutions were prepared using deionized water. Stock solutions of 1000 ppm were first prepared and stored in the dark. From these, 10 ppm of Crystal Violet (CV) and 20 ppm of Congo Red (CR) working solutions were freshly prepared before each experiment. These were used in photocatalysis, electrocatalysis, photolysis, and electrolysis tests.

II.8. Photocatalytic Activity Tests

II.8.1. Photolysis: Degradation without Catalyst

Photolysis is the process of breaking down chemical compounds using light energy, usually in the UV or visible spectrum. During this process, the target molecules or water absorb the energy from the photons, which creates reactive species (like hydroxyl radicals) that can start oxidation reactions.

Photolysis in this study was used as a control to investigate the impact of UV-A light (365 nm) on the degradation of the dye in the absence of a catalyst. This is beneficial in identifying if the dye is degrading with exposure to light only. It is beneficial in identifying the impact that photocatalysis or electrocatalysis produces compared to light.

1. 100mL of dye solution (CV-10ppm or CR-20ppm) was introduced into the graduated cylinder reactor in the absence of a catalyst.
2. The UV lamp (365 nm) was turned on, and the solution was irradiated for a specified duration (0–120 minutes).
3. At regular intervals (every 5 minutes), 2 mL samples were extracted using the sampling ports.
4. Determine the wavelength of the dye's maximum absorption (λmax) with a UV–Vis spectrophotometer.

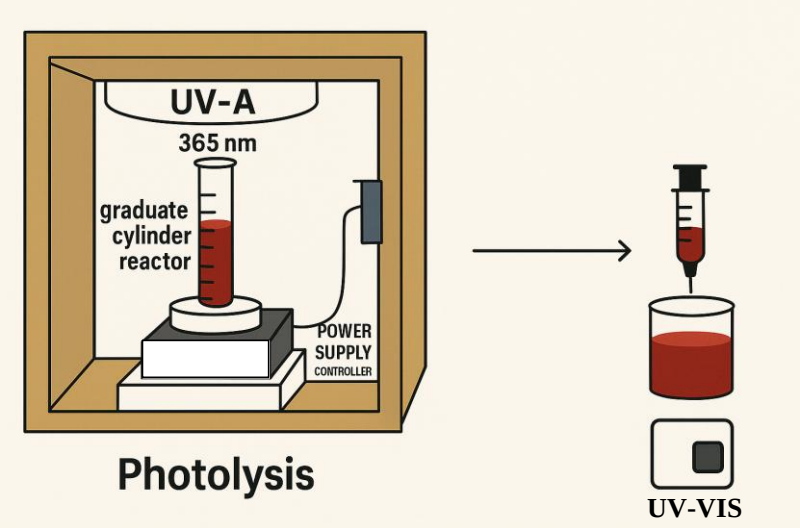

Figure II- 5. Schematic representation of the photolysis chambre.

II.8.2. Photocatalysis

Photocatalysis is a process driven by light in which electron-hole pairs are generated in a semiconductor material, often titanium dioxide (TiO_2), and initiate oxidation-reduction reactions. The resulting reactions generate reactive oxygen species (ROS), including hydroxyl radicals and superoxide anions, that can break down organic pollutants such as dyes into more harmless products.

We used photocatalysis to measure the ability of the TiO_2 and TiO_2/rGO nanomaterials they created to degrade under UV-A light (365 nm). We sought to find out how good each of the catalysts was at it and how good they were at filtering dye-containing water.

1. Initially, weigh exactly 0.1 g of the chosen catalyst (TiO_2 P25 or TiO_2/rGO), and mix it with 100 mL of the prepared dye solution. Stir the suspension properly for the homogeneous distribution of the catalyst in the liquid.
2. Let the dye catalyst mixture stir in the dark for around 30 minutes. This is a crucial step to allow the system to reach a stable adsorption–desorption equilibrium between the catalyst surface and the dye molecules.
3. Following equilibration, irradiate the suspension with UV light at 365 nm . Record this as the initiation of the irradiation time.
4. Every 5 minutes, pipette or syringe out 2 mL of the reaction mixture using a clean pipette or syringe. Sampling should be carried out for the duration of the experiment.
5. Each sample taken should be filtered immediately with a 0.45 µm syringe filter. This will eliminate the catalyst particles and leave the clear liquid for analysis.

6. Take a small sample of the clear liquid on the surface with a UV-Vis spectrophotometer. Record the absorbance for the wavelength at which the dye absorbs the most (λmax).
7. Repeat steps 4 and 6 for every time point based on how quickly the dye breaks down.[5]

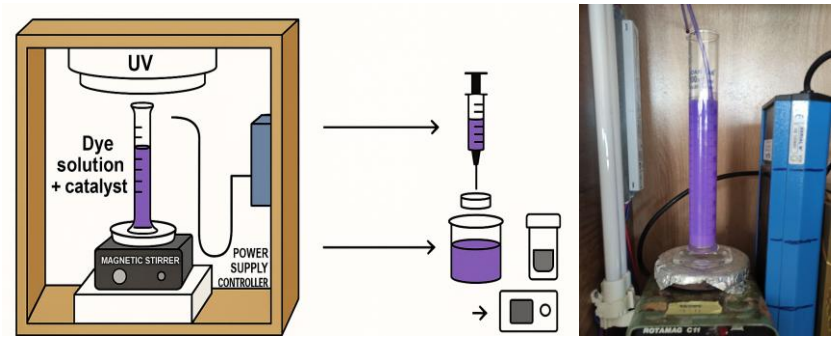

Figure II- 6. Schematic representation with real photo of the Photocatalytic degradation.

II.8.3. Electrocatalysis

Electrocatalysis involves acceleration of electrochemical reactions at the interface of an electrode by an external applied potential. Reactive intermediates like hydroxyl radicals (•OH) are formed at the interface of an electrode and an electrolyte during such a process.

Electrocatalysis has been employed herein as an assisting process of enhanced oxidation to help evaluate degradation efficiency of catalysts synthesized under electrostimulation:

The working electrode consisted of glassy carbon, Ag/AgCl reference electrode, and platinum wire counter electrode.

1. Powdered catalyst was deposited on the glassy carbon working electrode
2. The cell was filled with 1 M NaCl solution with the dye served as the electrolyte.
3. VoltaLab PGP201 potentiostat/galvanostat was used to impose controlled potential against the working electrode.
4. Current and future data were collected using VoltaMaster 4 software.[6]
5. Subsequent to given time electrolysis, concentrations of the dyes were examined by sampling and spectrophotometry.

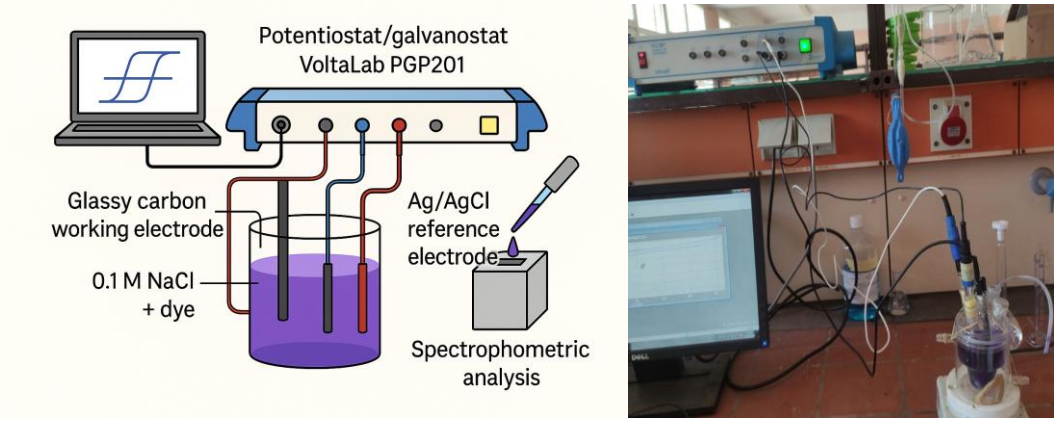

Figure II- 7. Schematic diagram with real photo of the electrocatalytic degradation setup.

II.8.4. Electrolysis: Direct Electrochemical Oxidation

Electrolysis is a process of direct electrochemical oxidation of contaminants at an electrode interface by applying an electric current or potential. Based on electrodes and electrolyte materials, oxidative species like hydroxyl radicals (•OH), chlorine-based oxidants (from NaCl), or ozone can be produced. The oxidative species then destroy and oxidize organic molecules present in solution.

Direct electrolysis in this research applied to provide a baseline measurement to assess how much the electric field itself would break down the dye under non-photocatalysis and non-electrocatalysis conditions.

1. The electrochemical cell setup was as in the electrcatalysis section.
2. A sample known solution of the dye was placed in the cell.
3. 1 M NaCl solution where the dye had been dissolved was added to the cell as the electrolyte
4. The powder catalyst (≈0.1g) was cast onto the glassy carbon working electrode
5. A constant current of 6 mA was provided via the potentiostat.
6. Electrolysis was performed for a planned period
7. Intervals were harvested and analyzed spectrophotometrically.[7]

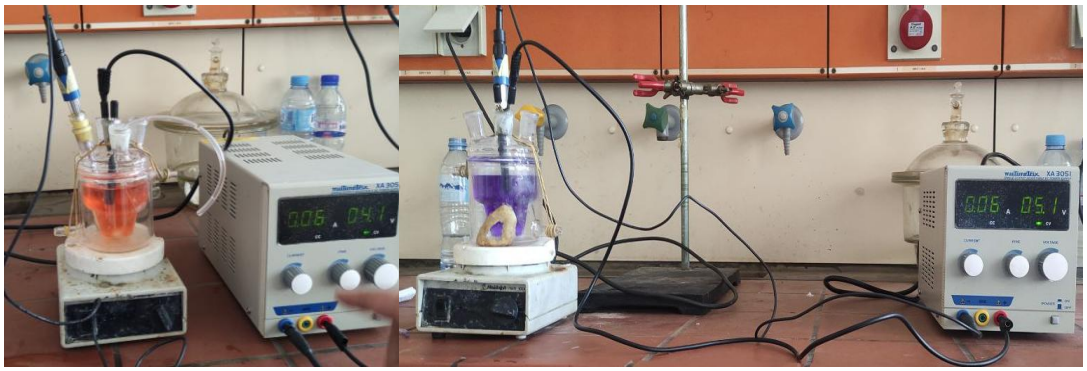

Figure II- 8. Electrolysis cell for CV/CR dyes degradation.

II.9. Characterization Techniques

II.9.1. Thin-Layer Chromatography

TLC is a quick analytical method used to separate and identify small organic molecules. In this study, it was employed to detect phytochemicals in the ***Ficus retusa*** leaf extract which employed to detect the role in the green synthesis of TiO_2 nanoparticles.

- **Stationary phase:** Pre-coated silica gel TLC plates (60 F_{254})
- **Mobile phase:** Acetone
- **Standard:** A phenol (1 mg/mL in distilled water)
- **Sample application:** Manual spotting using glass capillary tubes
- **Visualization:** Under UV light at 254 nm and 365 nm
- R_f values were calculated to support compound identification$\longmapsto R_f = D_{PE}/D_{PH}$

II.9.2 X-ray Diffraction

XRD is used to determine the crystalline structure and phase purity of materials. It was employed to analyze the phase composition of pure TiO_2, GO, and TiO_2/rGO nanohybrids and estimate crystallite size.

- **Instrument:** X-ray diffractometer with Cu Kα radiation (λ = 1.5406 Å)
- **Scanning range:** 2θ = 10°–80°
- **Step size:** 0.02°
- **Operating voltage and current:** 40 kV, 30 mA
- **Analysis:** Diffraction peaks were matched with ICDD standards.

Figure II- 9. Bruker D8 ADVANCE X-ray Diffractometer (XRD) system.

- Crystallite size estimated using the **Scherrer equation.**
- Distance between atomic layers (d) in the crystal. This allows us to identify the crystal structure and phase composition of a material. By using **Bragg's Law**[9],[10]

Table II- 2.Parameters in Bragg's Law and Scherrer Equation.

LAW	EQUATION	PARAMETER	MEANING
BRAGG	$n\lambda=2d\sin\theta$	n	Order of reflection (typically = 1)
		λ	X-ray wavelength (1.5406 Å for Cu Kα radiation)
		d	Interplanar spacing between atomic planes (in Å)
		θ	Diffraction angle (in degrees)
SCHERRER	$D=K\lambda/\beta\cos\theta$	D	Average crystallite size (in nm)
		K	Shape factor (typically 0.9 for spherical particles)
		λ	X-ray wavelength (same as in Bragg's Law)
		β	Full Width at Half Maximum (FWHM) of the diffraction peak (in radians)
		θ	Bragg angle (same as in Bragg's Law)

II.9.3. Scanning Electron Microscopy and Energy Dispersive X-ray spectroscopy

SEM provides surface morphology and topographical information, while EDX confirms elemental composition. Both techniques were used to examine particle morphology and verify the elemental constituents of TiO_2.

- **Instrument**: SEM with integrated EDX detector
- **Sample preparation:** Dried powders mounted on carbon tape and sputter-coated with gold
- **Imaging voltage:** 10–20 kV
- **Magnification:** Up to 50,000×
- **EDX:** Spectral analysis for Ti, O.[11]

II.9.4. Fourier Transform Infrared Spectroscopy

FTIR detects molecular vibrations to identify functional groups. It was used to confirm the presence of organic compounds to investigate the chemical interaction between TiO_2 and rGO.

- **Instrument:** FTIR-8400S. Fourier Transform Inrared.
- Spectrophotometer-SHIMADZU, equipped with a microcomputer.
- **Spectral range:** 4000–400 cm^{-1}
- **Resolution:** 4 cm^{-1}
- **Scan count:** 32 scans per sample
- **Sample preparation:** KBr pellet method for powder samples; ATR mode used when applicable[12]

II.9.5. UV–Visible Spectrophotometry (UV–Vis)

UV–Vis spectroscopy measures the light absorption characteristics of materials. This technique was used to analyze optical behavior and estimate band gap energies using the Kubelka–Munk function

Table II- 3. Analytical Methods, Governing Equations, and Their Specific Roles in the Photocatalytic Study

METHOD	LAW / BASIS	PURPOSE / APPLICATION
ABSORBANCE NORMALIZATION (OD/OD_0)	**Ratio from Beer–Lambert concept**	To track relative dye concentration changes during degradation over time
PSEUDO-FIRST-ORDER KINETICS	**$Ln\ (OD_0/OD_t) = kt$**	To determine rate constant ***k*** for photocatalytic degradation
DEGRADATION EFFICIENCY CALCULATION	**$\zeta\ (\%) = (1 - ODt/OD0) \times 100$**	To quantify dye removal effectiveness of each catalyst

- **Instrument:** UV–Vis spectrophotometer (e.g., Shimadzu UV-1800 or equivalent)
- **Wavelength range:** 200–800 nm
- **Cuvettes:** Quartz cuvettes (1 cm path length)
- **Sample preparation:** Dispersed in ethanol or distilled water via ultrasonication
- **Analysis:** Absorbance spectra used to calculate a band gap energy by plotting ($\alpha h\nu^{2}$) vs. hν[13],[14]

Figure II- 10. Shimadzu UV-1800 UV-Visible Spectrophotometer

II.10. Limitation of methodology

This study was faced with pragmatic limitations of restricted access to TTIP, time, and laboratory space. As such, degradation experiments were carried out under constant conditions, without varying important factors such as temperature, pH, and catalyst concentration. These are established factors affecting photocatalytic activity, and their exclusion raises analytical depth into question. Future studies should entail systematic exploration of such variables for further understanding and optimization of degradation performance.

Chapter III: Results and Discussion

III.1. Introduction

This chapter presents the experimental results of the synthesis and performance assessment of **TiO_2/rGO** nanohybrids, emphasizing their optical responses, structural characteristics, photocatalytic and electrocatalytic efficiency in Congo Red dye and Crystal Violet dye degradation.

III.2. Plant extract identification

III.2.1.TLC

Thin-layer chromatography (TLC) was used in the detection of phenolic compounds in ***Ficus retusa*** extract. The developed TLC plate with acetone and viewed under the UV light showed a spot in the plant extract lane that was equal in height and similar R_f (**~0.56**) to that of the phenol standard. This suggested that the extract must contain phenol or a phenolic compound with the same structure (**Figure III- 1**). This corroborates the free radical scavenging activity of the extract and suggests that it can be used as an environmentally friendly reducing agent.

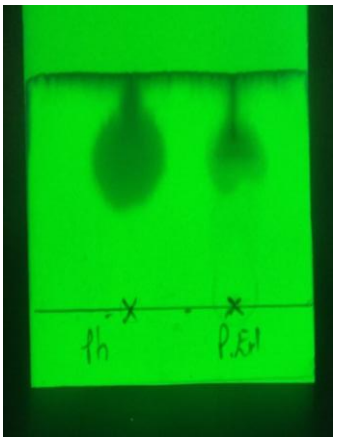

Figure III- 1. TLC analysis under UV light of phenolic standards (Ph) and the plant extract (PE)

- **Solvent front**: ~5.6 cm from baseline
- **Phenol spot (Ph)**: ~3.2 cm
- **Plant extract (PE)**: ~3.1

These ***Rf* values are almost identical**, indicating **co-migration** of the compound from the extract with the phenol standard.

III.3. Structural and Morphological Characterization

III.3.1 Fourier Transform Infrared Spectroscopy (FTIR)

FTIR spectra presented in (Figure III- 2) confirm the successful integration of reduced graphene oxide (**rGO**) into the **TiO_2** matrix. The **TiO_2** spectrum shows distinct vibrational modes associated with the **Ti–O–Ti** framework **(<800 cm^{-1}),** surface hydroxyl groups **(~3400 cm^{-1}**), and adsorbed water **(~1630 cm^{-1}),** which are characteristic of anatase-phase Titania synthesized via the sol–gel method.

With addition of **rGO**, the spectra have extra peaks at **1720 cm^{-1}** and **1600 cm^{-1}** due to **C=O** stretching and **C=C** skeletal vibrations, respectively. This confirms that the **rGO** has oxygen-containing and **sp^2**-hybridized carbon groups. With higher concentrations of rGO (**0.02 g, 0.04 g, 0.06 g**), these bands become stronger. This means that the dispersion is bigger and the two surfaces are more clearly interacting with each other.

The **O–H** region gets wider, and the **Ti–O–Ti** peaks move a little, which means that **Ti–O–C** bonds are forming. This means that there is a chemical interaction between **rGO** and **TiO_2**. These changes are important because they make it easier to separate charge carriers and slow down the rate at which electrons and holes recombine. These are two important things that improve the photocatalyst and electronic properties of the composite. The **TiO_2/rGO** sample with 0.06% loading had the best spectral features of all the samples that were tested. This meant that the interface had the most hybridization and synergy.

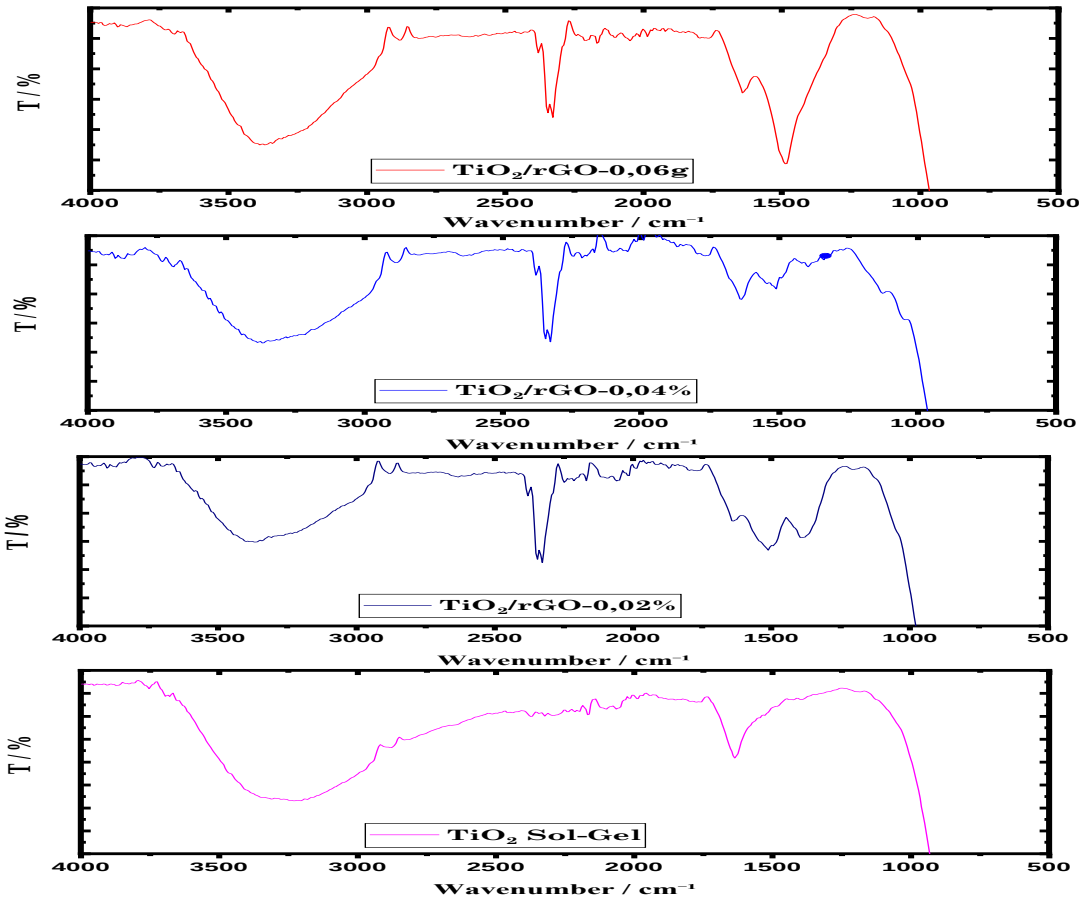

Figure III- 2. FTIR spectra of TiO_2/GO with varying GO compared to pure TiO_2 synthesized by the sol-gel method.

III.3.2. Scanning Electron Microscopy and Energy Dispersive X-ray Spectroscopy

Nanostructural analysis using SEM supplemented by EDX (Figure III- 3) were carried out for the anatase TiO_2 to establish the grain size, shape that the atomic and weight percentages of the elements Ti and O are 39.59 at.%, 66.24 wt.% and 60.41 at.%, 33.76 wt.% respectively.

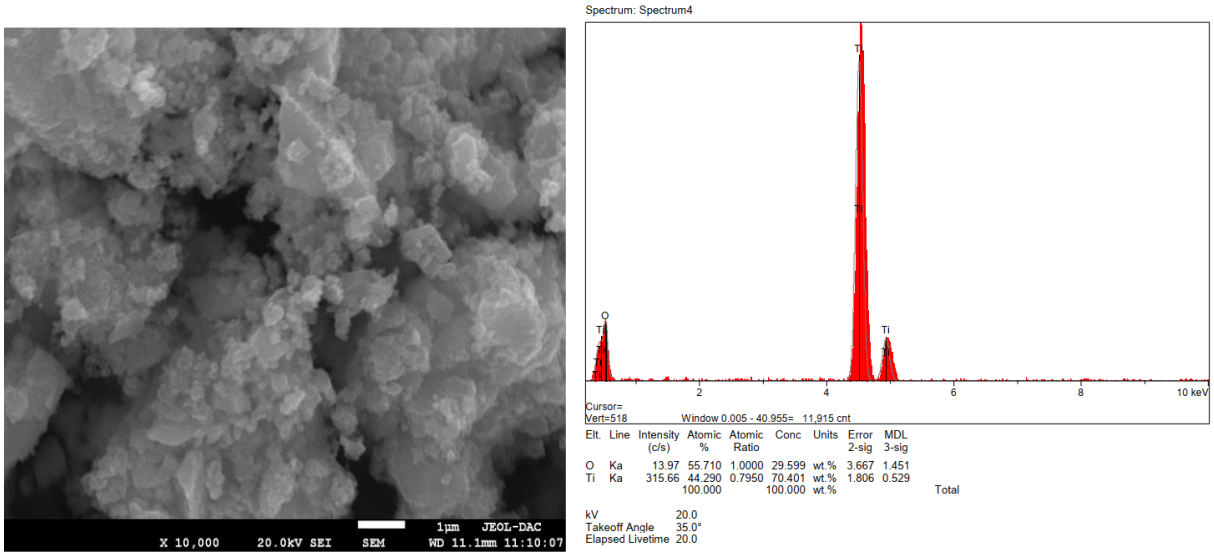

Figure III- 3. SEM image and EDX spectrum of TiO_2 nanoparticles.

III.3.3. X-ray Diffraction (XRD)

Identification of anatase and rutile phases; crystallite size determination using Scherrer's formula.

III.3.3.1. XRD of Titanium Dioxide TiO_2

The XRD pattern of the TiO_2 nanoparticles shows the typical diffraction peaks of the anatase phase. The most intense peak is $2\theta \approx 25.3°$with an interplanar spacing (d) of 0.3516 nm and a crystallite size (D) of 20 nm.

corresponding to the (101) plane (Appendix: PDF 00-001-0562). The other peaks in (Table III- 1) signify that anatase TiO_2 is highly crystalline. There is very little peak due to brookite phase appear, as supported by (Appendix: PDF 00-002-0514). This is an indication that the two phases can exist together, at least partially. Anatase is utilized in photocatalytic applications due to high surface area and increased mobility of the charge carrier. Intensity and peak sharpness define good crystallinity, achieved by sol-gel synthesis followed by calcination at 450 °C for 1 hour.

- **Major phase**: **Anatase TiO_2** (PDF 00-001-0562)
- **Minor peaks**: Small **Brookite TiO_2** contributions (PDF 00-002-0514)

Table III- 1. Key Diffraction Peaks for Anatase.

Miller indices (hkl)	**(101)**	**(004)**	**(200)**	**(105)**	**(211)**	**(204)**
2θ (degree)	**25.3**	**37.8°**	**48.0°**	**53.9°**	**55.1°**	**62.7°**

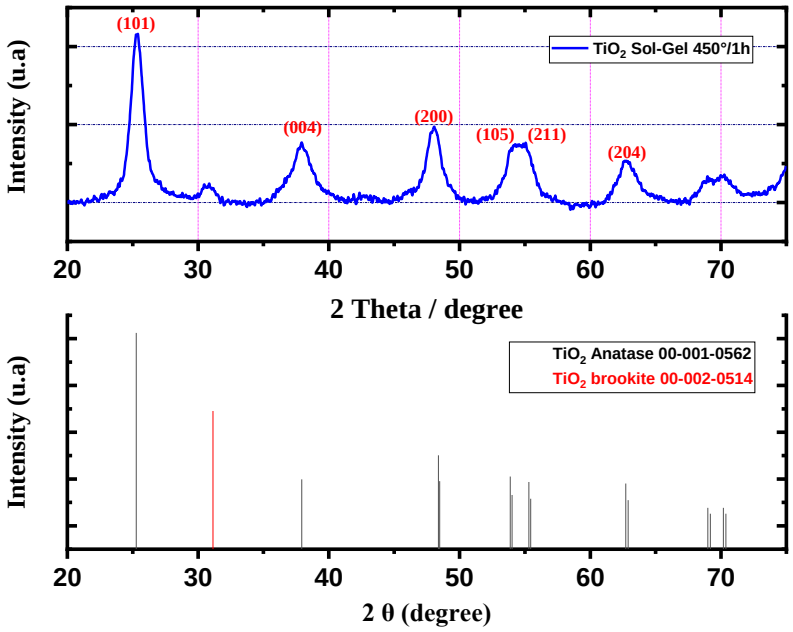

Figure III- 4. X-ray diffractogram of pure anatase TiO_2 nanoparticles.

III.3.3.2. XRD of Graphene Oxide GO

The XRD pattern of GO **(Figure III- 5**)prepared here consists of a prominent diffraction peak **at 2θ ≈ 11.2°** for the (001) plane of the crystal. The unique peak is the sign of successful oxidation of graphite and the formation of GO with an increased interlayer distance. The shift to the typical graphite peak at **~26.5°** (002 plane) to **~11.2°** defines the presence of oxygen-containing functional groups (i.e., hydroxyl, epoxy, carboxyl) and water molecule intercalation.

The interlayer distance was calculated using Bragg's law to be about **0.79 nm**, crystallite size **D=1.776nm** is applicable due to its amorphous and layered structure, consistent with literature reports on GO. The broadness of the peak also reflects partial randomness and the amorphous structure resulting from the oxidation process. These features confirm successful exfoliation and oxidation of graphite into graphene oxide.

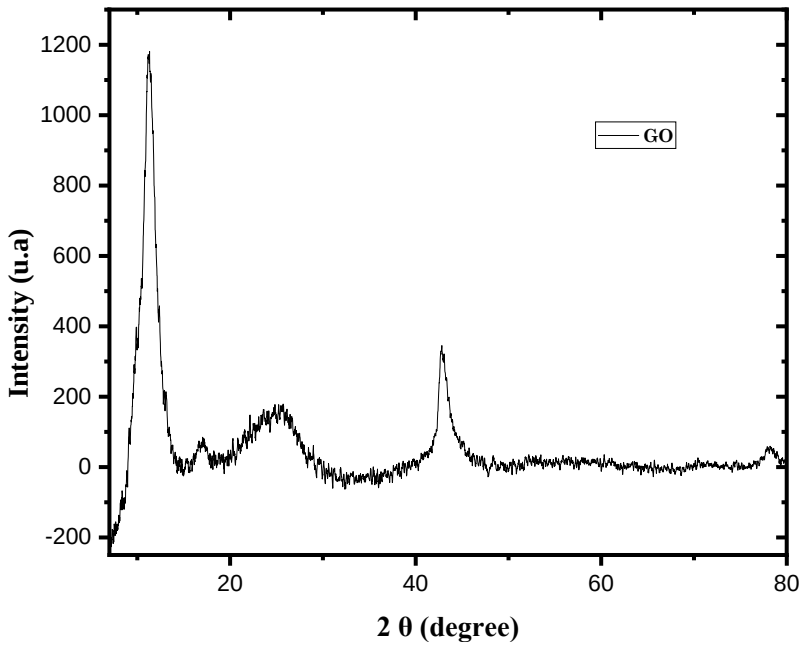

Figure III- 5. X-ray diffractogram of graphene oxide.

III.3.3.3. XRD of TiO_2/rGO

The XRD patterns of TiO_2/rGO composites (**Figure III- 6**)at varying loadings (0.02g, 0.04g, and 0.06g) indicate the retention of the anatase phase of TiO_2 by the dominance of the diffraction peaks at **2θ ≈ 25.3°** (101), 37.8° (004), and **48.0°** (200), consistent with (PDF 00-001-0562). No GO (~**11**°) or graphite (~**26.5°**) peaks were observed, which proves the efficient reduction of GO to **rGO** and uniform dispersal within the TiO_2 matrix. Additionally, the absence of new peaks confirms that no secondary crystalline phases formed during composite synthesis. The gradual reduction of anatase peak intensity with higher **rGO** content was a direct reflection of the marginal reduction in crystallite size and/or shielding effect caused by the sheets of rGO.

This intensity suppression suggests enhanced interaction of the TiO_2–rGO interface, likely due to physical encapsulation of TiO_2 nanoparticles by rGO or chemical bonding from oxygen-containing functional groups. Such kinds of interactions are beneficial for photocatalytic and charge separation performance through facilitating electron transfer and suppressing charge recombination.

Key Observations:

Anatase TiO_2 phase is retained:

- The major peaks (25.3°, 37.8°, 48.0°, etc.) are still clearly observed across all composites, indicating that the incorporation of rGO did **not alter the TiO_2 crystalline phase**.

No sharp GO/rGO peaks (~11° or ~26.5°):

- The absence of a distinct GO peak (~11°) and graphitic (002) peak (~26.5°) suggests:

Successful reduction of GO to rGO

- And/or **good dispersion and interaction with TiO_2**, which can obscure rGO's peak due to its lower content or disorder.

Peak Intensity Variation:

- A slight **decrease in TiO_2 peak intensity** with increasing rGO content is noted.
- This implies **reduced crystallite size or partial coverage of TiO_2 by rGO**, hindering X-ray diffraction from fully crystalline regions.
- **No new peaks** → Indicates **no new crystalline phase** formation between TiO_2 and rGO.

TiO_2/rGO-0.02g: The TiO_2/rGO composite with 0.02% rGO maintained the anatase (101) diffraction peak at $2\theta \approx 25.3°$, yielding a d-spacing of 0.3516 nm and a slightly reduced crystallite size of 23.1 nm.

TiO_2/rGO-0.04g: In the TiO_2/rGO-0.04% sample, the anatase (101) peak remained at $2\theta \approx 25.3°$, with a d-spacing of 0.3516 nm and a crystallite size (D) of 21.3 nm, showing a trend of decreasing grain size with increasing rGO content.

TiO_2/rGO-0.06g: For TiO_2/rGO-0.06%, the anatase (101) reflection was preserved at $2\theta \approx 25.3°$, with a d-spacing of 0.3516 nm and a further reduced crystallite size of 23.6 nm, suggesting enhanced interaction and partial encapsulation by rGO.

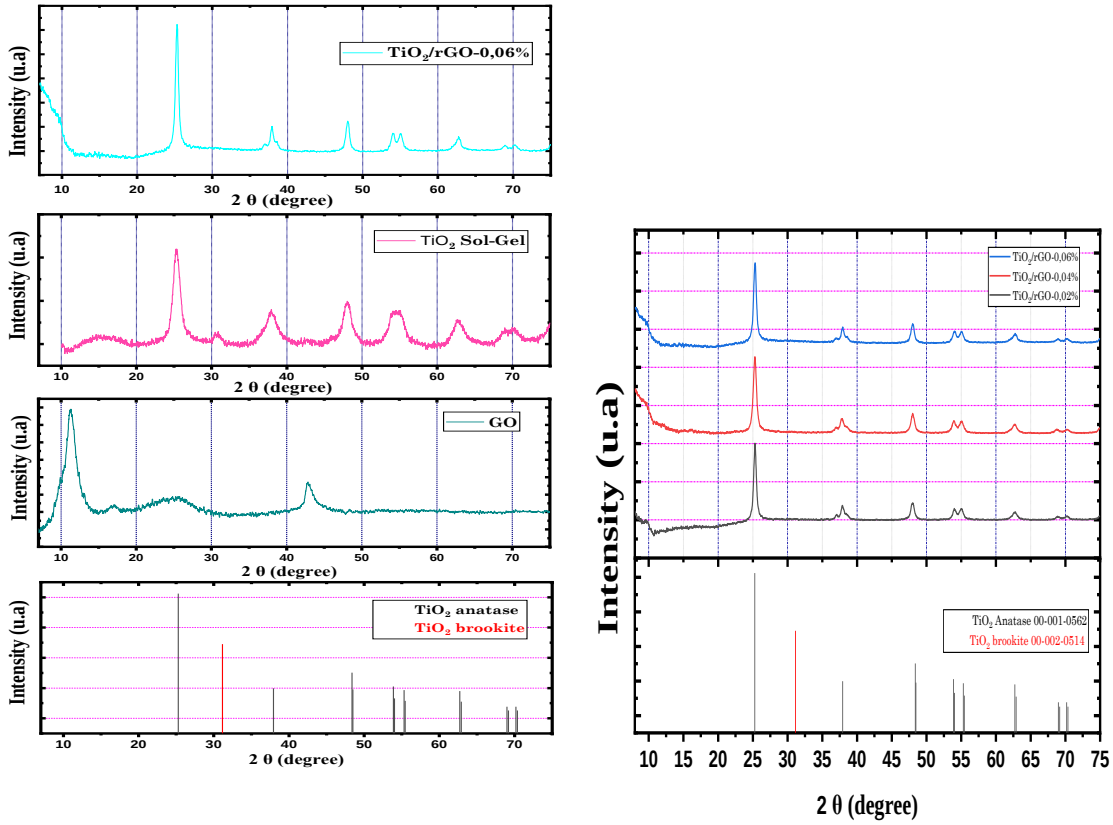

Figure III- 6. X-ray diffractogram of TiO_2/rGO synthesized with varying rGO contents (0.02%, 0.04%, and 0.06%), compared with TiO and graphene oxide.

III.4. Optical Properties and Spectral Calibration

III.4.1. UV spectrum of Dyes

Determination of λ_{max} for Crystal Violet and Congo Red used in catalytic experiments.

III.4.1.1. UV spectrum of Congo Red

The UV-Vis absorption spectrum of Congo Red (**20 ppm**) (Figure III- 7) indicates two characteristic absorption bands. The prominent peak, at about **498 nm**, due to π→π* transitions for the conjugated azo structure and it's responsible for the red color and the visible region absorption.

A second shoulder present in the **340–360 nm** region is related to n→π* transitions of non-bonding electrons on nitrogen atoms in the azo linkage. The spectral shape concurs with Congo Red's reported electronic transitions and verifies the selection of wavelength for tracking degradation.

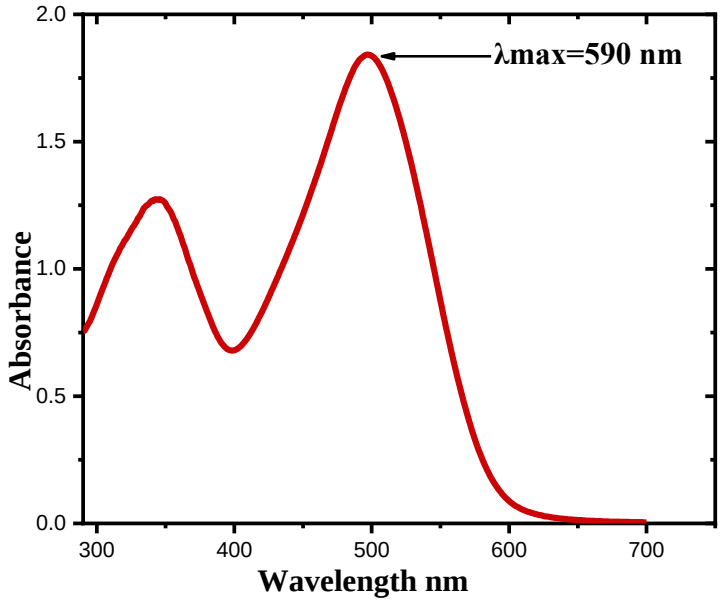

Figure III- 7. Absorbance spectrum of Congo Red.

III.4.1.2. UV spectrum of Crystal Violet

A sharp peak close to **590 nm** in Crystal Violet (**10 ppm**) UV-Vis absorption spectrum (Figure III- 8) is typical of π→π* transitions in its delocalized triphenylmethane backbone. The intense absorption is responsible for the compound's deep violet color.

There is also a weaker absorption band within the UV region (**290–320 nm**), possibly because of further π→π* transitions in aromatic ring systems on top of possible n→π* transitions from the nitrogen lone pairs of dimethylamino groups. By UV-Vis investigation, these spectral characteristics validate the photophysical property and structural stability of the dye.

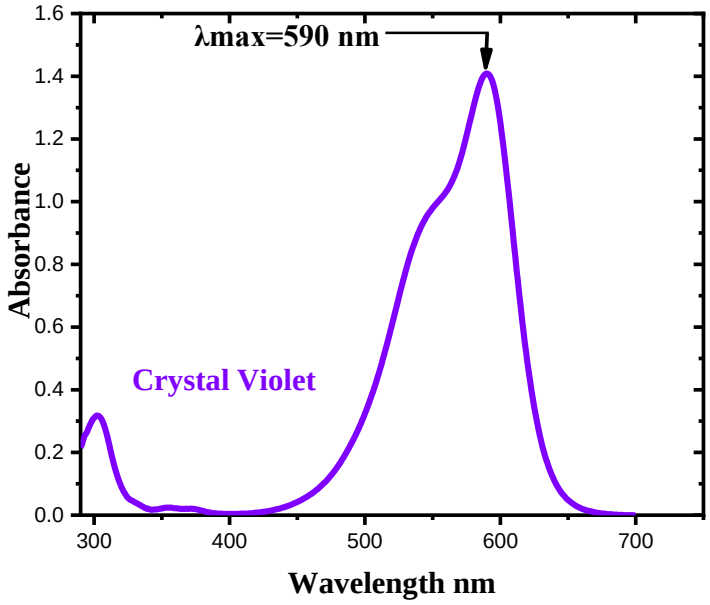

8

Figure III- 8. Absorbance spectrum of Crystal Violet.

III.4.2. Calibration Curves

Standard concentration-absorbance plots for CV and CR to quantify degradation efficiency.

III.4.2.1. Calibration Curve of Congo Red

UV-Vis absorbance at **λmax** was used to construct a calibration plot of Congo Red. The linearity of **y = 0.0116x + 0.0229** and **R^2 = 0.9989** signifies the impeccable linearity in the concentration range tested, as represented by (Figure III- 9). The high (R>0.9) figure verifies the reliability of the method for quantitative analysis. The slope is indicative of the procedure's sensitivity towards the concentration of Congo Red, and the smallest y-intercept is indicative of little or no interference due to the baseline. The linearity is proof of the application of UV-Vis spectrophotometry towards precise measurement of dye degradation.

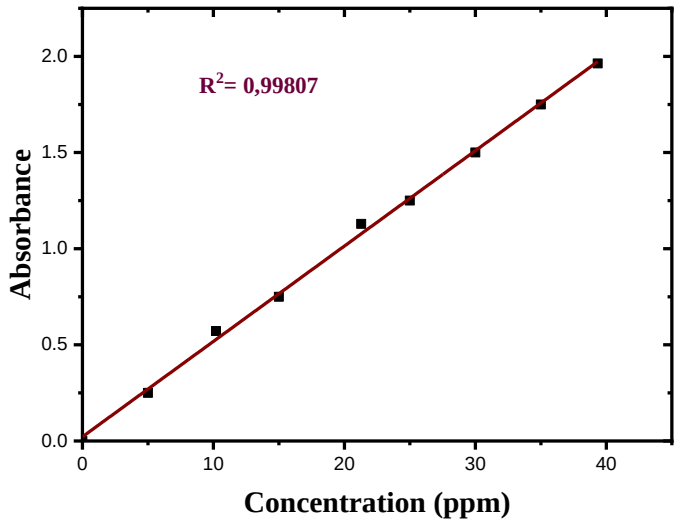

Figure III- 9. Calibration curve of Congo Red.

III.4.2.2. Calibration Curve of Crystal Violet

Crystal Violet calibration curve was linearly represented by the formula **y = 0.0332x + 0.0367**, **R² = 0.99999**, showing almost perfect linearity (Figure III- 10) The high slope yields excellent sensitivity, and trace concentrations can be measured.

Low y-intercept is a consequence of low background absorbance because of equipment or solvent, which guarantees the accuracy of the method. Calibration offers reliable and reproducible quantitative analysis of Crystal Violet in degradation studies.

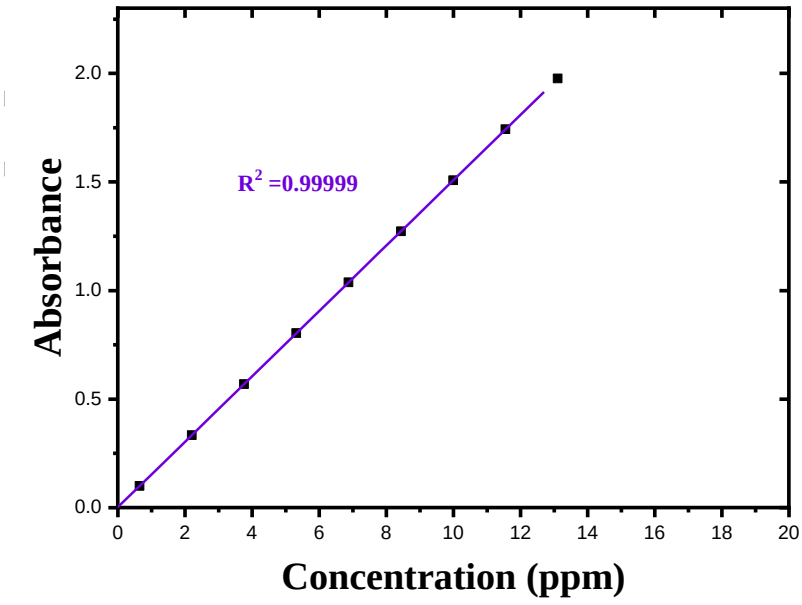

Figure III- 10. Calibration curve of Crystal Violet.

III.4.3. Kubelka–Munk function for Bandgap Estimation

To estimate the band gap of TiO_2, we used the Kubelka–Munk method that is applicable to powders. Reflectance values of UV-Vis spectroscopy are converted with the formula:

Where $$F(R) = \frac{(1-R)2}{2R}$$ **(1-III)**

R is reflectance. This function behaves similar to absorbance. A plot of $[\alpha \cdot h\nu]^2$ vs. photon energy $h\nu$ is traced out. Extrapolating the straight-line section of the graph (Figure III-11) to intersect the x-axis, we can find the band gap energy.

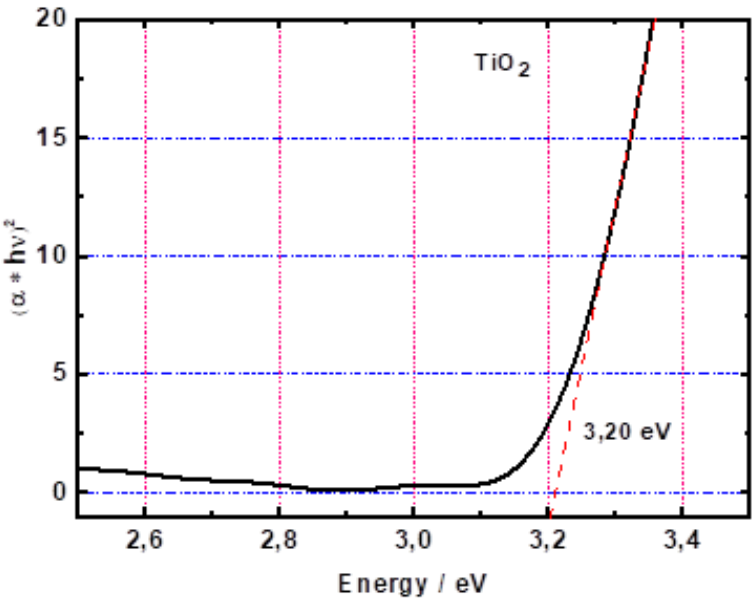

Figure III- 11. Plot of the Kubelka-Munk transformTiO_2.

III.5. Photolysis Activity

III.5.1. Photolysis (Homogenous)

In this experiment, we looked at how Congo Red (CR) and Crystal Violet (CV) dyes break down under UV light without a photocatalyst. The graph in (Figure III- 12) shows how the degradation rate changes over time and what the final photolysis efficiency is after 40 minutes of exposure. The results show that Congo Red degrades with a final photolysis efficiency of 34.81%. Crystal Violet, on the other hand, degrades with an efficiency of 19.09% under the same conditions. This means that Congo Red is more likely to break down when it's in direct sunlight. This is likely because the molecules are arranged differently and absorb UV light differently. Photolysis was the only thing that caused the breakdown, since there was no photocatalyst present. These results show that the two dyes react differently to UV light, which

shows how important it is to know how each dye acts when making processes for photodegradation or water treatment.

Crystal Violet is a triphenylmethane dye that is less likely to break down when it is exposed to light because of how its molecules are arranged. Azo dyes, on the other hand, often have chromophores that absorb UV light better, which speeds up the breakdown process.

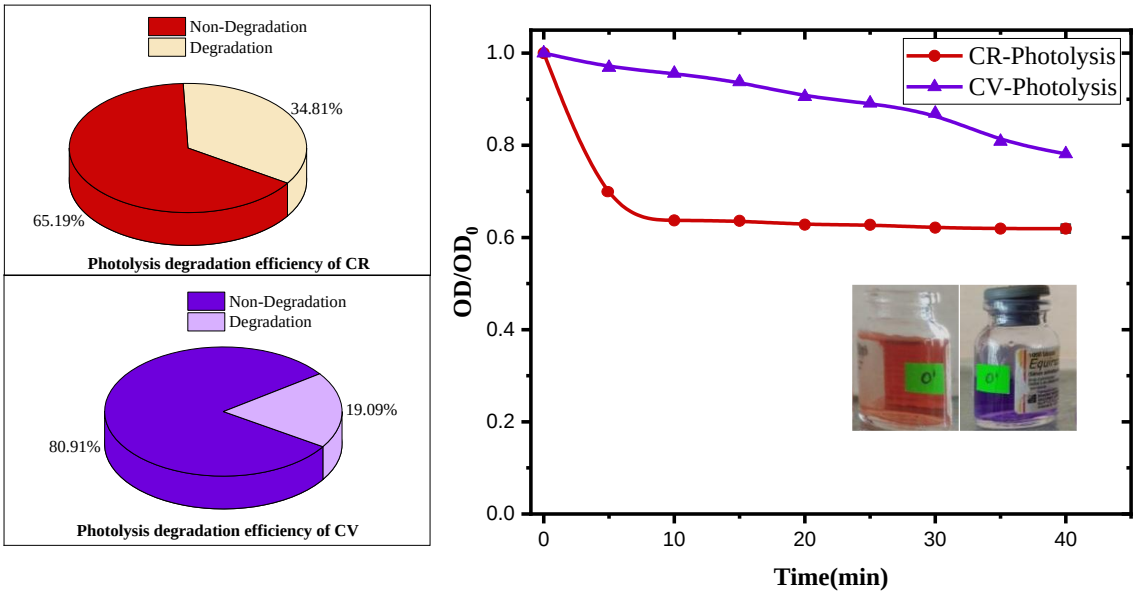

Figure III- 12. Photolysis kinetics and efficiencies degradation of CR and CV.

III.6. Photocatalytic Degradation Analysis

Time-resolved dye degradation with comparative analysis of catalyst performance.

III.6.1. Photocatalytic of Congo Red

We investigated the photocatalytic activity of **TiO_2/rGO** composites (Figure III- 13) with different **rGO** ratios (**0.02g**, **0.04g**, and **0.06g**) for the degradation of Congo Red (CR) dye (**20 ppm**) in this study. The results indicated the maximum sensitivity of **rGO** ratios on degradation performance.

The most photocatalytic activity was achieved for **TiO_2/rGO (0.04g),** which decomposed 99.8% of the material within 30 minutes of UV irradiation. This suggests that there is an ideal ratio between the photocatalytic characteristics of **rGO** in transferring electrons and those of TiO_2. **rGO** enhances the adsorption of dyes on surfaces and charge separation. TiO_2/rGO (**0.02g**) and TiO_2/rGO (**0.06g**) exhibited significantly lower efficiencies of 64.7% and 60.1%, respectively.

The poor performance at **0.02g** is due to a lack of **rGO** for charge transfer. The decrease at **0.06g** shows that there exists an excess **rGO**, and it can prevent the activation of **TiO_2** by UV light or even aid in recombination. This means there is an optimal **rGO** ratio, after which the photocatalytic benefit is lost. This non-linear behavior implies the very crucial need for nanocomposite composition optimization to yield best performance in advanced water treatment techniques.

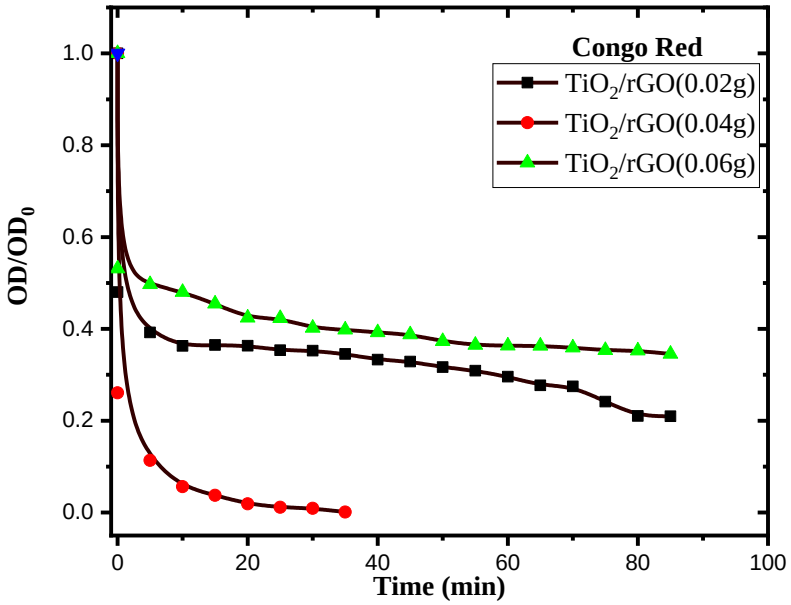

Figure III- 13. Kinetics of decolorization of CR byTiO2/rGO (0.02g;0.04g and 0.06g)

Having obtained the maximum degradation efficiency of TiO_2/rGO(0.04g), comparative analysis was carried out with commercial **P25** and pristine **TiO_2** to study their performance in detail. (Figure III- 14). The evidence succinctly describes the consistent performance enhancement with material modification. The reference photocatalyst **P25** utilized routinely was **87%** efficient, whereas pure **TiO_2** was considerably better at **98.96%** efficiency, likely by way of improved surface quality or enhanced crystallinity. With **TiO_2/rGO(0.04g)**, the best performing one, **99.89%** efficiency for near-complete degradation was achieved as evidence of the role of **rGO** in enhancing photocatalyst activity. The **rGO** is an excellent conductor of electrons, which reduces recombination of photo-generated electron-hole pairs and enhances dye adsorption through π–π interactions. Such a dramatic increase from **P25** to **TiO_2/rGO** demonstrates how judicious material design, more importantly, with nanostructured carbon supports, can profoundly enhance photocatalytic degradation. These findings validate the potential of **TiO_2/rGO** composites in building highly effective systems for environmental remediation and wastewater treatment.

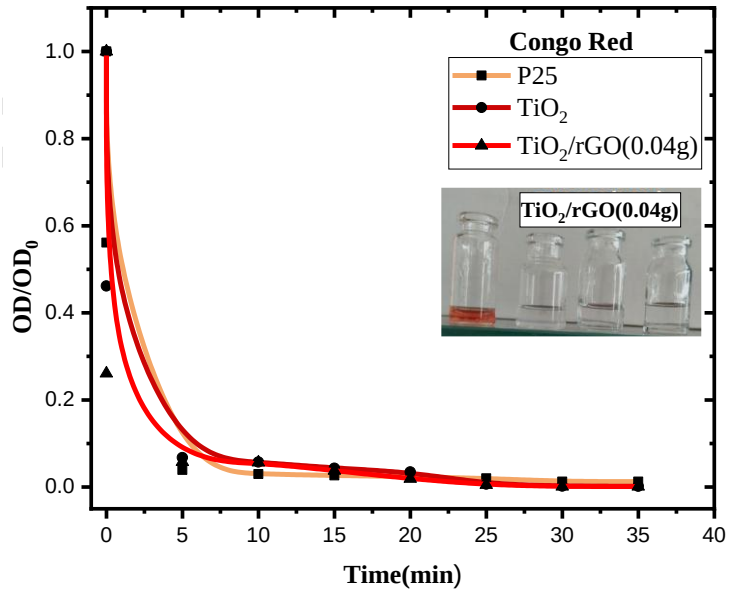

Figure III- 14. Photocatalytic kinetics of degradation of CR 20 ppm.

These results are supplemented by the corresponding pseudo-first-order kinetic plots (Figure III- 15). The highest rate constant was observed in the case of **TiO_2/rGO (0.04 g)**, **k = 0.17306 min^{-1})** followed by **TiO_2 (k = 0.1627 min^{-1})** and **P25 (k = 0.10399 min^{-1})**. The enhancement due to incorporation with **rGO** can be ascribed to the function as an electron sink, which prevents electron-hole recombination and thus results in improved photocatalysis under UV.

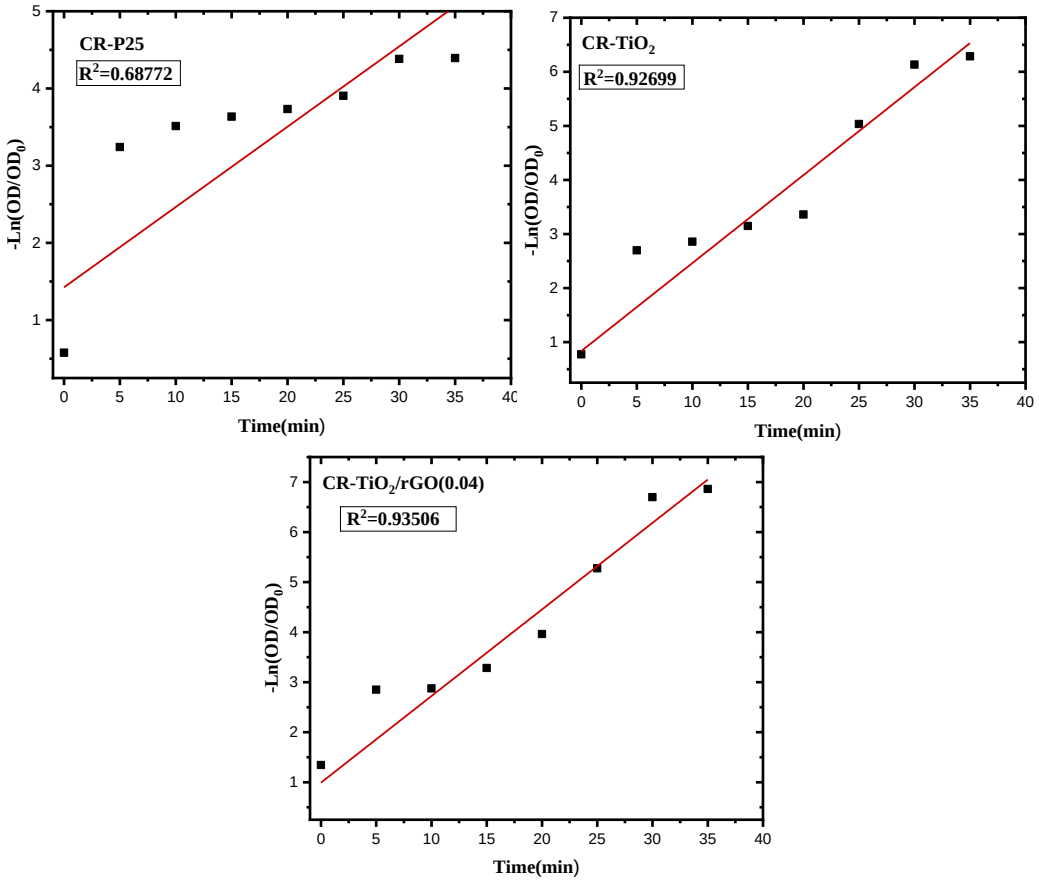

Figure III- 15. Pseudo-first order kinetics of photocatalytic removal of CR

III.6.2. Photocatalytic of Crystal Violet

A comparative degradation test of Crystal Violet dye (**10 ppm**) was carried out for commercial **P25**, pure **TiO_2**, and **TiO_2/rGO(0.04g)** under identical conditions (Figure III- 16). The degradation plots reflect differences in performance among the three photocatalysts. Commercial **P25**, the control in this case, reached a degradation efficiency of **98.36%,** while pure **TiO_2** showed a corresponding value of **98%,** Of particular note, **TiO_2/rGO(0.04g)** composite demonstrated optimum efficiency of **99.21%,** for which a notable enhancement in efficiency was caused by the introduction of reduced graphene oxide. Introduction of **rGO** would facilitate enhanced charge separation and inhibition of electron–hole recombination, besides increasing stronger adsorption of dye by **π–π** interactions with the aromatic rings of Crystal Violet. Such a performance trend reflects the significance of material engineering methodologies, primarily through the use of carbon-based nanostructures, to optimize photocatalytic degradation reactions. The study uncovers the prospects of **TiO_2/rGO** composites for the efficient removal of refractory organic pollutants during wastewater treatment processes.

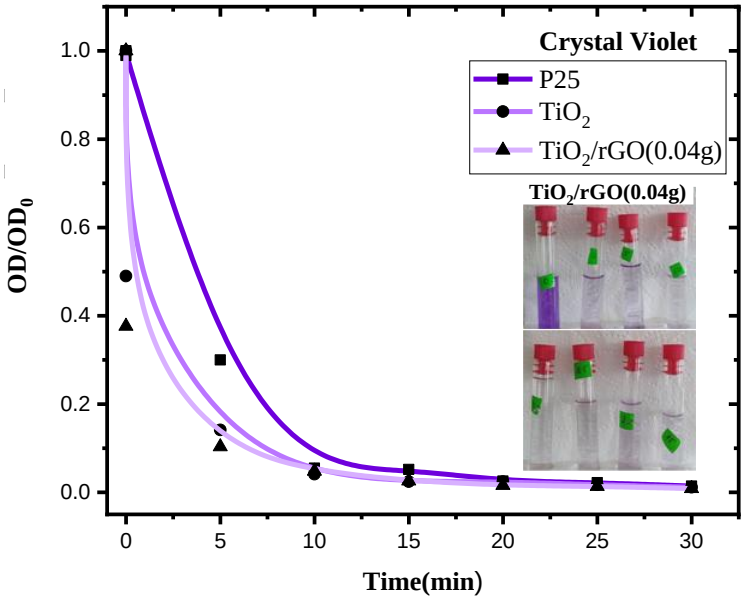

Figure III- 16. Kinetics degradation of CV10 ppm.

Kinetic analysis in (Figure III- 17) revealed the highest rate constant of **k = 0.14433 min⁻¹** in the case of **TiO₂/rGO(0.04g)**, succeeded by **P25** with **k = 0.13603 min⁻¹** and then **TiO₂** with **k = 0.0941 min⁻¹.** Although activity was exhibited by each of the catalysts, the presence of **rGO** significantly amplified the degradation kinetics, reinforcing its functional purpose of augmenting the photocatalytic response of the **TiO₂** matrix.

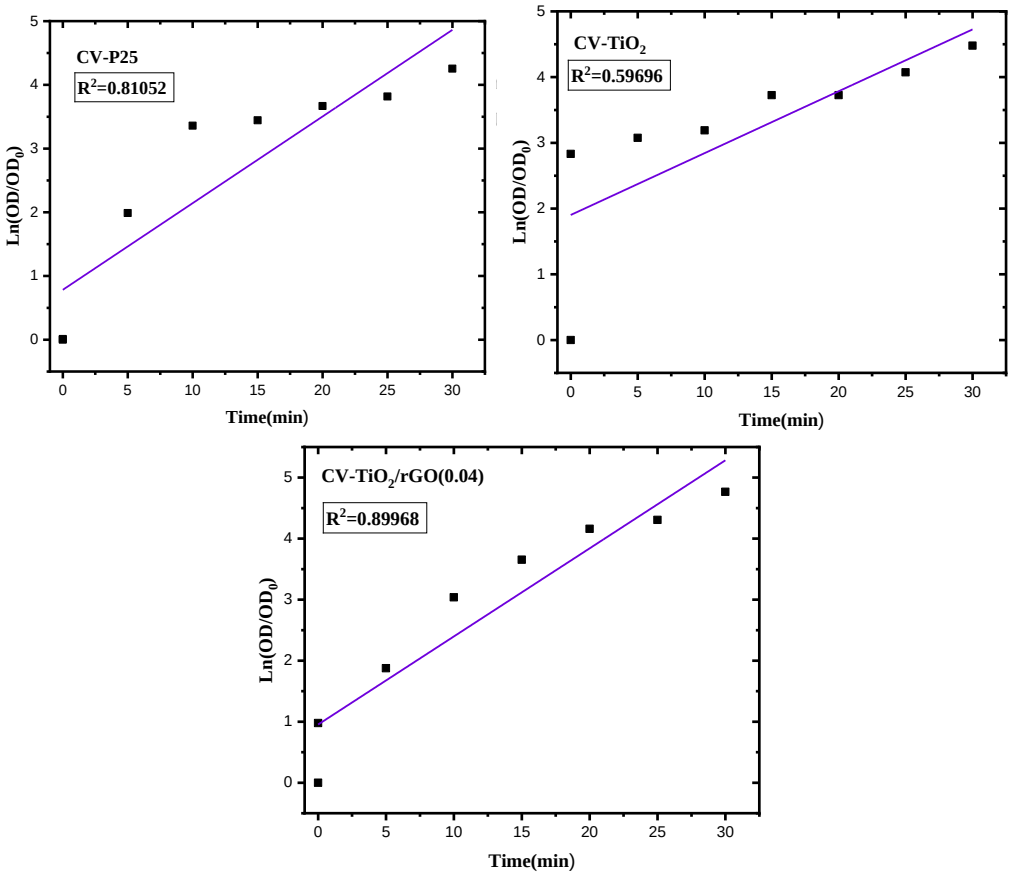

Figure III- 17. Pseudo-first-order kinetics of photocatalytic removal of CR.

III.7. Electrochemical Characterization and Activity

III.7.1. Cyclic Voltammetry of CR and CV

Cyclic voltammograms were performed on our electrodes in an electrochemical cell, which contains a mixture of **(1M NaCl + 10 ppm CV/ 20 ppm CR)** with a three-electrode assembly (Figure II- 7). The polarization curves were recorded in a potential range from **-1V to 1.6V**, and with a scanning speed equal to **50 mV.s^{-1}(**Figure III- 18**,**Figure III- 19**)**. From the results of this study, it can be seen that **TiO_2** increased the oxygen release overvoltage value, which is **1.42 V/Ag/AgCl**, the same for the **TiO_2/rGO(0.04g)** composite, and **P25**. This increase can be related to the chemical composition of the electrodes. Because the oxygen release overvoltage of an electrode is related to its chemical composition, its geometric factors. In general, electrodes with small particle sizes, which therefore have the fewest oxygen vacancies, exhibit the highest oxygen overvoltage values and better electrochemical activity.

In addition, the degradation of crystal violet/Congo red in solution by electro-oxidation can occur directly at the electrode surface or indirectly via oxidizing entities generated from the

supporting electrolyte. The use of sodium chloride as an electrolyte improves treatment efficiency with the in-situ generation of other oxidizing agents from it: dichlorine **Cl_2**, hypochlorous acid **HClO**, and the hypochlorite ion **ClO^-**, with one of these three species predominating depending on the pH of the medium. The latter are certainly less powerful oxidants than hydroxyl radicals, which can be generated from chloride.

$$2Cl^- \rightarrow Cl_2 + 2e^- \qquad \textbf{(III-2)}$$

$$Cl_2 + H_2O \rightarrow HClO + H^+ + Cl^- \qquad \textbf{(III-3)}$$

$$HClO \rightleftharpoons ClO^- + H^+ \qquad \textbf{(III-4)}$$

Note that these voltammograms typically illustrate a reversible redox process of TiO_2, TiO_2/rGO(0.04g), and P25; they are also characterized by an **Epa** peak and **Epc**.

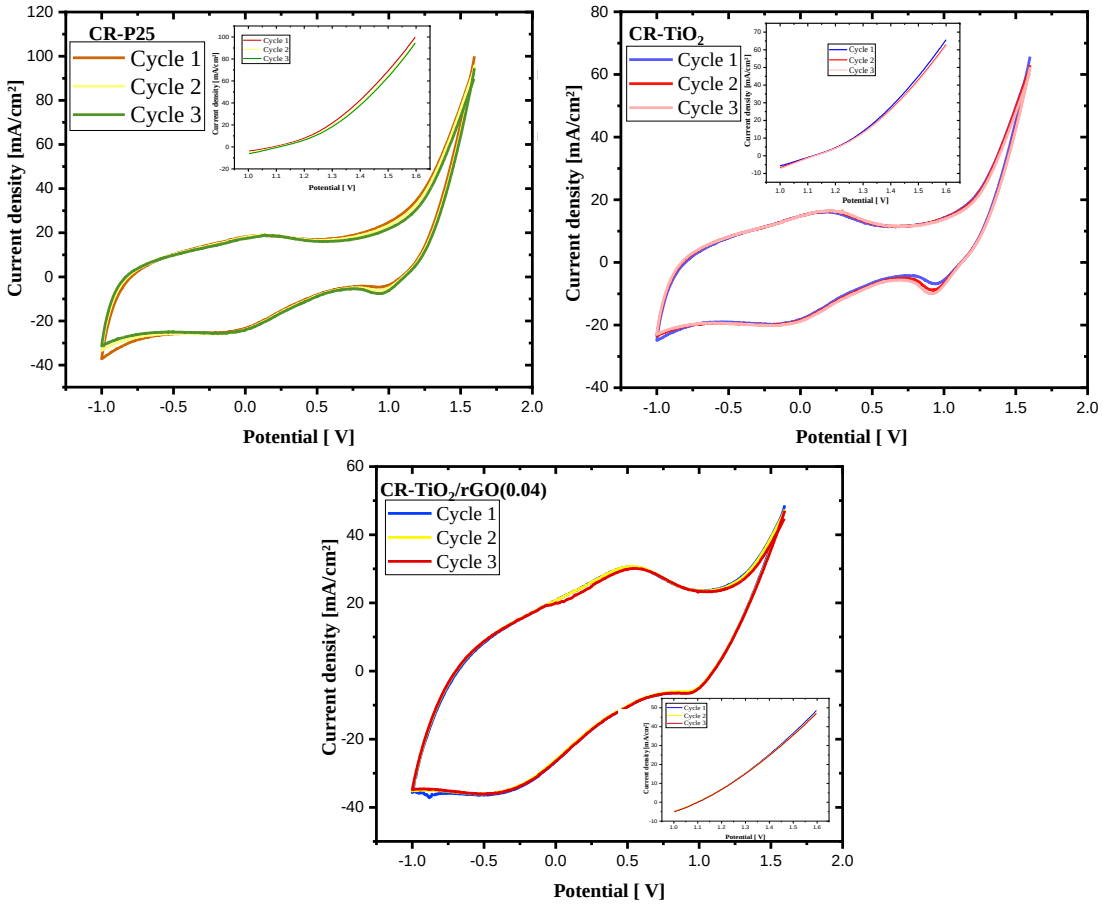

Figure III- 18. Cyclic voltammograms of CR degradation in 1 M NaCl at a scan rate of 50 mV·s⁻¹, using Ag/AgCl as the reference electrode.

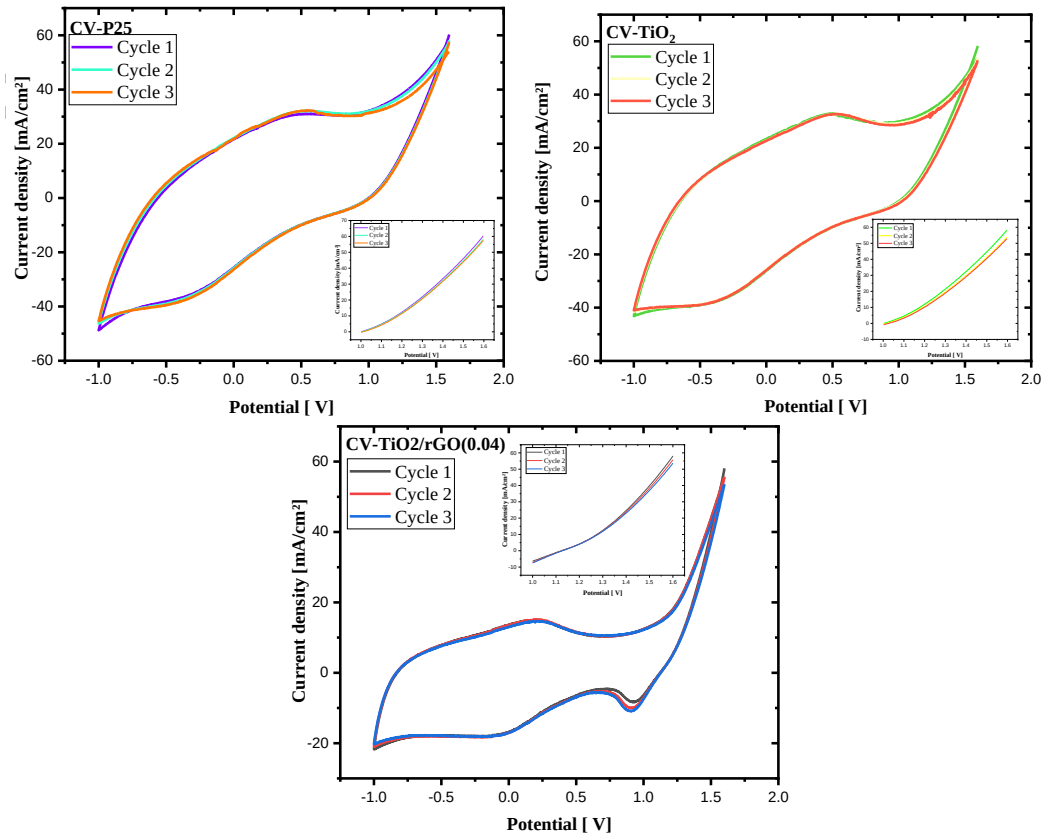

Figure III- 19. Cyclic voltammograms of CV degradation in 1 M NaCl at a scan rate of 50 mV·s⁻¹, using Ag/AgCl as the reference electrode.

III.7.2. Electrocatalytic Degradation Performance

III.7.2.1. Electrocatalytic Degradation Performance of Congo Red

The electrocatalytic degradation of Congo Red was studied under applied potential, and absorbance spectra are presented in (Figure III- 20). The **TiO_2/rGO(0.04g)** catalyst revealed maximum decrease in the absorbance at **498 nm** over **3 cycles**, establishing the high degradation efficiency and electrochemical stability of the catalyst.

Stable long-term performance of **TiO_2/rGO (0.04g)** can be ascribed to the intrinsic high conductivity of **rGO**, which makes a major contribution to the charge transport and initiates **ROS** on the electrode interface with efficiency of **97.28%**. Pure **TiO_2** and **P25**, on the other hand, exhibited degrading performance with efficiency of **96.41%**;**96.3%** respectively, reflecting poor electrochemical stability coupled with slower degradation. Kinetics compared with **TiO_2/rGO (0.04g)**.

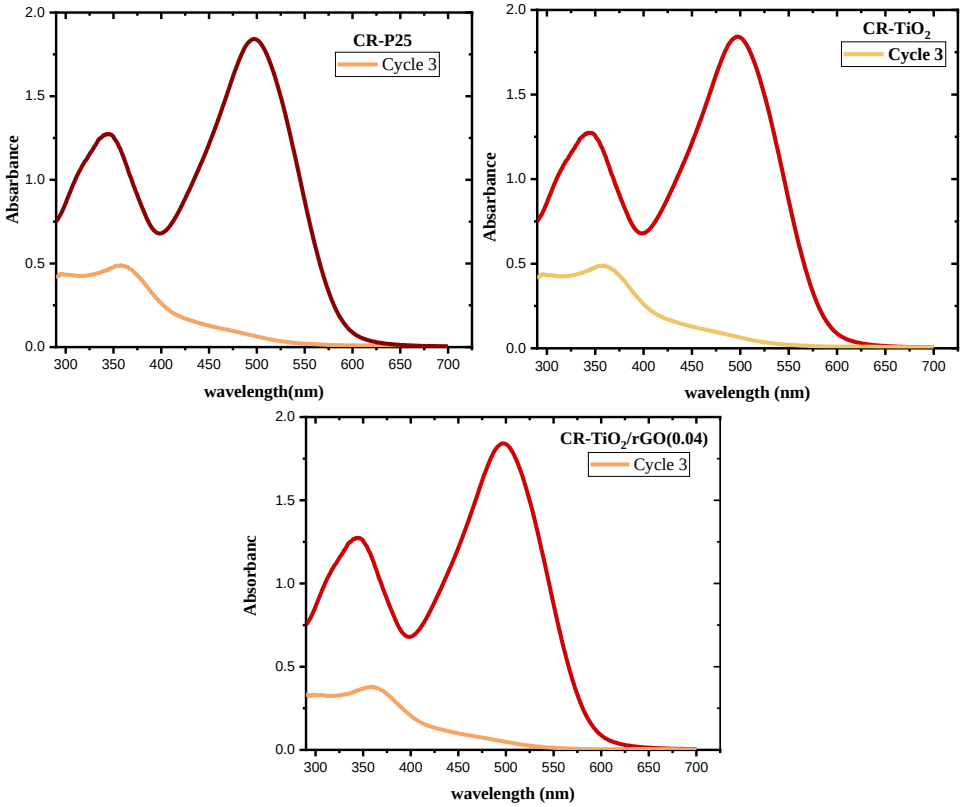

Figure III- 20. Absorbance spectra illustrating the degradation of CR during Electrocatalysis.

III.7.2.2. Electrocatalytic Degradation Performance of Crystal Violet

Similarly, the same was true for Crystal Violet degradation (Figure III- 21). **TiO_2/rGO(0.04g)** also saw the most severe quenching of the **590 nm** absorption peak upon electrolysis with efficiency of **99,87%**, most significantly by the third cycle. It is an indication of its increased electrocatalytic activity and structural stability upon prolonged electrochemical operation.

TiO_2 had moderate activity with efficiency of **94.6 %**, while pure **P25**was least active because of low electric conductivity and reduced redox reactivity with efficiency of **98.5%**. These findings reinforce the benefit of **rGO** in augmenting short and long term electrocatalytic performance of **TiO_2** based material.

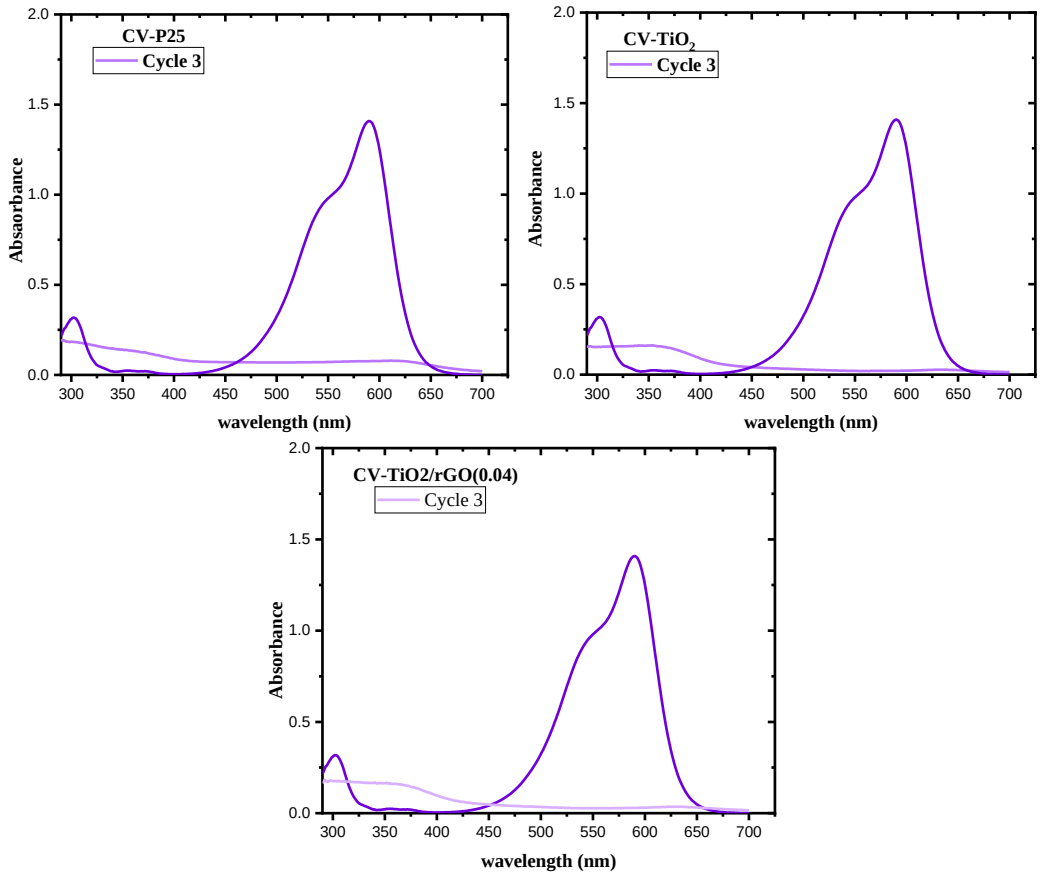

Figure III- 21. Absorbance spectra illustrating the degradation of CV during Electrocatalysis.

III.8. Electrolysis degradation Analysis

III.8.1. Electrolysis of Congo Red

Electrochemical degradation of Congo Red under constant current of **6 mA** was determined by absorbance analysis (Figure III- 22). Maximum degradation efficiency **98.41%** in **2min** was noted in the case of **TiO_2/rGO(0.04g)**. This improved performance is due to the synergistic effect of **rGO** to enhance electrical conductivity and facilitate interfacial electron transfer, resulting in effective formation of **ROS** that are responsible for degradation of the dye. Pure **TiO_2** exhibited comparatively modest performance with efficiency of **98.31%** in **3min**, while **P25** had the less degradation efficiency **97.82%** in **6min** presumably due to limited electrochemical surface activity and poor charge transfer kinetics.

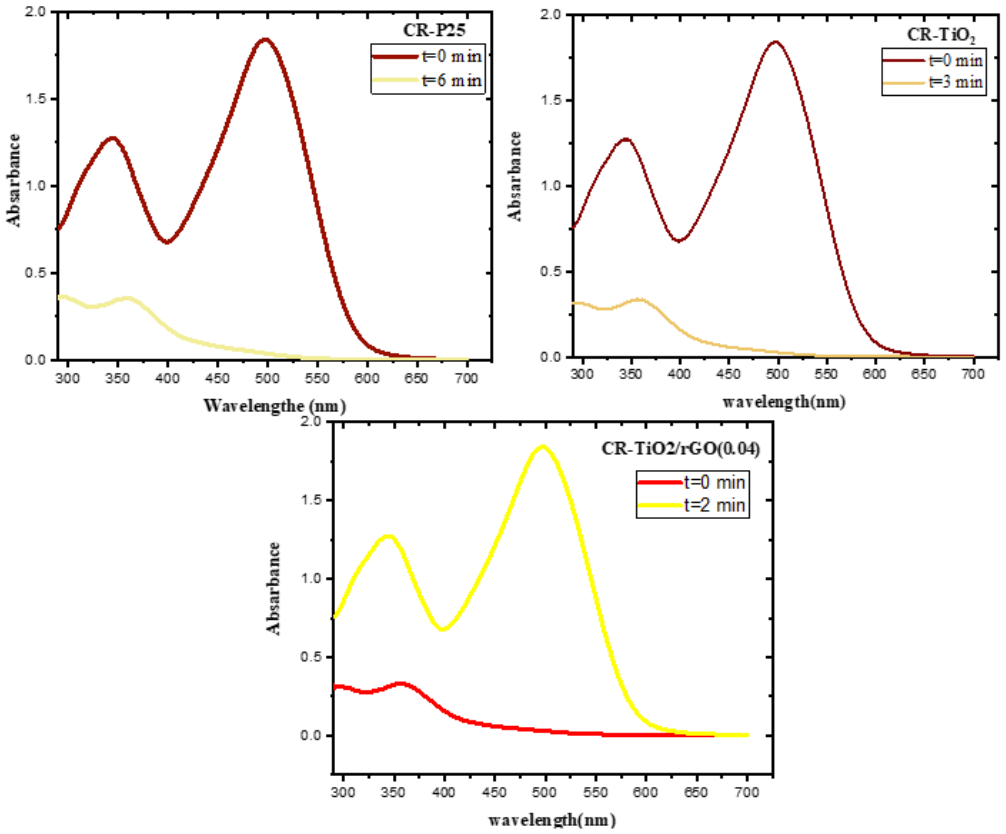

Figure III- 22. Absorbance spectra illustrating the degradation of CR during Electrolysis.

III.8.2. Electrolysis of Crystal Violet

Electrolysis of Crystal Violet under the same condition **6 mA** gave the same results as well (Figure III- 23). **TiO_2/rGO(0.04g)** again showed the highest degradation capacity with near complete removal of the **590 nm** absorbance peak within **3min** with degradation efficiency of **98.5%**. The enhanced activity is due to improved adsorption of the dye and improved electron mobility provided by **rGO**.

TiO_2 demonstrated low degradation activity, which was lowest for **P25** efficiency of **98.01%** in **4min**; **96.59%** in **7min** respectively. These findings highlight the critical role played by the **rGO** in providing fast charge mobility and ease of catalytic surface interactions, two features of prime importance for effective dye degradation in electrochemical systems.

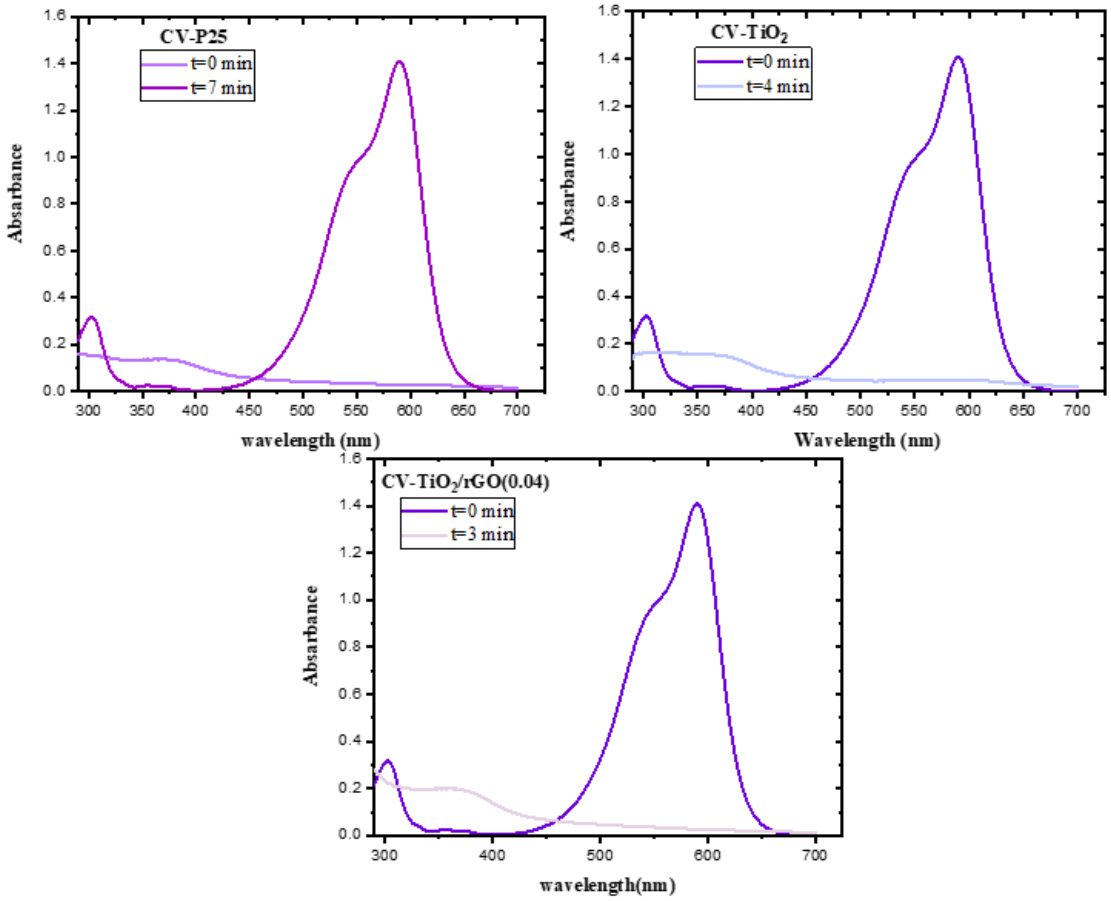

Figure III- 23. Absorbance spectra illustrating the degradation of CV during Electrolysis.

III.9. Comparative Analysis of Degradation Systems

The relative degradation efficiencies of TiO_2, P25, and TiO_2/rGO under various treatment modalities photocatalysis, electrocatalysis, and electrolysis are depicted in (Figure III- 24,Figure III- 25) respectively, for CR and CV.

In photocatalyst applications, **TiO_2/rGO (0.04 g)** performed better than pure **TiO_2** and **P25** consistently. The reasons behind this superior activity are the improvement in the separation of carriers, mobility of electrons, and adsorption of the dye provided by the component of **rGO**. Remarkably, **rGO** is both an electron transport agent and an electron acceptor, which helps in inhibiting recombination and promoting enhanced photocatalyst activity.

Under electrolytic and electrocatalytic conditions **6 mA**, all catalysts had better degradation efficiencies, with less significant differences between them, which implies that the driving of the redox reaction overcomes inherent material constraints. Despite this, **TiO_2/rGO**

still had a slight edge, especially as far as operational stability in terms of efficiency over cycles, supporting again the positive contribution of **rGO** to all the tested degradation systems.

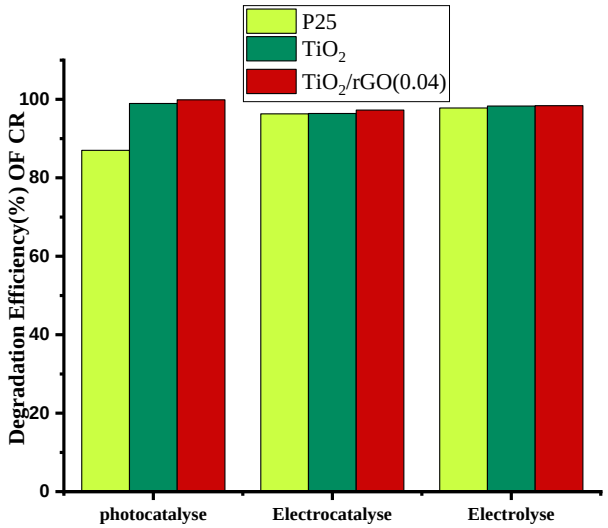

Figure III- 24. Bar chart presents the degradation efficiency (%) of CR.

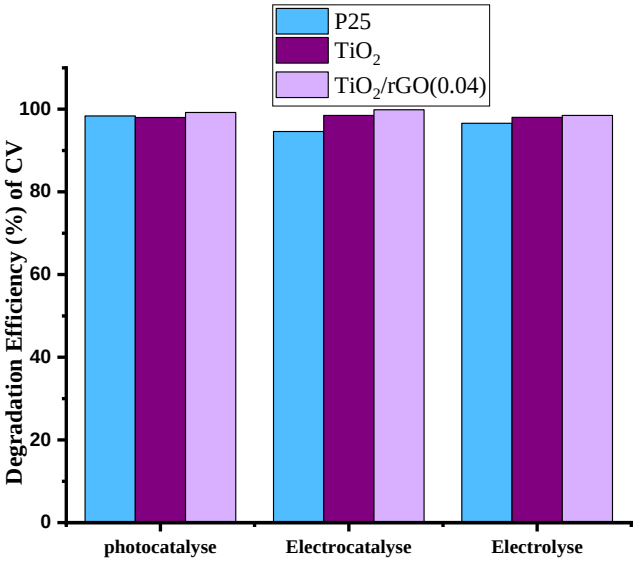

Figure III- 25. Bar chart presents the degradation efficiency (%) of CV.

III.10. Conclusions

This chapter demonstrates the effective synthesis, characterization, and functional assessment of **TiO_2/rGO** nanocomposites as next-generation catalytic systems to degrade dyes. Structural analysis validated the retention of anatase **TiO_2** and successful loading of **rGO**, while **FTIR, XRD**, and **SEM-EDX** corroborated the creation of a hybrid nanostructure with improved interfacial features.

Optical and electrochemical analysis revealed superior photocatalytic and electrocatalytic activities of the composite TiO_2/rGO, and especially 0.04 g loading, when compared with pure TiO_2 and commercial P25. The reasons are mainly due to increased charge separation, improved conductivity, and intensified surface reactivity provided by the presence of rGO.

Comparative studies between photocatalytic, electrocatalytic, and electrolytic modes ensured that although all systems are improved by the input of external energy (electric or light), coupling with rGO strongly enhances catalytic efficiency, particularly under photocatalytic conditions.

In general, TiO_2/rGO composites offer a promising approach to the efficient and sustainable removal of recalcitrant organic pollutants in water environments.

General Conclusions

This thesis investigated the photocatalytic degradation of synthetic dyes from wastewater using green-synthesized titanium dioxide/reduced graphene oxide (**TiO_2/rGO**) nanohybrids. The study aimed at the environmental issue generated by synthetic dyes in that they are chemically stable, toxic, and refractive against conventional wastewater treatment methods.

Literature was reviewed thoroughly to describe the synthesis, structure, and environmental impact of synthetic dyes, such as those of Congo Red and Crystal Violet. The review also compared various dye removal technologies and limitations of physical, chemical, and biological treatments. Advanced oxidation processes, and heterogeneous semiconductor photocatalysis more specifically, proved to be efficient alternatives.

Trying to enhance the **TiO_2** photocatalytic efficiency, which is limited by its wide bandgap and high recombination rate of electrons-holes, the current research proposed the synthesis of **TiO_2/rGO** nanocomposites. The nanohybrids were synthesized using a green sol-gel process with the ***Ficus retusa*** leaf extract as the green reducing and stabilizing agent. The used method of synthesis avoided toxic chemicals and was consistent with sustainable and environmental-friendly nanomaterial construction guidelines.

Structural analysis of synthesized materials with **FTIR, SEM, XRD**, and **UV-Vis** confirmed successful **rGO** addition into the **TiO_2** matrix and demonstrated favourable structural and optical properties. Photocatalytic performance of nanohybrids was evaluated by degradation studies with UV irradiation. Results were that the efficiency of degradation of both model dyes was higher for **TiO_2/rGO** composites compared to unmodified **TiO_2**. Additionally, electrocatalytic and electrochemical experiments confirmed material potential for widespread use in water treatment systems.

Finally, the results confirm green-synthesized **TiO_2/rGO** nanohybrids are effective photocatalysts for dye degradation in water. The presence of **rGO** is beneficial for charge separation, increases surface area, and improves photocatalytic activity. Green synthesis with plant extracts is a promising low-cost, low-footprint approach to the synthesis of advanced functional materials.

Follow-up studies will have to tackle the development of visible-light sensitivity, long-term stability and reusability assessments of the catalysts, and testing in real wastewater samples to assess scalability and practicability to industrial wastewater treatment.

General Introduction References

[1] A. K. Yadav *et al.*, "Sustainable Napier Grass (Pennisetum purpureum) Biochar for the Sorptive Removal of Acid Orange 7 (AO7) from Water," *Processes*, vol. 12, no. 6, p. 1115, Jun. 2024, doi: 10.3390/PR12061115/S1.

[2] M. Mehta, M. Sharma, K. Pathania, P. K. Jena, and I. Bhushan, "Degradation of synthetic dyes using nanoparticles: a mini-review," *Environmental Science and Pollution Research*, vol. 28, no. 36, pp. 49434–49446, Sep. 2021, doi: 10.1007/S11356-021-15470-5/METRICS.

[3] E. H. Alici and G. Arabaci, "The Enzymatic Decolorization of Textile Dyes by the Immobilized Peroxidase from Chard Leaves (Beta vulgaris Subspecies cicla)," *avestia.com*, 2019, doi: 10.11159/ICCPE19.123.

[4] M. Misra, K. Akansha, A. Sachan, and S. G. Sachan, "Removal of Dyes from Industrial Effluents by Application of Combined Biological and Physicochemical Treatment Approaches," *Combined Application of Physico-Chemical and Microbiological Processes for Industrial Effluent Treatment Plant*, pp. 365–407, Jan. 2020, doi: 10.1007/978-981-15-0497-6_17.

[5] M. B. Ceretta, D. Nercessian, and E. A. Wolski, "Current Trends on Role of Biological Treatment in Integrated Treatment Technologies of Textile Wastewater," Mar. 25, 2021, *Frontiers Media S.A.* doi: 10.3389/fmicb.2021.651025.

[6] T. N Lotha, V. Sorhie, P. Bharali, and L. Jamir, "Advancement in Sustainable Wastewater Treatment: A Multifaceted Approach to Textile Dye Removal through Physical, Biological and Chemical Techniques," *ChemistrySelect*, vol. 9, no. 11, p. e202304093, Mar. 2024, doi: 10.1002/SLCT.202304093;WGROUP:STRING:PUBLICATION.

[7] P. Krystynik and P. Krystynik, "Advanced Oxidation Processes (AOPs) – Utilization of Hydroxyl Radical and Singlet Oxygen," Jun. 2021, doi: 10.5772/INTECHOPEN.98189.

[8] Y. Chabanyuk, "Assessing toxicity of titanium dioxide (TiO2) nanoparticles on Pseudomonas species biofilms," May 2021, doi: 10.32920/RYERSON.14663781.V1.

[9] X. Jiang and J. Wang, "Enhanced photocatalytic activity of three-dimensional TiO2/reduced graphene oxide aerogel by efficient interfacial charge transfer," *Appl Surf Sci*, vol. 612, p. 155849, Mar. 2023, doi: 10.1016/J.APSUSC.2022.155849.

[10] P. C. Sruthi and P. D. Shima, "Green synthesis of Ag/RGO nanohybrid using Terminalia Arjuna bark extract as a recyclable catalyst for the reduction of toxic nitroaromatics and azo dyes," *Mater Lett*, vol. 377, p. 137371, Dec. 2024, doi: 10.1016/J.MATLET.2024.137371.

[11] R. Kausar, S. N. Arshad, and S. Khan, "Green Synthesis of Ag-TiO2 -SiO2 Nanocomposite using Azadirachta indica Leaf Extract and Evaluation of Biological Activities: Green Synthesis of Ag-TiO2 Nanocomposite using Azadirachta indica Leaf Extract," *Journal of Chemistry and Material Sciences (JCMS)*, pp. 86–91, Dec. 2024, doi: 10.71120/J.CHEM.MATER.SCI..V1I2.3466.

Chapter I References

[1] S. Dutta, B. Gupta, S. K. Srivastava, and A. K. Gupta, "Recent advances on the removal of dyes from wastewater using various adsorbents: a critical review," *Mater Adv*, vol. 2, no. 14, pp. 4497–4531, Jul. 2021, doi: 10.1039/D1MA00354B.

[2] R. Al-Tohamy *et al.*, "A critical review on the treatment of dye-containing wastewater: Ecotoxicological and health concerns of textile dyes and possible remediation approaches for environmental safety," *Ecotoxicol Environ Saf*, vol. 231, p. 113160, Feb. 2022, doi: 10.1016/J.ECOENV.2021.113160.

[3] Q. Liu, "Pollution and Treatment of Dye Waste-Water," *IOP Conf Ser Earth Environ Sci*, vol. 514, no. 5, p. 052001, May 2020, doi: 10.1088/1755-1315/514/5/052001.

[4] J. Sharma, S. Sharma, and V. Soni, "Classification and impact of synthetic textile dyes on Aquatic Flora: A review," *Reg Stud Mar Sci*, vol. 45, p. 101802, Jun. 2021, doi: 10.1016/J.RSMA.2021.101802.

[5] J. H. Choi, "Dye," *Encyclopedia of Color Science and Technology*, pp. 1–7, 2013, doi: 10.1007/978-3-642-27851-8_182-1.

[6] P. Singh, Ed., "Dye Pollution from Textile Industry," 2024, doi: 10.1007/978-981-97-5341-3.

[7] S. Sinha, N. Jahan, and P. R. Agrawal, "Dyes and Unveiling the Environmental Story of Dye Pollution," pp. 31–63, 2024, doi: 10.1007/978-981-97-5341-3_3.

[8] S. Benkhaya, S. M'rabet, and A. El Harfi, "Classifications, properties, recent synthesis and applications of azo dyes," *Heliyon*, vol. 6, no. 1, Jan. 2020, doi: 10.1016/j.heliyon.2020.e03271.

[9] M. Tripathi *et al.*, "Recent Strategies for the Remediation of Textile Dyes from Wastewater: A Systematic Review," *Toxics 2023, Vol. 11, Page 940*, vol. 11, no. 11, p. 940, Nov. 2023, doi: 10.3390/TOXICS11110940.

[10] H. Zollinger, *Color chemistry: syntheses, properties, and applications of organic dyes and pigments*. 2003. Accessed: May 26, 2025. [Online]. Available: https://books.google.com/books?hl=en&lr=&id=0Ynge4E5rqYC&oi=fnd&pg=PA1&dq=H.+Zollinger,+Color+Chemistry:+Syntheses,+Properties,+and+Applications+of+Organic+Dyes+and+Pigments&ots=pWuzR3jzcm&sig=qfLa_KFqpKIkITOiOpByw32eWt0

[11] K. CARR, "Dyes for Ink Jet Printing," *Colorants for Non-Textile Applications*, pp. 1–34, 2000, doi: 10.1016/B978-044482888-0/50032-5.

[12] A. Mancuso *et al.*, "Photocatalytic Degradation of Crystal Violet Dye under Visible Light by Fe-Doped TiO2 Prepared by Reverse-Micelle Sol–Gel Method," *Nanomaterials 2023, Vol. 13, Page 270*, vol. 13, no. 2, p. 270, Jan. 2023, doi: 10.3390/NANO13020270.

[13] G. Xia and H. Wang, "Squaraine dyes: The hierarchical synthesis and its application in optical detection," *Journal of Photochemistry and Photobiology C: Photochemistry Reviews*, vol. 31, pp. 84–113, Jun. 2017, doi: 10.1016/J.JPHOTOCHEMREV.2017.03.001.

[14] "Colorimetric Analysis of Salt-free Reactive Dyes on Textile Materials." Accessed: May 26, 2025. [Online]. Available: https://textilelearner.net/salt-free-reactive-dyes/

[15] A. Jamil *et al.*, "Photocatalytic degradation of disperse dye Violet-26 using TiO2 and ZnO nanomaterials and process variable optimization," *Journal of Materials Research and Technology*, vol. 9, no. 1, pp. 1119–1128, Jan. 2020, doi: 10.1016/J.JMRT.2019.11.035.

[16] A. Khalil, C. Mangwandi, M. A. Salem, S. Ragab, and A. El Nemr, "Orange peel magnetic activated carbon for removal of acid orange 7 dye from water," *Sci Rep*, vol. 14, no. 1, pp. 1–23, Dec. 2024, doi: 10.1038/S41598-023-50273-3;SUBJMETA=169,172,638,639,704,896;KWRD=POLLUTION+REMEDIATION.

[17] U. Yunusa, B. Usman, and M. B. Ibrahim, "Cationic dyes removal from wastewater by adsorptive method: A systematic in-depth review", doi: 10.5281/ZENODO.5101197.

[18] L. M. Sanchez, R. P. Ollier, J. S. Gonzalez, and V. A. Alvarez, "Nanocomposite materials for dyes removal," *Handbook of Nanomaterials for Industrial Applications*, pp. 922–951, Jan. 2018, doi: 10.1016/B978-0-12-813351-4.00053-5.

[19] Z. Yaneva, D. Ivanova, N. Nikolova, and M. Toneva, "Organic dyes in contemporary medicinal chemistry and biomedicine. I. From the chromophore to the bioimaging/bioassay agent," *Biotechnology and Biotechnological Equipment*, vol. 36, no. 1, pp. 1–14, Dec. 2022, doi: 10.1080/13102818.2022.2039077;SUBPAGE:STRING:FULL.

[20] L. Ouettar, E. K. Guechi, O. Hamdaoui, N. Fertikh, F. Saoudi, and A. Alghyamah, "Biosorption of Triphenyl Methane Dyes (Malachite Green and Crystal Violet) from Aqueous Media by Alfa (Stipa tenacissima L.) Leaf Powder," *Molecules 2023, Vol. 28, Page 3313*, vol. 28, no. 8, p. 3313, Apr. 2023, doi: 10.3390/MOLECULES28083313.

[21] H. A. Begum, M. A. Islam, and T. Muslim, "Equilibrium and Kinetic Studies of Adsorption of Aqueous Crystal Violet by Peanut Shells," *Bangladesh Pharmaceutical Journal*, vol. 17, no. 2, pp. 163–171, Feb. 2015, doi: 10.3329/BPJ.V17I2.22335.

[22] S. I. Siddiqui *et al.*, "Investigation of Congo Red Toxicity towards Different Living Organisms: A Review," *Processes 2023, Vol. 11, Page 807*, vol. 11, no. 3, p. 807, Mar. 2023, doi: 10.3390/PR11030807.

[23] K. Meghwal, S. Kumawat, C. Ameta, and N. K. Jangid, "Effect of dyes on water chemistry, soil quality, and biological properties of water," *Impact of Textile Dyes on Public Health and the Environment*, pp. 90–114, Nov. 2019, doi: 10.4018/978-1-7998-0311-9.CH005.

[24] M. B. Hoque *et al.*, "Unraveling the ecological footprint of textile dyes: A growing environmental concern," *Pollution Study*, vol. 5, no. 2, p. 3014, Dec. 2024, doi: 10.54517/PS.V5I2.3014.

[25] R. Kant and R. Kant, "Textile dyeing industry an environmental hazard," *Nat Sci (Irvine)*, vol. 4, no. 1, pp. 22–26, Dec. 2011, doi: 10.4236/NS.2012.41004.

[26] A. Kargupta, K. Dutta, D. Roychoudhury, S. Rana, and S. N. Talapatra, "Toxicity, Genotoxicity and Ecotoxicity of Food Colourants Especially Synthetic Dyes and its Metabolites: An in silico Approach," *Asian Journal of Chemistry*, vol. 34, no. 11, pp. 2955–2960, Oct. 2022, doi: 10.14233/AJCHEM.2022.23987.

[27] D. Goswami, J. Mukherjee, C. Mondal, and B. Bhunia, "Bioremediation of azo dye: A review on strategies, toxicity assessment, mechanisms, bottlenecks and prospects," *Science of The Total Environment*, vol. 954, p. 176426, Dec. 2024, doi: 10.1016/J.SCITOTENV.2024.176426.

[28] K. T. Chung, "Azo dyes and human health: A review," *J Environ Sci Health C Environ Carcinog Ecotoxicol Rev*, vol. 34, no. 4, pp. 233–261, Oct. 2016, doi: 10.1080/10590501.2016.1236602,.

[29] X. Xie *et al.*, "Effect of Enhanced Hydrolytic Acidification Process on the Treatment of Azo Dye Wastewater," *Molecules*, vol. 28, no. 9, p. 3930, May 2023, doi: 10.3390/MOLECULES28093930.

[30] D. Kumar Yeruva, P. Ranadheer, A. Kiran Kumar, and S. Venkata Mohan, "Tri-phasic engineered wetland system for effective treatment of azo dye-based wastewater," *NPJ Clean Water*, vol. 2, no. 1, pp. 1–8, Dec. 2019, doi: 10.1038/S41545-019-0037-Y;SUBJMETA=172,2805,704,706;KWRD=ENVIRONMENTAL+SCIENCES,WATER+RESOURCES.

[31] X. Zhang *et al.*, "Simultaneous photocatalytic and microbial degradation of dye-containing wastewater by a novel g-C3N4-P25/photosynthetic bacteria composite," *PLoS One*, vol. 12, no. 3, p. e0172747, Mar. 2017, doi: 10.1371/JOURNAL.PONE.0172747.

[32] G. M. D. Ferreira *et al.*, "Adsorption of red azo dyes on multi-walled carbon nanotubes and activated carbon: A thermodynamic study," *Colloids Surf A Physicochem Eng Asp*, vol. 529, pp. 531–540, Sep. 2017, doi: 10.1016/J.COLSURFA.2017.06.021.

[33] A. M. Ismail, A. A. Menazea, and H. Ali, "Selective adsorption of cationic azo dyes onto zeolite nanorod-based membranes prepared via laser ablation," *Journal of Materials Science: Materials in Electronics*, vol. 32, no. 14, pp. 19352–19367, Jul. 2021, doi: 10.1007/S10854-021-06453-W/METRICS.

[34] A. Khan, P. Ju, Z. Han, and C. Ni, "A comprehensive review on adsorptive removal of azo dyes using functional materials," *iwaponline.comA Khan, P Ju, Z Han, C NiAQUA—Water Infrastructure, Ecosystems and Society, 2024•iwaponline.com*, vol. 73, no. 2, pp. 266–285, Feb. 2024, doi: 10.2166/AQUA.2024.292/1370284/JWS0730266.PDF.

[35] M. Tripathi *et al.*, "Recent Strategies for the Remediation of Textile Dyes from Wastewater: A Systematic Review," *Toxics 2023, Vol. 11, Page 940*, vol. 11, no. 11, p. 940, Nov. 2023, doi: 10.3390/TOXICS11110940.

[36] M. Jargalsaikhan, J. Lee, A. Jang, and S. Jeong, "Efficient Removal of Azo Dye from Wastewater Using the Non-Toxic Potassium Ferrate Oxidation–Coagulation Process," *Applied Sciences 2021, Vol. 11, Page 6825*, vol. 11, no. 15, p. 6825, Jul. 2021, doi: 10.3390/APP11156825.

[37] F. Akter and Y. Dong, "Investigation of removing orange II azo dye from wastewater through an oxidation process," *Appl Water Sci*, vol. 14, no. 11, pp. 1–13, Nov. 2024, doi: 10.1007/S13201-024-02311-2/METRICS.

[38] P. Navarro, J. A. Gabaldón, and V. M. Gómez-López, "Degradation of an azo dye by a fast and innovative pulsed light/H2O2 advanced oxidation process," *Dyes and Pigments*, vol. 136, pp. 887–892, Jan. 2017, doi: 10.1016/J.DYEPIG.2016.09.053.

[39] K. Kato and T. Shirai, "Highly efficient water purification by WO3-based homo/heterojunction photocatalyst under visible light," *J Alloys Compd*, vol. 901, p. 163434, Apr. 2022, doi: 10.1016/J.JALLCOM.2021.163434.

[40] B. Kamenická, "Chemical degradation of azo dyes using different reducing agents: A review," *Journal of Water Process Engineering*, vol. 61, p. 105350, May 2024, doi: 10.1016/J.JWPE.2024.105350.

[41] D. Goswami, J. Mukherjee, C. Mondal, and B. Bhunia, "Bioremediation of azo dye: A review on strategies, toxicity assessment, mechanisms, bottlenecks and prospects," *Science of The Total Environment*, vol. 954, p. 176426, Dec. 2024, doi: 10.1016/J.SCITOTENV.2024.176426.

[42] G. B. Singh, A. Vinayak, G. Mudgal, and K. K. Kesari, "Azo dye bioremediation: An interdisciplinary path to sustainable fashion," *Environ Technol Innov*, vol. 36, p. 103832, Nov. 2024, doi: 10.1016/J.ETI.2024.103832.

[43] J. Kyziol-Komosinska, A. Dzieniszewska, S. Pasieczna-Patkowska, A. Kołbus, and J. Czupioł, "Compost as Green Adsorbent for the Azo Dyes: Structural Characterization and Dye Removal Mechanism," *Korean Journal of Chemical Engineering*, vol. 41, no. 12, pp. 3227–3243, Nov. 2024, doi: 10.1007/S11814-024-00254-7/METRICS.

[44] N. Madima, K. K. Kefeni, S. B. Mishra, and A. K. Mishra, "TiO2-modified g-C3N4 nanocomposite for photocatalytic degradation of organic dyes in aqueous solution," *Heliyon*, vol. 8, no. 9, p. e10683, Sep. 2022, doi: 10.1016/J.HELIYON.2022.E10683/ASSET/00EE24FE-A749-4070-808A-DAB95558E6DC/MAIN.ASSETS/GR11.JPG.

[45] H. Yang *et al.*, "ZnS/CuFe2O4/MXene ternary heterostructure photocatalyst for efficient adsorption and photocatalytic degradation of azo dyes under visible light: Synergistic effect, mechanism, and application," *Chemosphere*, vol. 339, p. 139797, Oct. 2023, doi: 10.1016/J.CHEMOSPHERE.2023.139797.

[46] C. Illahi, W. E. F. Hutabarat, N. Nurdini, F. Failamani, and G. T. M. Kadja, "Photocatalytic degradation of azo dyes over MXene-based catalyst: Recent developments and future prospects," *Next Nanotechnology*, vol. 6, p. 100055, Jan. 2024, doi: 10.1016/J.NXNANO.2024.100055.

[47] M. A. Abu-Dalo, S. A. Al-Rosan, B. A. Albiss, M. A.; Al-Rosan, S. A.; Albiss, and B. A. Photocatalytic, "Photocatalytic Degradation of Methylene Blue Using Polymeric Membranes Based on Cellulose Acetate Impregnated with ZnO Nanostructures," *Polymers 2021, Vol. 13, Page 3451*, vol. 13, no. 19, p. 3451, Oct. 2021, doi: 10.3390/POLYM13193451.

[48] A. Turolla, A. Piazzoli, J. Farner Budarz, M. R. Wiesner, and M. Antonelli, "Experimental measurement and modelling of reactive species generation in TiO2 nanoparticle photocatalysis," *Chem Eng J*, vol. 271, p. 260, Jul. 2015, doi: 10.1016/J.CEJ.2015.03.004.

[49] H. Y. Ma, L. Zhao, L. H. Guo, H. Zhang, F. J. Chen, and W. C. Yu, "Roles of reactive oxygen species (ROS) in the photocatalytic degradation of pentachlorophenol and its main toxic intermediates by TiO2/UV," *J Hazard Mater*, vol. 369, pp. 719–726, May 2019, doi: 10.1016/J.JHAZMAT.2019.02.080.

[50] T. Liu *et al.*, "Synergistic Effect of Charge Separation and Multiple Reactive Oxygen Species Generation on Boosting Photocatalytic Degradation of Fluvastatin by ZnIn2S4/Bi2WO6 Z-Scheme Heterostructured Photocatalytst," *Toxics*, vol. 10, no. 10, p. 555, Oct. 2022, doi: 10.3390/TOXICS10100555/S1.

[51] R. Ameta, M. S. Solanki, S. Benjamin, and S. C. Ameta, "Photocatalysis," *Advanced Oxidation Processes for Wastewater Treatment: Emerging Green Chemical Technology*, pp. 135–175, Feb. 2018, doi: 10.1016/B978-0-12-810499-6.00006-1.

[52] J. Ângelo, L. Andrade, L. M. Madeira, and A. Mendes, "An overview of photocatalysis phenomena applied to NOx abatement," *J Environ Manage*, vol. 129, pp. 522–539, Nov. 2013, doi: 10.1016/j.jenvman.2013.08.006.

[53] N. M. Chauke, R. L. Mohlala, S. Ngqoloda, and M. C. Raphulu, "Harnessing visible light: enhancing TiO2 photocatalysis with photosensitizers for sustainable and efficient environmental solutions," *Frontiers in Chemical Engineering*, vol. 6, p. 1356021, Feb. 2024, doi: 10.3389/FCENG.2024.1356021/XML/NLM.

[54] S. B. Madduri and R. R. Kommalapati, "Photocatalytic Degradation of Azo Dyes in Aqueous Solution Using TiO2 Doped with rGO/CdS under UV Irradiation," *Processes*, vol. 12, no. 7, p. 1455, Jul. 2024, doi: 10.3390/PR12071455/S1.

[55] N. Qutub, P. Singh, S. Sabir, S. Sagadevan, and W. C. Oh, "Enhanced photocatalytic degradation of Acid Blue dye using CdS/TiO2 nanocomposite," *Sci Rep*, vol. 12, no. 1, pp. 1–18, Dec. 2022, doi: 10.1038/S41598-022-

09479-0;SUBJMETA=172,301,638,639,704,925;KWRD=CHEMISTRY,ENVIRONMENTAL+SCIENCES,MATERIALS+SCIENCE,NANOSCIENCE+AND+TECHNOLOGY.

[56] H. Barkouch *et al.*, "Bismuth-doped TiO2 enable solar photocatalytic water treatment," *Opt Mater (Amst)*, vol. 146, p. 114507, Dec. 2023, doi: 10.1016/J.OPTMAT.2023.114507.

[57] D. R. Eddy *et al.*, "Heterophase Polymorph of TiO2 (Anatase, Rutile, Brookite, TiO2 (B)) for Efficient Photocatalyst: Fabrication and Activity," *Nanomaterials 2023, Vol. 13, Page 704*, vol. 13, no. 4, p. 704, Feb. 2023, doi: 10.3390/NANO13040704.

[58] D. A. Akuma, H. Lund, T. T. Hoa Duong, F. Fufa, J. Strunk, and N. Steinfeldt, "Optimization of Anatase TiO2 Photocatalyst for Diclofenac Degradation by Using Response Surface Methodology," *Applied Sciences (Switzerland)*, vol. 15, no. 3, p. 1401, Feb. 2025, doi: 10.3390/APP15031401.

[59] F. Amano, A. Yamamoto, and J. Kumagai, "Highly Active Rutile TiO2 for Photocatalysis under Violet Light Irradiation at 405 nm," *Catalysts*, vol. 12, no. 10, p. 1079, Oct. 2022, doi: 10.3390/CATAL12101079/S1.

[60] Z. Chen, J. Xiong, and G. Cheng, "Recent advances in brookite phase TiO2-based photocatalysts toward CO2 reduction," *Fuel*, vol. 357, p. 129806, Feb. 2024, doi: 10.1016/J.FUEL.2023.129806.

[61] A. E. Shalan, A. M. Elseman, and M. M. Rashad, "Controlling the Microstructure and Properties of Titanium Dioxide for Efficient Solar Cells," *Titanium Dioxide - Material for a Sustainable Environment*, Jun. 2018, doi: 10.5772/INTECHOPEN.72494.

[62] S. P. Pitre, T. P. Yoon, and J. C. Scaiano, "Titanium dioxide visible light photocatalysis: surface association enables photocatalysis with visible light irradiation," *Chemical Communications*, vol. 53, no. 31, pp. 4335–4338, Apr. 2017, doi: 10.1039/C7CC01952A.

[63] I. TatlIdil, M. Sökmen, C. Breen, F. Clegg, C. K. Buruk, and E. BacaksIz, "Degradation of Candida albicans on TiO2 and Ag-TiO2 thin films prepared by sol-gel and nanosuspensions," *J Solgel Sci Technol*, vol. 60, no. 1, pp. 23–32, Oct. 2011, doi: 10.1007/S10971-011-2546-0/METRICS.

[64] L. Vilas Vilela, L. Ruiz-Rubio, H. Wang, S. J. Armakovi´carmakovi´c, M. M. Savanovi´csavanovi´c, and S. A. Armakovi´c, "Titanium Dioxide as the Most Used Photocatalyst for Water Purification: An Overview," *Catalysts 2023, Vol. 13, Page 26*, vol. 13, no. 1, p. 26, Dec. 2022, doi: 10.3390/CATAL13010026.

[65] A. Thakur, S. Kumar, and V. S. Rangra, "Synthesis of reduced graphene oxide (rGO) via chemical reduction," *AIP Conf Proc*, vol. 1661, no. 1, May 2015, doi: 10.1063/1.4915423/588473.

[66] C. B. Anucha, I. Altin, E. Bacaksiz, and V. N. Stathopoulos, "Titanium dioxide (TiO_2)-based photocatalyst materials activity enhancement for contaminants of emerging concern (CECs) degradation: In the light of

modification strategies," *Chemical Engineering Journal Advances*, vol. 10, p. 100262, May 2022, doi: 10.1016/J.CEJA.2022.100262.

[67] F. Zhang *et al.*, "Recent Advances and Applications of Semiconductor Photocatalytic Technology," *Applied Sciences 2019, Vol. 9, Page 2489*, vol. 9, no. 12, p. 2489, Jun. 2019, doi: 10.3390/APP9122489.

[68] N. M. Chauke, A. Ngqalakwezi, and M. Raphulu, "Transformative advancements in visible-light-activated titanium dioxide for industrial wastewater remediation," *International Journal of Environmental Science and Technology 2025 22:9*, vol. 22, no. 9, pp. 8521–8552, Feb. 2025, doi: 10.1007/S13762-025-06397-2.

[69] P. S. Basavarajappa, S. B. Patil, N. Ganganagappa, K. R. Reddy, A. V. Raghu, and C. V. Reddy, "Recent progress in metal-doped TiO2, non-metal doped/codoped TiO2 and TiO2 nanostructured hybrids for enhanced photocatalysis," *Int J Hydrogen Energy*, vol. 45, no. 13, pp. 7764–7778, Mar. 2020, doi: 10.1016/J.IJHYDENE.2019.07.241.

[70] A. K. Bhunia, "Type-II heterostructure of semiconducting CdS nanoparticle-ZnO nanoflake arrays for visible light dependent enhanced photocatalytic activity," *Sci Rep*, vol. 15, no. 1, pp. 1–14, Dec. 2025, doi: 10.1038/S41598-025-88141-X;SUBJMETA=172,639,692,700,704,766,925;KWRD=ENVIRONMENTAL+SCIENCES,HEALTH+CARE,NANOSCIENCE+AND+TECHNOLOGY,PHYSICS.

[71] S. K. Nadikatla, V. B. Chintada, T. R. Gurugubelli, and R. Koutavarapu, "Review of Recent Developments in the Fabrication of ZnO/CdS Heterostructure Photocatalysts for Degradation of Organic Pollutants and Hydrogen Production," *Molecules 2023, Vol. 28, Page 4277*, vol. 28, no. 11, p. 4277, May 2023, doi: 10.3390/MOLECULES28114277.

[72] F. Khan, M. S. Khan, S. Kamal, M. Arshad, S. I. Ahmad, and S. A. A. Nami, "Recent advances in graphene oxide and reduced graphene oxide based nanocomposites for the photodegradation of dyes," *J Mater Chem C Mater*, vol. 8, no. 45, pp. 15940–15955, Dec. 2020, doi: 10.1039/D0TC03684F.

[73] F. Dai *et al.*, "Preparation and Characterization of Reduced Graphene Oxide /TiO2 Blended Polyphenylene sulfone Antifouling Composite Membrane With Improved Photocatalytic Degradation Performance," *Front Chem*, vol. 9, p. 753741, Oct. 2021, doi: 10.3389/FCHEM.2021.753741.

[74] N. Shakeel, I. Piwoński, A. Kisielewska, M. Krzywiecki, D. Batory, and M. Cichomski, "Morphology-Dependent Photocatalytic Activity of Nanostructured Titanium Dioxide Coatings with Silver Nanoparticles," *International Journal of Molecular Sciences 2024, Vol. 25, Page 8824*, vol. 25, no. 16, p. 8824, Aug. 2024, doi: 10.3390/IJMS25168824.

[75] S. Abela *et al.*, "Photocatalytic Activity of Titanium Dioxide Nanotubes Following Long-Term Aging," *Nanomaterials*, vol. 11, no. 11, p. 2823, Nov. 2021, doi: 10.3390/NANO11112823.

[76] S. Mathew *et al.*, "Cu-Doped TiO2: Visible Light Assisted Photocatalytic Antimicrobial Activity," *Applied Sciences 2018, Vol. 8, Page 2067*, vol. 8, no. 11, p. 2067, Oct. 2018, doi: 10.3390/APP8112067.

[77] A. Das *et al.*, "Origin of the Improved Photoelectrochemical and Photocatalytic Activity in a ZnO-TiO2 Nanohybrid Revealed by Experimental and Density Functional Theory Studies," *Journal of Physical Chemistry Letters*, vol. 15, no. 29, pp. 7524–7532, Jul. 2024, doi: 10.1021/ACS.JPCLETT.4C01641/ASSET/IMAGES/LARGE/JZ4C01641_0005.JPEG.

[78] S. Prabakaran, K. D. Nisha, S. Harish, J. Archana, and M. Navaneethan, "Yttrium incorporated TiO2/rGO nanocomposites as an efficient charge transfer layer with enhanced mobility and electrical conductivity," *J Alloys Compd*, vol. 885, Dec. 2021, doi: 10.1016/J.JALLCOM.2021.160936.

[79] E. T. Mombeshora and E. Muchuweni, "Dynamics of reduced graphene oxide: synthesis and structural models," *RSC Adv*, vol. 13, no. 26, pp. 17633–17655, Jun. 2023, doi: 10.1039/D3RA02098C.

[80] S. Yadav *et al.*, "An Update on Graphene Oxide: Applications and Toxicity," *ACS Omega*, vol. 7, no. 40, pp. 35387–35445, Oct. 2022, doi: 10.1021/ACSOMEGA.2C03171/ASSET/IMAGES/LARGE/AO2C03171_0018.JPEG.

[81] N. G. de Barros *et al.*, "Graphene Oxide: A Comparison of Reduction Methods," *C-Journal of Carbon Research*, vol. 9, no. 3, p. 73, Sep. 2023, doi: 10.3390/C9030073/S1.

[82] Y. Hu and H. Gao, "Chemical synthesis of reduced graphene oxide: a review," *Minerals and Mineral Materials*, vol. 2, no. 2, Jul. 2023, doi: 10.20517/MMM.2023.07.

[83] K. Tadyszak, J. K. Wychowaniec, and J. Litowczenko, "Biomedical applications of graphene-based structures," *Nanomaterials*, vol. 8, no. 11, Nov. 2018, doi: 10.3390/NANO8110944.

[84] Q. Hu, A. Nag, L. Zhang, and K. Wang, "Reduced graphene oxide-based composites for wearable strain-sensing applications," *Sens Actuators A Phys*, vol. 345, p. 113767, Oct. 2022, doi: 10.1016/J.SNA.2022.113767.

[85] X. Jiao, Y. Qiu, L. Zhang, and X. Zhang, "Comparison of the characteristic properties of reduced graphene oxides synthesized from natural graphites with different graphitization degrees," *RSC Adv*, vol. 7, no. 82, pp. 52337–52344, Nov. 2017, doi: 10.1039/C7RA10809E.

[86] R. Selvam *et al.*, "Study of Different Properties of Graphene Oxide (GO) and Reduced Graphene Oxide (rGO)," *Engineering Proceedings 2023, Vol. 59, Page 84*, vol. 59, no. 1, p. 84, Dec. 2023, doi: 10.3390/ENGPROC2023059084.

[87] A. Mondal, A. Prabhakaran, S. Gupta, and V. R. Subramanian, "Boosting Photocatalytic Activity Using Reduced Graphene Oxide (RGO)/Semiconductor Nanocomposites: Issues and Future Scope," *ACS Omega*, vol. 6, no. 13,

pp. 8734–8743, Apr. 2021, doi: 10.1021/ACSOMEGA.0C06045/ASSET/IMAGES/LARGE/AO0C06045_0003.JPEG.

[88] H. A. A. Jamjoum, K. Umar, R. Adnan, M. R. Razali, and M. N. Mohamad Ibrahim, "Synthesis, Characterization, and Photocatalytic Activities of Graphene Oxide/metal Oxides Nanocomposites: A Review," *Front Chem*, vol. 9, p. 752276, Sep. 2021, doi: 10.3389/FCHEM.2021.752276/XML/NLM.

[89] L. H. Verástegui-Domínguez, N. Elizondo-Villarreal, D. I. Martínez-Delgado, and M. Á. Gracia-Pinilla, "Eco-Friendly Reduction of Graphene Oxide by Aqueous Extracts for Photocatalysis Applications," *Nanomaterials 2022, Vol. 12, Page 3882*, vol. 12, no. 21, p. 3882, Nov. 2022, doi: 10.3390/NANO12213882.

[90] M. Kocijan, L. Ćurković, T. Radošević, and M. Podlogar, "Enhanced Photocatalytic Activity of Hybrid rGO@TiO2/CN Nanocomposite for Organic Pollutant Degradation under Solar Light Irradiation," *Catalysts 2021, Vol. 11, Page 1023*, vol. 11, no. 9, p. 1023, Aug. 2021, doi: 10.3390/CATAL11091023.

[91] N. T. P. Thanh *et al.*, "Investigating for Photocatalytic Activity of Hybrid TiO2/Reduced Graphene Oxide and Application in Reducing VOCs," *Bulletin of Chemical Reaction Engineering & Catalysis*, vol. 19, no. 1, pp. 79–85, Apr. 2024, doi: 10.9767/BCREC.20042.

[92] H. Cruz *et al.*, "The Potential of rGO@TiO2 Photocatalyst for the Degradation of Organic Pollutants in Water," *Sustainability 2022, Vol. 14, Page 12703*, vol. 14, no. 19, p. 12703, Oct. 2022, doi: 10.3390/SU141912703.

[93] P. N. O. Gillespie and N. Martsinovich, "Origin of Charge Trapping in TiO2/Reduced Graphene Oxide Photocatalytic Composites: Insights from Theory," *ACS Appl Mater Interfaces*, vol. 11, no. 35, pp. 31909–31922, Sep. 2019, doi: 10.1021/ACSAMI.9B09235/ASSET/IMAGES/LARGE/AM9B09235_0003.JPEG.

[94] W. Yan, F. He, S. Gai, P. Gao, Y. Chen, and P. Yang, "A novel 3D structured reduced graphene oxide/TiO2 composite: synthesis and photocatalytic performance," *J Mater Chem A Mater*, vol. 2, no. 10, pp. 3605–3612, Feb. 2014, doi: 10.1039/C3TA14718E.

[95] D. Perumal, E. L. Albert, and C. A. C. Abdullah, "Green Reduction of Graphene Oxide Involving Extracts of Plants from Different Taxonomy Groups," *Journal of Composites Science 2022, Vol. 6, Page 58*, vol. 6, no. 2, p. 58, Feb. 2022, doi: 10.3390/JCS6020058.

[96] H. Awang, N. I. Talalah, H. Awang, and N. I. Talalah, "Synthesis of Reduced Graphene Oxide-Titanium (rGO-TiO2) Composite Using a Solvothermal and Hydrothermal Methods and Characterized via XRD and UV-Vis," *Natural Resources*, vol. 10, no. 2, pp. 17–28, Feb. 2019, doi: 10.4236/NR.2019.102002.

[97] A. Basso Peressut *et al.*, "Reduced Graphene Oxide/Waste-Derived TiO2 Composite Membranes: Preliminary Study of a New Material for Hybrid Wastewater Treatment," *Nanomaterials*, vol. 13, no. 6, p. 1043, Mar. 2023, doi: 10.3390/NANO13061043/S1.

[98] L. L. Tan, W. J. Ong, S. P. Chai, and A. R. Mohamed, "Reduced graphene oxide-TiO2 nanocomposite as a promising visible-light-active photocatalyst for the conversion of carbon dioxide," *Nanoscale Res Lett*, vol. 8, no. 1, pp. 1–9, Nov. 2013, doi: 10.1186/1556-276X-8-465/FIGURES/4.

[99] E. D. H. Kong *et al.*, "GO/TiO2-Related Nanocomposites as Photocatalysts for Pollutant Removal in Wastewater Treatment," *Nanomaterials 2022, Vol. 12, Page 3536*, vol. 12, no. 19, p. 3536, Oct. 2022, doi: 10.3390/NANO12193536.

[100] S. Subhapriya and P. Gomathipriya, "Green synthesis of titanium dioxide (TiO2) nanoparticles by Trigonella foenum-graecum extract and its antimicrobial properties," *Microb Pathog*, vol. 116, pp. 215–220, Mar. 2018, doi: 10.1016/j.micpath.2018.01.027.

[101] S. kazemi *et al.*, "Recent advances in green synthesized nanoparticles: from production to application," *Materials Today Sustainability*, vol. 24, p. 100500, Dec. 2023, doi: 10.1016/J.MTSUST.2023.100500.

[102] G. Bhattacharya, S. Sas, S. Wadhwa, A. Mathur, J. McLaughlin, and S. S. Roy, "Aloe vera assisted facile green synthesis of reduced graphene oxide for electrochemical and dye removal applications," *RSC Adv*, vol. 7, no. 43, pp. 26680–26688, May 2017, doi: 10.1039/C7RA02828H.

[103] T. K. N. Tran *et al.*, "Green synthesis of titanium dioxide nanoparticles using green tea (Camellia sinensis) extract: Characteristics and applications," *Green Processing and Synthesis*, vol. 14, no. 1, Jan. 2025, doi: 10.1515/GPS-2024-0226/ASSET/GRAPHIC/J_GPS-2024-0226_FIG_011.JPG.

[104] "Green Synthesis of Neem-based Zinc Oxide and Titanium Dioxide Nanoparticles for Enhanced Antimicrobial Functionalization of DBD Plasma Treated Silk and Corn Fabrics," *NanoWorld J*, vol. 9, Dec. 2023, doi: 10.17756/NWJ.2023-S5-076
.

[105] P. Tippayawat, N. Phromviyo, P. Boueroy, and A. Chompoosor, "Green synthesis of silver nanoparticles in aloe vera plant extract prepared by a hydrothermal method and their synergistic antibacterial activity," *PeerJ*, vol. 2016, no. 10, p. e2589, 2016, doi: 10.7717/PEERJ.2589/SUPP-2.

[106] heba Hassan, E. Attia, S. Desoukey, K. Mohamed, and M. Kamel, "Quantitative Analysis of Total Phenolic and Total Flavonoid Constituents of some Ficus species," *Journal of advanced Biomedical and Pharmaceutical Sciences*, vol. 2, no. 1, pp. 38–40, Jan. 2019, doi: 10.21608/JABPS.2018.5945.1027.

[107] A. E. D. Mahmoud, N. El-Maghrabi, M. Hosny, and M. Fawzy, "Biogenic synthesis of reduced graphene oxide from Ziziphus spina-christi (Christ's thorn jujube) extracts for catalytic, antimicrobial, and antioxidant potentialities," *Environ Sci Pollut Res Int*, vol. 29, no. 59, p. 89772, Dec. 2022, doi: 10.1007/S11356-022-21871-X.

[108] A. Singhal, N. Singhal, A. Bhattacharya, and A. Gupta, "Synthesis of silver nanoparticles (AgNPs) using Ficus retusa leaf extract for potential application as antibacterial and dye decolourising agents," *Inorganic and Nano-*

Metal Chemistry, vol. 47, no. 11, pp. 1520–1529, Nov. 2017, doi: 10.1080/24701556.2017.1357604;CTYPE:STRING:JOURNAL.

[109] "Photo of the leaves of Ficus retusa posted by DaylilySLP - Garden.org." Accessed: May 27, 2025. [Online]. Available: https://garden.org/plants/photo/571614/

[110] G. Liu *et al.*, "Enhanced catalytic effect of TiO2@rGO synthesized by one-pot ethylene glycol-assisted solvothermal method for MgH2," *J Alloys Compd*, vol. 881, p. 160644, Nov. 2021, doi: 10.1016/J.JALLCOM.2021.160644.

[111] U. Hikmah *et al.*, "In-Situ Sol-Gel Method of TiO_2-reduced Graphene Oxide as Photocatalyst," pp. 72–80, May 2023, doi: 10.2991/978-94-6463-148-7_8.

[112] Z. A. M. Alaizeri, H. A. Alhadlaq, S. Aldawood, and N. A. Y. Abduh, "Green synthesis of ZnO-TiO 2 /RGO nanocomposites using Senna surattensis extract: a novel approach for enhanced anticancer efficacy and biocompatibility," *RSC Adv*, vol. 14, no. 24, pp. 16685–16695, May 2024, doi: 10.1039/D4RA01634C.

[113] M. H. Olana, F. K. Sabir, E. T. Bekele, and B. A. Gonfa, "Citrus sinensis and Musa acuminata Peel Waste Extract Mediated Synthesis of TiO2/rGO Nanocomposites for Photocatalytic Degradation of Methylene Blue under Visible Light Irradiation," *Bioinorg Chem Appl*, vol. 2022, no. 1, p. 5978707, Jan. 2022, doi: 10.1155/2022/5978707.

[114] G. B. Yitagesu, D. T. Leku, and G. A. Workneh, "Green Synthesis of TiO2 Using Impatiens rothii Hook.f. Leaf Extract for Efficient Removal of Methylene Blue Dye," *ACS Omega*, vol. 8, no. 46, pp. 43999–44012, Nov. 2023, doi: 10.1021/ACSOMEGA.3C06142/ASSET/IMAGES/LARGE/AO3C06142_0013.JPEG.

[115] S. Ying *et al.*, "Green synthesis of nanoparticles: Current developments and limitations," *Environ Technol Innov*, vol. 26, p. 102336, May 2022, doi: 10.1016/J.ETI.2022.102336.

[116] T. S. Algarni, A. M. Al-Mohaimeed, N. A. Y. Abduh, R. A. Habab, and S. M. Alqahtani, "Green Synthesis of Mixed ZnO-SnO2 Nanoparticles for Solar-Assisted Degradation of Synthetic Dyes," *Catalysts 2023, Vol. 13, Page 1509*, vol. 13, no. 12, p. 1509, Dec. 2023, doi: 10.3390/CATAL13121509.

[117] M. Ali *et al.*, "GREEN SYNTHESIS OF METAL OXIDE NANOPARTICLES FOR SOLAR CELL EFFICIENCY ENHANCEMENT," *Spectrum of Engineering Sciences*, vol. 3, no. 4, pp. 765–773, Apr. 2025, doi: 10.5281/zenodo.15267111.

[118] U. M. Balasubramanian, S. V. Murugaiyan, and T. Marimuthu, "Sustainable robust green synthesis of nanoparticles from waste aquatic plants and its application in environmental remediation," *Water Science and Technology*, vol. 84, no. 12, pp. 3599–3615, Dec. 2021, doi: 10.2166/WST.2021.471.

[119] F. Zanbili and A. Poursattar Marjani, "Innovative green and bio-based approaches for photosensitive nanoparticle synthesis: a review on methodologies, characterization, and applications," *Micro and Nano Systems Letters 2025 13:1*, vol. 13, no. 1, pp. 1–36, Mar. 2025, doi: 10.1186/S40486-025-00223-7.

[120] H. Singh *et al.*, "Revisiting the Green Synthesis of Nanoparticles: Uncovering Influences of Plant Extracts as Reducing Agents for Enhanced Synthesis Efficiency and Its Biomedical Applications," *Int J Nanomedicine*, vol. 18, pp. 4727–4750, Aug. 2023, doi: 10.2147/IJN.S419369.

[121] A. I. Osman *et al.*, "Synthesis of green nanoparticles for energy, biomedical, environmental, agricultural, and food applications: A review," *Environmental Chemistry Letters 2024 22:2*, vol. 22, no. 2, pp. 841–887, Jan. 2024, doi: 10.1007/S10311-023-01682-3.

[122] M. S. Samuel *et al.*, "A Review on Green Synthesis of Nanoparticles and Their Diverse Biomedical and Environmental Applications," *Catalysts 2022, Vol. 12, Page 459*, vol. 12, no. 5, p. 459, Apr. 2022, doi: 10.3390/CATAL12050459.

[123] V. P. Aswathi, S. Meera, C. G. A. Maria, and M. Nidhin, "Green synthesis of nanoparticles from biodegradable waste extracts and their applications: a critical review," *Nanotechnology for Environmental Engineering*, vol. 8, no. 2, p. 1, Jun. 2022, doi: 10.1007/S41204-022-00276-8.

Chapter II References

[1] Z. A. M. Alaizeri, H. A. Alhadlaq, S. Aldawood, and N. A. Y. Abduh, "Green synthesis of ZnO-TiO2/RGO nanocomposites using Senna surattensis extract: a novel approach for enhanced anticancer efficacy and biocompatibility," *RSC Adv*, vol. 14, no. 24, pp. 16685–16695, May 2024, doi: 10.1039/D4RA01634C.

[2] KHELLAF Noureddine, "Synthèse par voie sol-gel et caractérisation d'un photocatalyseur composite La0.5Sr0.5MnO3/TiO2 vis-à-vis de la production d'hydrogène et d'oxygène," UNIVERSITE FERHAT ABBAS SETIF-1, 2018.

[3] L. Otmani, R. Doufnoune, Y. Benguerba, and A. Erto, "Experimental and theoretical investigation of the interaction of sulfonated graphene oxide with polyvinylalcohol/poly (4-styrenesulfonic) complex," *J Mol Liq*, vol. 284, pp. 599–606, Jun. 2019, doi: 10.1016/j.molliq.2019.04.034.

[4] C. A. De Caro, M. Toledo, and H. Claudia, "UV/Vis Spectrophotometry-Fundamentals and Applications." [Online]. Available: https://www.researchgate.net/publication/321017142

[5] Y. Ammari, K. Elatmani, S. Qourzal, I. Bakas, E. Ejakouk, and Y. Ait-Ichou, "colorant bleu de méthylène en présence de dioxyde de titane (TiO2), en suspension aqueuse (Kinetic study of the photocatalytic degradation of methylene blue …," *jmaterenvironsci.com*, vol. 7, no. 2, pp. 671–678, 2016, Accessed: Jun. 12, 2025. [Online]. Available: http://www.jmaterenvironsci.com/Document/vol7/vol7_N2/79-JMES-2103-2015-Ammari.pdf

[6] I. Diouf, P. Drogui, E. H. M. Diop, S. M. Lo, M. Rumeau, and C. G. M. Diop, "Degradation of the crystal violet by electro-oxidation on ti/tio 2 and ti/iro 2 -ruo 2 electrodes: Study of the effects of operating parameters on the process efficiency," *Revue des Sciences de l'Eau*, vol. 31, no. 4, pp. 327–339, 2018, doi: 10.7202/1055592AR.

[7] Samia SAAIDIA, "Dégradation d'un colorant cationique par photocatalyse, électro-oxydation et leur couplage," 2018.

[8] A. Ali, Y. W. Chiang, and R. M. Santos, "X-ray Diffraction Techniques for Mineral Characterization: A Review for Engineers of the Fundamentals, Applications, and Research Directions," *Minerals 2022, Vol. 12, Page 205*, vol. 12, no. 2, p. 205, Feb. 2022, doi: 10.3390/MIN12020205.

[9] A. Monshi, M. R. Foroughi, M. R. Monshi, A. Monshi, M. R. Foroughi, and M. R. Monshi, "Modified Scherrer Equation to Estimate More Accurately Nano-Crystallite Size Using XRD," *World Journal of Nano Science and Engineering*, vol. 2, no. 3, pp. 154–160, Sep. 2012, doi: 10.4236/WJNSE.2012.23020.

[10] A. Yaseen Sharaf Zeebaree *et al.*, "Sustainable engineering of plant-synthesized TiO2 nanocatalysts: Diagnosis, properties and their photocatalytic performance in removing of methylene blue dye from effluent. A review," *Current Research in Green and Sustainable Chemistry*, vol. 5, p. 100312, Jan. 2022, doi: 10.1016/J.CRGSC.2022.100312.

[11] H. Zhang *et al.*, "Synthesis and characterization of TiO2/graphene oxide nanocomposites for photoreduction of heavy metal ions in reverse osmosis concentrate," *RSC Adv*, vol. 8, no. 60, pp. 34241–34251, 2018, doi: 10.1039/C8RA06681G;

[12] P. Makuła, M. Pacia, and W. Macyk, "How To Correctly Determine the Band Gap Energy of Modified Semiconductor Photocatalysts Based on UV-Vis Spectra," *Journal of Physical Chemistry Letters*, vol. 9, no. 23, pp. 6814–6817, Dec. 2018, doi: 10.1021/ACS.JPCLETT.8B02892/SUPPL_FILE/JZ8B02892_LIVESLIDES.MP4.

[13] J. A. Myers, B. S. Curtis, and W. R. Curtis, "Improving accuracy of cell and chromophore concentration measurements using optical density," *BMC Biophysics 2013 6:1*, vol. 6, no. 1, pp. 1–16, Apr. 2013, doi: 10.1186/2046-1682-6-4.

Appendix

Name and formula

Reference code:	00-001-0562
Mineral name:	Anatase
PDF index name:	Titanium Oxide
Empirical formula:	O_2Ti
Chemical formula:	TiO_2

Crystallographic parameters

Crystal system:	Tetragonal
Space group:	I41/amd
Space group number:	141
a (Å):	3,7300
b (Å):	3,7300
c (Å):	9,3700
Alpha (°):	90,0000
Beta (°):	90,0000
Gamma (°):	90,0000
Measured density (g/cm^3):	3,90
Volume of cell (10^6 pm^3):	130,36
Z:	4,00
RIR:	-

Status, subfiles and quality

Status:	Marked as deleted by ICDD
Subfiles:	Inorganic Mineral Alloy, metal or intermetalic
Quality:	Blank (B)

Comments

Deleted by:	Deleted by NBS card 21-1272, see 4-477.
Color:	Brown
General comments:	T.P. to a-anatase at 642 C. To rutile at 915.
Optical data:	A=2.4880, B=2.561, Sign=-

References

Primary reference:	Hanawalt. et al., *Anal. Chem.*, **10**, 475, (1938)
Optical data:	*Dana's System of Mineralogy, 7th Ed.*
Unit cell:	*Dana's System of Mineralogy, 7th Ed.*

Peak list

No.	h	k	l	d [A]	2Theta[deg]	I [%]
1	1	0	1	3,52000	25,281	100,0
2	1	0	3	2,37000	37,934	24,0
3	2	0	0	1,88000	48,376	40,0
4	1	0	5	1,70000	53,888	28,0
5				1,66000	55,296	24,0
6	2	1	3	1,48000	62,728	24,0
7	1	1	6	1,36000	68,999	8,0
8				1,34000	70,178	8,0
9	1	0	7	1,26000	75,374	11,0
10	3	0	3	1,16000	83,219	6,0
11	3	1	4	1,05000	94,381	3,0
12	3	1	6	0,95000	108,357	2,0
13	4	0	2	0,91300	115,066	2,0
14	4	1	1	0,89400	119,001	2,0

Stick Pattern

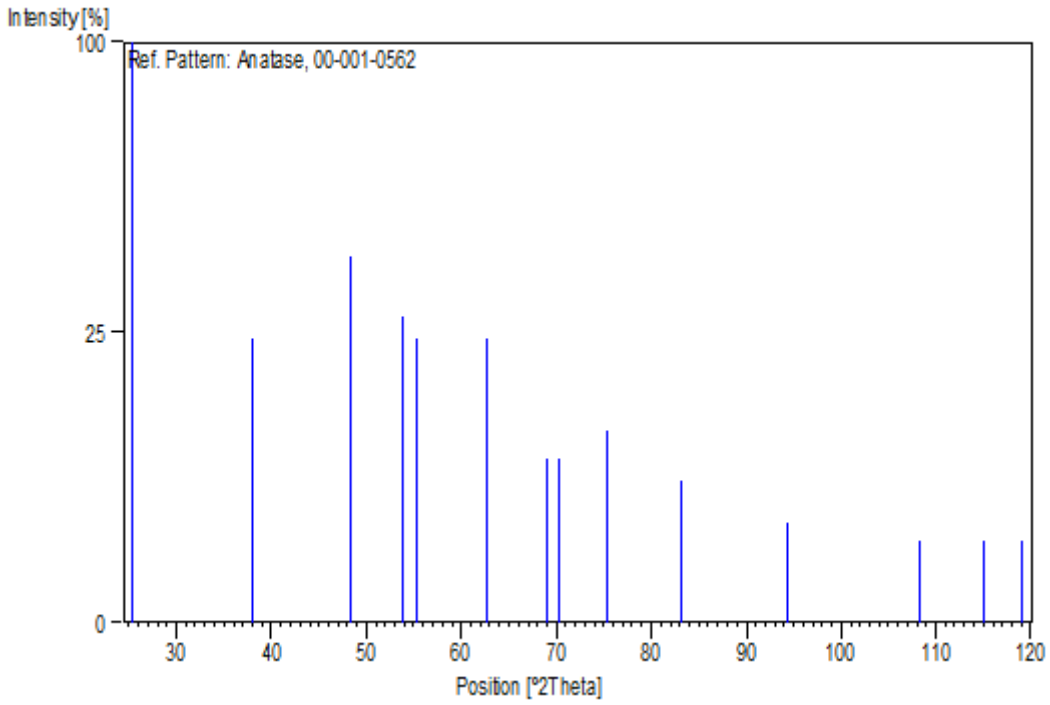

Name and formula

Reference code: 00-002-0514

Mineral name: Brookite
PDF index name: Titanium Oxide

Empirical formula:	O_2Ti
Chemical formula:	TiO_2

Crystallographic parameters

Crystal system:	Orthorhombic
Space group:	Pbca
Space group number:	61
a (Å):	9,1660
b (Å):	5,4360
c (Å):	5,1350
Alpha (°):	90,0000
Beta (°):	90,0000
Gamma (°):	90,0000
Measured density (g/cm^3):	4,14
Volume of cell (10^6 pm^3):	255,86
Z:	8,00
RIR:	-

Status, subfiles and quality

Status:	Marked as deleted by ICDD
Subfiles:	Inorganic Mineral Alloy, metal or intermetalic
Quality:	Doubtful (O)

Comments

Deleted by:	see A. Pabst letter of July 4, 1953.
Color:	Yellow, blue
General comments:	Transforms to tetragonal at 700 C. Decomposes at 2227 C.
Optical data:	A=2.5831, B=2.5843, Q=2.7004, Sign=+
Melting point:	1825

References

Primary reference:	Crystallographic Laboratory, Cambridge, England, UK., *Private Communication*
Optical data:	*Dana's System of Mineralogy, 7th Ed.*

Peak list

No.	h	k	l	d [A]	2Theta[deg]	I [%]
1	1	1	1	3,46000	25,727	60,0
2				3,22000	27,681	100,0
3	2	1	1	2,87000	31,138	60,0
4	1	0	2	2,45000	36,650	80,0
5	0	2	1	2,39000	37,604	5,0
6	4	0	0	2,29000	39,312	5,0
7	2	0	2	2,24000	40,227	5,0
8				2,17000	41,584	40,0

9	2	2	1	2,12000	42,612	5,0
10				2,04000	44,370	30,0
11	4	1	1	1,95000	46,535	30,0
12	3	2	1	1,88000	48,376	40,0
13	3	1	2	1,84000	49,498	20,0
14	1	3	1	1,68000	54,582	100,0
15	5	1	1	1,65000	55,660	20,0
16	4	1	2	1,62000	56,783	60,0
17	2	3	1	1,60000	57,559	20,0
18	6	0	0	1,53000	60,459	20,0
19	6	1	0	1,48000	62,728	20,0
20	0	2	3	1,45000	64,179	40,0
21	1	2	3	1,43000	65,186	20,0
22	2	3	2	1,41000	66,229	20,0
23	0	4	0	1,36000	68,999	80,0
24	3	3	2	1,34000	70,178	20,0
25	3	2	3	1,31000	72,033	10,0
26	1	1	4	1,24000	76,809	10,0
27	4	4	0	1,17000	82,352	20,0
28	7	2	1	1,15000	84,107	30,0
29	4	0	4	1,12000	86,907	30,0
30	4	3	3	1,09000	89,934	40,0
31				1,08000	90,998	20,0
32	7	3	1	1,04000	95,578	40,0

Stick Pattern

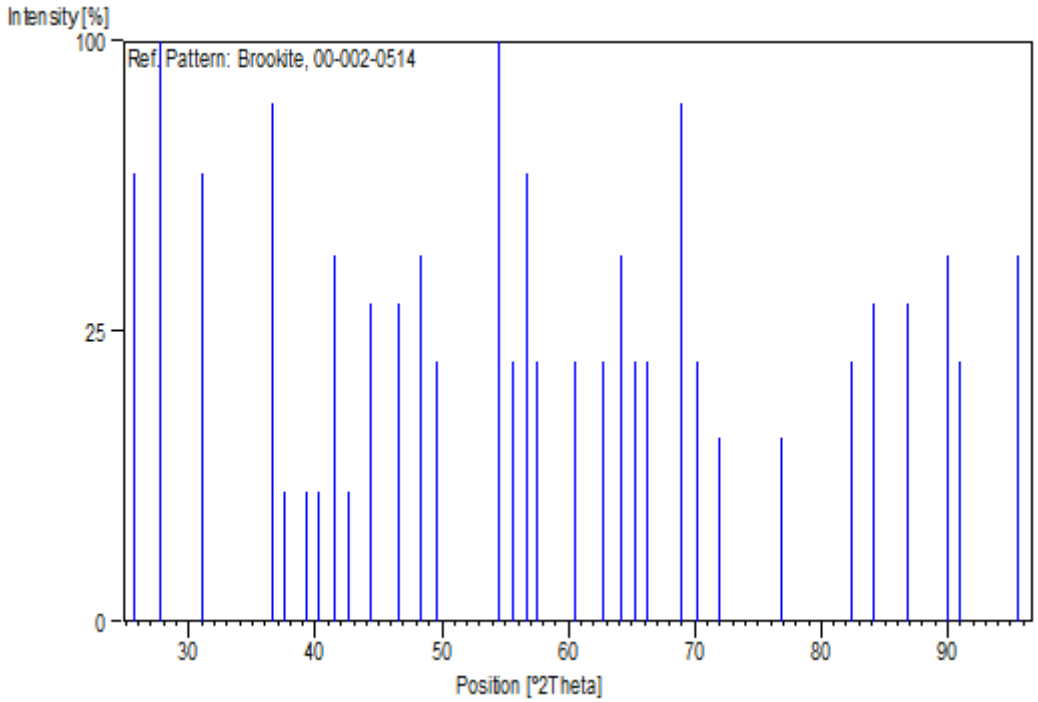

Résumé

Ce travail propose un procédé écologique de dégradation des colorants organiques (rouge Congo et violet cristal) à l'aide de nanohybrides TiO_2/rGO. Le matériau synthétisé par voie sol-gel et à partir d'extraits de feuilles de *Ficus retusa* a montré une dégradation efficace du colorant sous irradiation UV. Le rGO a permis de pallier les défauts du TiO_2 et constitue donc un candidat intéressant pour le traitement des eaux usées.

Mots clés : Photocatalyse ; dioxyde de titane (**TiO_2**) ; oxyde de graphène réduit (**rGO**) ; synthèse verte ; nanocomposites ; Rouge Congo (**CR**) ; Cristale Violet (**CV**).

ملخص

يقترح هذا العمل طريقة لتحلل الأصباغ العضوية (الأحمر الكونغولي والبنفسجي الكريستالي) باستخدام مركبات نانوية هجينة من TiO_2/rGO. وقد أظهر المركب المحضر بطريقة السول-جيل، وبالاعتماد على مستخلصات أوراق نبات الفيكس ريتوزا، فعالية عالية في تحلل الصبغة تحت إشعاع الأشعة فوق البنفسجية. وساهم وجود أكسيد الغرافين المختزل (rGO) في التغلب على عيوب ثاني أكسيد التيتانيوم(TiO_2) ، مما يجعله مرشحًا واعدًا لمعالجة مياه الصرف.

الكلمات المفتاحية.

التحفيز الضوئي؛ ثاني أكسيد التيتانيوم(TiO_2) ؛ أكسيد الجرافين المختزل(rGO) ؛ التخليق الأخض ؛ نانوهجين؛ الكونغو الأحمر (CR)؛ كريستال فيوليت.(CV)

Abstract

This work proposes an environmentally friendly process to degrade organic dyes (**CR**) and (**CV**) by using **TiO_2/rGO** nanohybrids. Sol-gel and ***Ficus retusa*** leaf extract synthesized material exhibited effective dye degradation under UV irradiation. The **rGO** enhanced the shortcomings of TiO_2 and thus it is a useful candidate for wastewater treatment.

Keywords: Photocatalysis; titanium dioxide (**TiO_2**); reduced graphene oxide (**rGO**); green synthesis; nanohybride; Congo Red(**CR**); Crystal Violet(**CV**).